1-1-2008

Uncertainty analysis of net heat release rate predictions in a single cylinder pilot compression ignited natural gas engine

Brandon T Marvel

UNCERTAINTY ANALYSIS OF NET HEAT RELEASE RATE PREDICTIONS IN A SINGLE CYLINDER PILOT COMPRESSION IGNITED NATURAL GAS ENGINE

By

Brandon T. Marvel

A Thesis
Submitted to the Faculty of
Mississippi State University
in Partial Fulfillment of the Requirements
for the Degree of Master of Science
in Mechanical Engineering
in the Department of Mechanical Engineering

Mississippi State, Mississippi

December 2008

UNCERTAINTY ANALYSIS OF NET HEAT RELEASE RATE PREDICTIONS

IN A SINGLE CYLINDER PILOT COMPRESSION

IGNITED NATURAL GAS ENGINE

By

Brandon T. Marvel

Approved:

Kalyan K. Srinivasan Assistant Professor of Mechanical Engineering (Director of Thesis)	Louay M. Chamra Professor and Interim Department Head of Mechanical Engineering (Committee Member)
Pedro Mago Associate Professor of Mechanical Engineering (Committee Member)	Steve Daniewicz Professor of Mechanical Engineering (Graduate Coordinator)

Sarah A. Rajala, Ph.D
Dean of Engineering
Earnest W. and Mary Ann Deavenport, Jr., Chair

Name: Brandon T. Marvel

Date of Degree: December 14, 2008

Institution: Mississippi State University

Major Field: Mechanical Engineering

Major Professor: Dr. Kalyan K. Srinivasan

Title of Study: UNCERTAINTY ANALYSIS OF NET HEAT RELEASE RATE PREDICTIONS IN A SINGLE CYLINDER PILOT COMPRESSION IGNITED NATURAL GAS ENGINE.

Pages in Study: 119

Candidate for Degree of Master of Science

A zero dimensional single zone model was developed to determine the crank resoled heat release rate at various injection timings (15°-60° BTDC) and the associated uncertainties from a pilot ignited natural gas engine. The uncertainty analysis examines the percentage contribution from various sources of error, including cylinder pressure measurements, intake manifold pressure measurements, and the impact of assumptions such as constant versus temperature dependent specific heat ratios. In particular, uncertainty percentage contributions and uncertainty magnification factors were used to quantify and compare the uncertainties in heat release rates using temperature dependent specific heat ratio correlations to constant specific heat ratio assumption. It is demonstrated that the error associated with the constant specific heat ratio assumption contributes to about 40 percent error (full scale value) in the net heat release estimates in comparison to using temperature dependent specific heat ratio correlations.

ACKNOWLEDGEMENTS

The author expresses his sincere gratitude for all the invaluable assistance and motivation that he received during this research. First and foremost, I would like to thank God for without His blessings and company I would be lost. To my parents, Larry and Jacqueline Marvel, I thank you for your unconditional love and support throughout my years. To Dr. Kalyan Srinivasan, I am grateful for the experience to work by your side these past two years. I know there were times that we both had our doubts but you kept faith in me and for that I'm grateful. To my friends, Richard Jackson, Blake Hargrove, Daniel Bozone and Rhett Graves, I thank you for your continual support and the swift kicks in the rear for when I lost focus. Lastly, I would like to express my sincere gratitude towards the staff and faculty of the Mechanical Engineering Department at Mississippi State University. Without their dedication to learning and hard work during my undergraduate years this Masters would not have been possible.

TABLE OF CONTENTS

LIST OF TABLES

LIST OF FIGURES

NOMENCLATURE

a	Crank Radius (m)
A_s	Stoichiometric Molar Air-Fuel Ratio
$BTDC$	Before Top Dead Center
C_p	Specific Heat at Constant Pressure ($m^2/K\text{-}s^2$)
C_v	Specific Heat at Constant Volume ($m^2/K\text{-}s^2$)
$dU/d\theta$	Rate of Internal Energy Release per Crank Angle (kJ)
$IMEP$	Indicated Mean Effective Pressure (bar)
IW	Indicated Work (kJ)
l	Connecting Rod Length (m)
m	In-cylinder Mass (kg)
mf	Mass Fraction
MW	Molecular Weight (kg/kmol)
P	In-cylinder Pressure (bar)
Q	Rate of Heat Release (kJ)
R	Gas Constant (J/kg-K)
T	In-cylinder Temperature (K)
U_x	Uncertainty of Subscript Variable
UMF	Uncertainty Magnification Factor

UPC	Uncertainty Percentage Contribution
V	Instantaneous In-cylinder Volume (m^3)
W	Work done by the Engine (kJ)

Greek

γ	Specific Heat Ratio
θ	Crank Angle
Φ	Equivalence Ratio

Subscripts

dot	Flow Rate
EVO	Exhaust Valve Opening
EVC	Exhaust Valve Closure
inj	Injection
IVO	Intake Valve Opening
IVC	Intake Valve Closure
o	Initial Condition

CHAPTER 1

INTRODUCTION

Global concerns of environmental effects due to emissions of internal combustion engines (ICEs) and fossil fuel consumption have forced engine researchers to reevaluate the combustion process. Alternative fuels such as propane, natural gas and biodiesel as well as hybrid drive trains have been proposed as possible solutions in recent years. Still, as governments continue to impose stricter emissions regulations, researchers are pressed to find an environmentally friendly and fuel efficient solution to the modern ICE.

In 1947, the governor of California, Earl Warrens, supported state legislature which set into motion the Air Pollution Control Act. This act was the first of its kind in the United States. The U.S. government shortly recognized California's emission concerns in 1955 when congress passed the Clean Air Act. Though concern for air pollution due to emissions was on the rise, it wasn't until the 1970's that federal and state legislature began placing strict regulations on the production of oxides of nitrogen (NO_x); the primary contributors to smog (Muzio & Quartucy, 1997). Nitrogen dioxide (NO_2) when combined with ultra-violet radiation forms ground level ozone (photochemical smog). Ozone is a volatile oxidizing compound that causes significant health risks to humans such as inflammation of the lungs and asthma. One study predicted that ground level ozone is responsible for nearly 20 deaths per day in the United States alone (Bell et

al., 2004). In addition to oxides of nitrogen, the emissions of combustion include carbon dioxide (CO_2), a green-house gas associated with global warming, and unburned hydro-carbons (HC), particulate matter (PM) or soot and carbon monoxide (CO).

If the environmental and health risks of emissions alone were not enough to advocate engine research, in recent years there has been a growing concern of the future availability of fossil fuels. The burning of fossil fuels, fuels refined from crude oil, supplies 40% of the world's total energy usage and 96% of the world's transportation energy. The United States contributes to one-quarter of the world's oil consumption, seven billion barrels annually. Of the seven billion barrels, two thirds is imported which translates to seven trillion dollars spent on imported oil over the past thirty years. Sixty-seven percent of the U.S. oil is used for ground transportation, i.e. gasoline and diesel powered engines.

The gasoline powered engine (spark ignition engine) has an energy efficiency of about thirty percent while diesel or compression ignited engines are about forty percent efficient. In laymen terms, at best, less than half of the energy produced by the burning of fuel in an ICE is converted into usable work. To relate these efficiencies to the annual U.S. consumption, only 2.11 billion barrels of the 4.69 billion barrels of oil used for ground transportation is converted to usable work, the other 2.58 billion barrels is lost to thermal and mechanical inefficiencies within the combustion process. Increasing modern engine efficiencies is the primary concern of academic research. Many studies have proposed alternative fuels or dual-fuel injection, using diesel as an ignition sources for natural gas, as a means to increase the ICE efficiency (Srinivasan et al., 2006, Krishnan et al., 2006).

In general, performance evaluation of internal combustion engines involve the measurement of the following parameters, brake torque (Nm), brake power (kW), indicated mean effective pressure (kPa), brake mean effective pressure (kPa), burned mass fraction (X_b) and the rate of heat release (ROHR). From these test parameters the efficiencies and specific fuel consumption (the technical equivalent of fuel economy) (g/kW-h) of a given engine can be derived. The indicated mean effective pressure is a measure of the cylinder pressure used in the determination of engine work per cycle. The term "indicated" is used "…to identify the impact of the compression, combustion and expansion processes on engine performance" (Heywood, 1998, pp. 48). The brake mean effective pressure is used to evaluate the usable power delivered by the engine. The brake power in addition to the friction power can be used as an estimate of the indicated power of an engine. Both the indicated and brake mean effective pressures allow the comparison of engines irrespective of engine size and are particularly useful metrics to compare two engines operating under similar conditions. The burned mass fraction is a representation of the temporal or crank-resolved history of mass burned in the cylinder. Coupled with the range of crank angles in which combustion occurs, the mass fraction burn portrays the quality of combustion in a given engine (Shayler & Wiseman, 1990). Similar to the mass fraction burn profile, the rate of heat release quantifies the amount of energy released during combustion and how much of the energy released is loss to heat transfer.

In order for researchers to determine the aforementioned test parameters, the engine piston position and corresponding in-cylinder pressure are required. The former is measured using an optical encoder mounted on the engine's drive shaft. The optical

encoder is essentially a square wave generator. By counting the waves generated, it is possible to determine the crank angle corresponding to the instantaneous position of the piston. The in-cylinder pressure is measured by mounting a piezoelectric pressure transducer within the cylinder. The piezoelectric transducer is a device that consists of a quartz piezoelectric crystal, which generates a voltage when subjected to a normal stress (or pressure). The voltage generated is linearly related to the pressure (within a certain operating temperature range, which is why the piezoelectric crystal is made of quartz since quartz can withstand high temperatures); therefore, the instantaneous cylinder pressure can be estimated from the voltage characteristics of the piezoelectric transducer. The accuracy of the optical encoder is limited to the manufacturer specified resolution and the phasing of the device to the top dead center (TDC) of the engine (Krishnan, 2001**)**. In-cylinder pressure data acquisition has many errors that are due to the violent nature of combustion and are difficult to overcome. Thermal shock, the rapid expansion and/or contraction of the transducer's diaphragm, is caused by large temperature differentials during combustion. These temperature variations apply an additional force against the quartz causing inaccuracies within the pressure reading. These errors are minimized greatly by adequately cooling the quartz crystal with cooling water (Krishnan, 2001). In addition to thermal shock errors, the piezoelectric pressure transducer is a differential pressure device, and therefore, requires a reference pressure to obtain an accurate representation of in-cylinder pressure measurements. Academic and industrial debate over where to reference the in-cylinder pressure data has given rise to additional uncertainties within its measurement. These uncertainties have typically been presented as estimation by the researchers or the uncertainty has been quantified by comparing two

or more alternatives methods in acquiring engine data. Few, if any studies, have presented a quantitative method to evaluate these uncertainties.

Uncertainty analysis provides a concrete means of quantifying the uncertainty introduced by variables within engine testing. Uncertainty analysis is the process of quantifying the uncertainty percentage contribution (UPC) and uncertainty magnification factor (UMF) of each variable. The uncertainty percentage contribution value is a measurement of "how much" the respective variable contributes to the total uncertainty of the calculated quantity. The uncertainty magnification factor demonstrates the degree in which uncertainties within a given variable propagate through the data reduction equation and its potential to affect the total uncertainty of the quantity of interest. Uncertainty analysis is a viable tool for preliminary experimental design. It provides a basis for the experimentalist to understand which of the measured variables contribute the most error to the total uncertainty, and how to effectively reduce the respective measurement errors.

Herein lays the focus of this thesis. First an in-depth review of the existing literature on in-cylinder pressure measurement, and the estimation of the rate of heat release, indicated work and indicated mean effective pressure (imep) from these in-cylinder pressure measurements and the respective uncertainties involved in these estimations will be presented. This will be followed by detailed uncertainty estimates of the heat release rate schedules of pilot ignited natural gas engine along with a discussion of results, conclusions and recommendations for future work.

CHAPTER 2

LITERATURE REVIEW

This chapter presents an overview of the research work that has been done on engine testing. In particular, the studies on in-cylinder pressure data acquisition that focus on pressure transducer selection, mounting techniques and crank angle resolution are of prime interest. The errors associated within these variables greatly affect the accuracy in the evaluation of the rate of heat release, indicated mean effective pressure, mass fraction burn and thermal efficiency of an engine. Several early investigations including those of Brown (1967), Lancaster et al. (1975) and Amann (1985) provided preliminary insight to such errors. This insight allowed future studies such as Randolph (1990a, 1990b) and Brunt and Lucas (1991) to quantify the errors involved in-cylinder pressure data acquisition through a series of sensitivity analyses.

Without the corresponding crank angle, the pressure data is virtually useless to researchers. Determining the piston's position is achieved by instrumenting the engine's drive shaft with an optical encoder. An optical encoder consists of a rotating disk with an encoded opaque and translucent pattern, light source and light sensor. A pulse is generated when the light source detected by the light sensor is interrupted by the opaque section of the encoded pattern (National Instruments, 2006). These pulses translate to a fixed amount of piston displacement. Though instrumenting the engine with an optical

encoder is a relatively easy task and has few additional errors associated besides the physical limitations of the device (crank angle resolution), researchers must take care to ensure that the device is phased appropriately with the engine. That is to say that the zero reading of the optical encoder corresponds to either the engine's top dead or bottom dead center.

2.1 Cylinder Pressure

In-cylinder pressure data is one of the cornerstones in engine testing. In conjunction with the in-cylinder volume, in-cylinder pressure data is used to determine the mass within the cylinder, temperature during the combustion cycle and the rate of heat release. These quantities in turn are used by experimenters to evaluate the work output and indicated mean effective pressure of a particular engine. The indicated mean effective pressure is used in comparing the efficiency between two or more engines. With the advancement of technology, in-cylinder pressure data acquisition has become more accurate, precise and rapid. Modern computer technology and data acquisition hardware/software have given researchers a deeper understanding of processes occurring during combustion. The study of combustion analysis increased within academic communities with the introduction of the piezoelectric pressure transducer, an example is shown in Figure 2.1. The piezoelectric pressure transducer is based upon the principle of piezoelectricity, or in laymen terms the ability of certain materials (typically quartz) to generate electric potential in response to an external mechanical stress (pressure). The generated electric potential or charge is proportional to the applied stress and can be converted into a measurable change in voltage by means of a charge amplifier. Because

the measure pressured is a differential reading, a reference pressure must be acquired beforehand. The reference pressure is typically taken as the average pressure from the inlet manifold.

Perhaps one of the first papers addressing the errors associated with in-cylinder pressure measurement was written by Brown (1967). Brown's extensive research demonstrated the factors contributing to errors in determining the indicated mean effective pressure. Brown states that phasing of the top dead center and absolute pressure referencing are the dominant sources of error in imep evaluation. Other sources of errors in engine testing are addressed in detail and include errors associated with pressure transducer mounting, sensitivity, hysteresis and vibration. Lancaster et al. (1975) performed a detailed comparison of piezoelectric pressure transducers when the device was relatively new to the engineering community. Though the pressure transducer has evolved considerably since the study was performed, Lancaster et al. provided a comprehensive, preliminary insight on the errors associated with cylinder pressure measurement using the piezoelectric transducer – errors that researchers are still trying to minimize today. The errors included, but were not limited to, thermal effects upon the transducer's diaphragm, discontinuities caused by physical dynamics when mounting the transducer within the cylinder, and appropriately referencing the data collected since the piezoelectric pressure transducer is a differential measuring device.

A detailed study of cylinder pressure data and its usage in engine testing was published by Amann (1985). The article discussed methodology of acquiring pressure data, calculating heat release schedules, mass-burned estimates, cyclic variability and spark timing as well as briefly discussing the effects of abnormal combustion. Though the

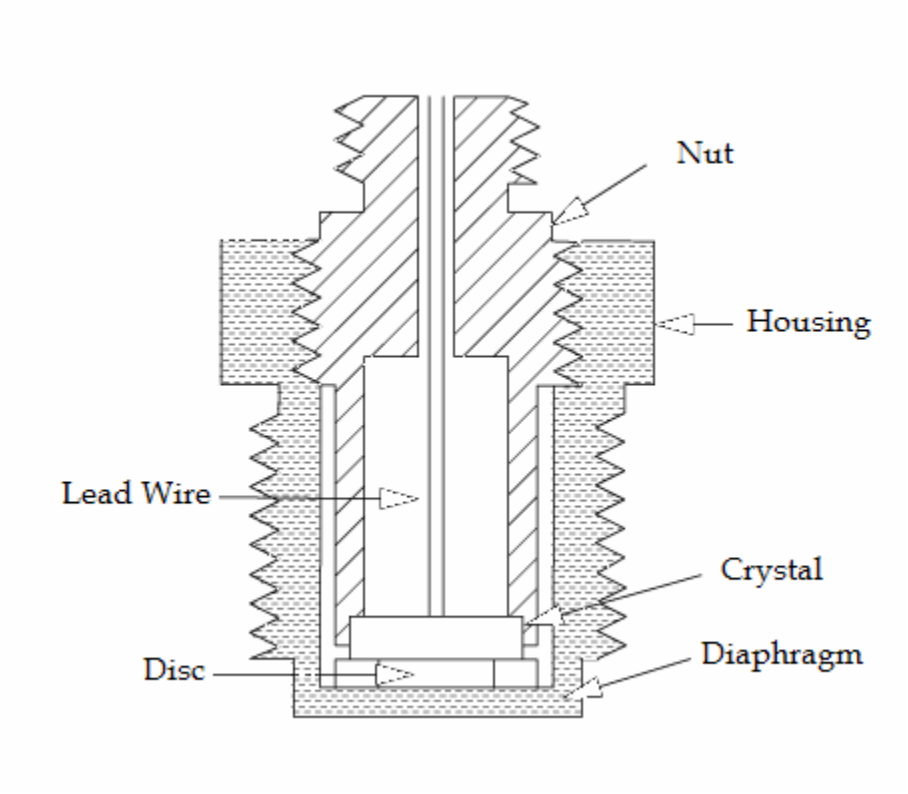

Figure 2.1 Schematic of a Piezoelectric Pressure Transducer [Freeman et al., 2008]

author provided little data of his own, the article was an excellent review of previous studies and methodology in engine testing.

A drawback to the piezoelectric pressure transducer is its sensitivity to temperature. This is particularly significant in engine testing due to the high temperature combustion environment within the engine cylinders. The effect of temperature on the piezoelectric pressure transducer is known as thermal shock; a phenomena which can result in excessive drift in the output signal over time. Position of the piezoelectric pressure transducer within the cylinder (referred to as mounting techniques) can alleviate the effects of thermal shock. Randolph (1990b) addressed mounting techniques for the piezoelectric pressure transducer within the cylinder. The study observed the effects of three different mounting techniques and presented the advantages and disadvantages of each. The mounting techniques included flush mounting, single passage mounting, and multiple passage mounting. It was concluded that at standard operating conditions the multiple-slot design was most appropriate as it reduced errors caused by thermal shock and cyclic variability.

2.2 Pressure Referencing

The pressure reading from the piezoelectric pressure transducer is a differential reading and thereby requires a reference pressure before the readings can be of any use in engine testing. Nine different methods of cylinder pressure referencing were evaluated by Randolph (1990a). The methods included three of the more commonly accepted means of pressure referencing which are intake manifold referencing, polytropic index referencing and intra-cycle pressure referencing by means of a second transducer. Randolph

demonstrated the advantages and disadvantages of each method and concluded that thermal shock and cyclic variability are the primary factors influencing error within cylinder pressure measurement. It was noted that these sources of error could be minimized by careful discretion when selecting a pressure transducer and choosing the intake manifold as the location for referencing the inlet bottom dead center pressure.

Further study was conducted on two of the nine referencing methods Randolph listed (Brunt & Pond 1997). Brunt et al. evaluated cylinder pressure referencing by means of inlet manifold pressure referencing (IMPR) and polytropic index pressure referencing (PIPR). They concluded that though both methods produced similar results the IMPR method is better suited for low engine speeds due to its susceptibility to thermal shock and linearity errors while the PIPR method should be implemented for combustion analysis. The authors noted that the PIPR is affected by signal noise and has tendency to produce high cyclic variability and that these errors should be given considerable care when evaluating the rate of heat release.

2.3 Crank Angle Resolution

Brunt and Lucas (1991) discuss the effects of crank angle resolution on cylinder pressure analysis. The authors discussed the advantages of using optical encoders that have a high crank angle resolution. The primary advantage of using high resolution is that the hardware is able to "better" detect pressure variations during combustion as the accuracy in determining the piston location is increased. In addition, the pressure data can be more accurately phased with higher resolution optical encoders. Nevertheless, there are some disadvantages associated with high resolution optical encoders presented by the

authors. The disadvantages include: lower engine speeds required for testing, fewer combustion cycles are obtained, noise sensitivity is increased and computer hardware demands increase. The authors concluded that due to noise sensitivity errors, optical encoders with a resolution between 0.5 degrees and 1.0 degrees are adequate for compression ignition engines while a 1.0 degree resolution is suitable for compression ignition systems. In regards to the effect crank angle resolution has on the indicated mean effective pressure calculation, Brunt and Lucas (1991) write, "…relatively coarse CA [crank angle] resolution could be used without incurring significant errors".

Typically the determination of TDC is accomplished by plotting the logarithmic pressure versus the logarithmic volume for the motoring pressure data; the pressure within the cylinder without combustion occurring. However, Hribernik (1998) proposed a statistical method in determining the TDC. He claims his method allows for accuracy within 0.025 degrees. Hribernik recommends that TDC be determined within 0.1 degrees to avoid significant errors when evaluating the indicated mean effective pressure and that the statistical method be implemented as it is more accurate than the traditional method. Lapuerta et al. (2000) in their sensitivity analysis of the rate of heat release agree with Hribernik that TDC phasing errors propagate significantly into the indicated mean effective pressure calculations via estimations in the rate of heat release.

2.4 Heat Release Analysis

Karim (1968) performed an analysis of the rate of heat release in pilot injected natural gas combustion. Using a zero-dimensional single zone model, the study concluded that the effective heat release rates proceeded in two stages – combustion of

the pilot spray and surrounding gases followed by the combustion of the remaining bulk gaseous fuel. Further study using the cylinder pressure data to calculate the mass fraction burn and rate of heat release was performed by Hayes and Savage (1986). The study focused on comparing the Krieger and Borman heat release model (1967) to a simple thermodynamics-based heat release model. The results comparing the rate of heat release and the mass fraction burned were presented and the authors concluded that the simple heat release model "qualitatively agreed" with the Krieger and Borman method. This conclusion was advantageous to the engines research community as the simple heat release model has fewer variables to take into account than the more complex Krieger and Borman model.

2.5 IMEP Calculations

The indicated mean effective pressure – the net work per unit of displaced volume (Ferguson & Kirkpatrick, 2001) – or imep is a useful quantity in comparing two engines using the same fuel and is used extensively in engine research and development. Brunt and Emtage (1996) point out that there are two primary concerns when determining the imep from acquired pressure data; the pressure data itself with respect to crank angle and the "…integration of cylinder pressure and cylinder volume" (Brunt & Emtage, 1996). To address these concerns, the authors reviewed the effects of alternative imep equations and the physical impact of hardware devices such as the optical encoder resolution, noise and duration of combustion. At coarse crank angle resolutions ($\theta > 0.5$ deg), the authors note that significant differences occurred between the evaluation methods of the imep, but that at fine resolutions these differences were negligible. The most prominent sources of error

within the imep calculation were due to thermal shock (2%) and crank angle phasing (1.2 bar at 2% error).

Despite the fact that many studies have been preformed on in-cylinder pressure data acquisition, crank angle resolution, imep, and rate of heat release, few, if any, provide a quantitative explanation of the errors associated with these parameters. Without fully understanding the effect of error propagation the terms used by the authors such as “better”, “adequate” and/or “good” have little meaning in describing the accuracy of their results. Uncertainty analysis appropriately defines the quality of experimental results by means of confidence intervals, thereby providing statistical merit when comparing the effects of alternative test methods.

CHAPTER 3

METHODOLOGY

The focus of this study is to apply detailed uncertainty analysis to cylinder pressure data acquired in a single-cylinder direct-injection pilot-ignited natural gas compression ignition engine at various injection timings (15° BTDC - 60° BTDC). The pressure data was provided by Srinivasan et al. (2004, 2006a, 2006b). The in-cylinder pressure data was used to calculate the rate of heat release (ROHR), indicated work (IW) and indicated mean effective pressure (IMEP). The goal of the detailed uncertainty analysis is to obtain quantitative assessments of the effect of uncertainties in cylinder pressure data on ROHR, IW and IMEP. The raw in-cylinder pressure data file contained the motoring (without combustion) pressure data for 50 cycles of the engine and 150 cycles of firing data for the range of injection timings investigated. Each cycle contained 1440 recorded measurements. These 1440 points obtained from a 0.5 degree resolution optical encoder correspond to 720 degrees of shaft revolution or one full combustion cycle.

3.1 Pressure Data

Since the measured pressure values are differential values, a reference pressure is needed to obtain the absolute cylinder pressure. As discussed in detailed by Randolph

(1990a), setting the pressure at BDC equal to the average absolute intake manifold pressure is deemed acceptable by the engine testing community. The remaining pressures within the data set are then appropriately scaled to the reference pressure hence becoming absolute measurements of in-cylinder pressure. It is important to note that pressure referencing adds to the errors associated with in-cylinder pressure measurement as there are inherent uncertainties in all calibration devices. However, these uncertainties are addressed later and prove to be negligible when compared to the other uncertainties within engine testing.

It is useful to average the pressure data over multiple cycles of the combustion process to reduce the effects of noise and cyclic variations such that the average pressure curve is more representative of the engine at a given operating condition. The reduction in noise and cyclic variability in the pressure data facilitates more accurate computations of the indicated mean effective pressure, rate of heat release, in-cylinder temperature and mass fraction burn. Lancaster et al. (1975) studied the effects of cycle-to-cycle variations on cylinder pressure data and proposed that at least 300 cycles are needed to ensure the accuracy of the average pressure curve. However, as noted by Brunt and Emtage (1996), limitations within data acquisition systems forces experimenters to use less than 300 cycles. For this study 150 cycles of the firing pressure data and 50 cycles of the motoring pressure data were used. A simple numerical average was used to obtain these averages and the equation used is given as

$$P_{avg} = \sum_{x=0}^{\left(N_{cycle}-1\right)} \frac{P(i,x)}{N_{cycle}} \tag{3.1}$$

where P_{avg} is the average pressure across the cycles in bar and N_{cycle} is the number of cycles. Since the first entry of an array in MathCad™ is denoted by zero (rather than one) the last entry of the summation array needed to be inputted as N_{cycle} minus one.

A smoothing algorithm was applied twice to the averaged pressure data for both motoring and firing to further reduce noise within the pressure data. The algorithm applied was given by Stone (1999) as:

$$P_{smooth} = \frac{P_{avg_{k-1}} + 2 \cdot P_{avg_k} + P_{avg_{k+1}}}{4} \tag{3.2}$$

The in-cylinder volume as a function of crank angle was determined as

$$V(\theta) := V_c + \frac{\pi}{4} \cdot b^2 \cdot \left[l + a - \left[\left(l^2 - a^2 \sin(\theta)^2 \right)^{.5} + a \cdot \cos(\theta) \right] \right] \tag{3.3}$$

where V_c is the clearance volume in cubic meters, b is the bore in meters, l is the connecting rod length in meters and a is the crank radius in meters. The values for the geometric attributes of the engine (bore, stroke length, crank radius, etc.) were predetermined and given by Srinivasan (2006a & 2006b).

3.2 Phasing of the Pressure Data

Before the averaged firing pressure data can be analyzed, one must first address the phasing of the pressure-crank angle curve. The accuracy of the phasing process depends upon the accuracy with which the TDC is determined in the engine by the

optical encoder. If the optical encoder was not correctly aligned with the engine TDC then the measured pressures would be out of synchronization with the crank angle at which they actually occurred. It is important to note that absolute determination of the engine TDC is nigh impossible. However, a relatively accurate means of ensuring the pressure data is phased correctly with crank angle is done by plotting the logarithmic values of the motoring pressure versus the logarithmic values of the in-cylinder volume (Heywood, 1988). If cross over is apparent then the pressure data is out of phase. An example of cross over in inappropriately phased pressure data is given in Figure 3.1 followed by correctly phased pressure data shown in Figure 3.2.

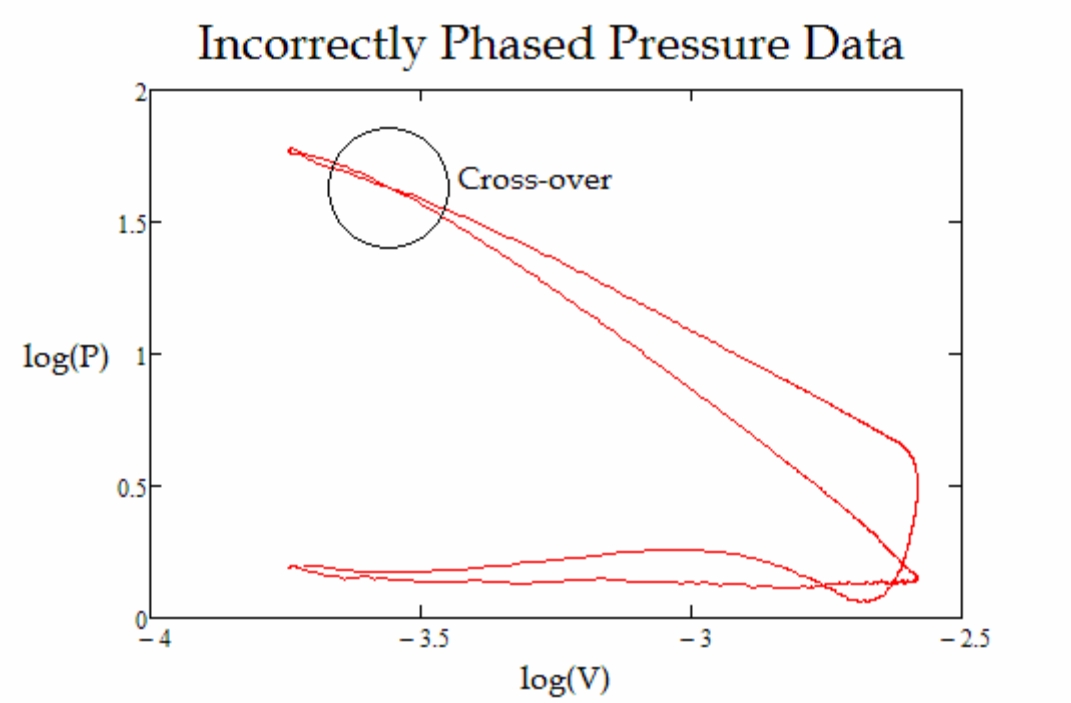

Figure 3.1 Incorrectly phased pressure data with the presence of cross over

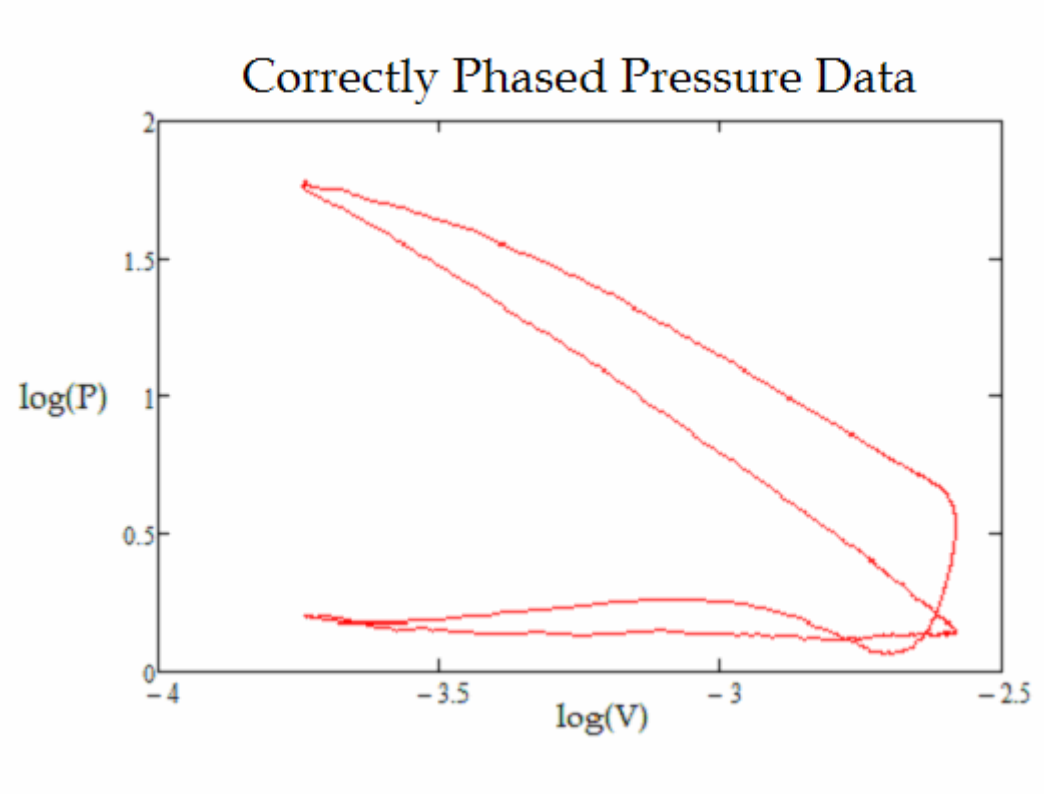

Figure 3.2 Correctly phased pressure versus volume log chart

Cross-over is remedied by adjusting the corresponding crank angle for the motoring pressure data point by a value C_1 multiplied by the crank angle resolution of 0.5 crank angle degrees (denoted as theta). The constant C_1, whose value could be any integer, was found to be equal to zero. It is important to note that severely retarding the engine, values of C_1 less than zero, will exhibit cross over effects in the log P versus log V curve. The opposite effect occurs with excessive advancement, values of C_1 greater than zero, and the compression and expansion lines bulge outward. Hence engineering sense must be implied when phasing the pressure data in this manner.

3.3 Combustion Modeling

The combustion process of internal combustion engines is a complex process involving the transfer of energy from a chemical state (unburned fuel), to a thermal state (combustion) and finally to a kinetic state by means of shaft work. As with most engineering models, assumptions are needed to simplify the original complex phenomena into a more manageable form that still maintains the integrity of the actual physical process. Since the unknown quantities outnumber the mathematical equations derived from the conservation equations (equations of mass, energy and momentum conservation which ultimately govern the combustion process), combustion models have been developed to alleviate these limitations. Heywood (1988, p. 749) divided the various engine combustion models available into three categories that progress in difficulty as one moves down the list. The classifications are as follows:

1. Zero dimensional
2. Quasi-dimensional
3. Multi-dimensional

3.3.1 Zero Dimensional Modeling

Zero dimensional models are the most basic of the three categories. They simplify the combustion process into a thermodynamic system solely dependent upon energy and/or mass interaction at the system boundary. The zero dimensional models can be further divided into single, two and multi zone models. A zero order single zone combustion model simplifies the mass within the cylinder homogeneous throughout the entire combustion process. A zero order two zone model separates the mass into an unburned zone and burned zone. Finally a zero order multi zone model attempts to distinguish multiple thermodynamic systems within the cylinder consisting of unburned, burned and mixtures of both unburned and burned zones. Though the zero dimensional models are the simplest in design, they are widely used throughout the engine testing community because of their practicality and relative accuracy in portraying the combustion process.

3.3.2 Quasi and Multi-Dimensional Modeling

The quasi-dimensional models expand upon the thermodynamic analysis of the zero dimensional models, but include the specific geometric features of a given engine. These features include but are not limited to the spark-ignition engine flame or the spray

pattern of diesel fuel into the cylinder (Heywood, 1988, p. 749). Multi-dimensional models, perhaps the most inclusive models to date, incorporate the effects of fluid dynamics in conjunction with the geometric features and thermodynamics that impact combustion. Due to the increase in complexity of the models, quasi-dimensional and multi-dimensional models require more hardware demands and man-hours to accurately record the inclusion of such variables. Though such models provide greater accuracy in describing the combustion process, the increase in hardware demands hinders their information to cost ratio; thereby rendering them impractical for day-to-day engine analysis.

For this work a zero dimensional single zone model was implemented in determining the average rate of heat release, work, and imep. The working fluid within the cylinder during combustion can be represented as a single thermodynamic system. The assumptions used in the model were as follows:

- Pressure is spatially uniform at any given crank angle
- Mass within the cylinder is constant
- Combustion is viewed as a series of equilibrium states
- Pressure taken at the intake manifold is equal to in-cylinder BDC
- All gases are ideal gases

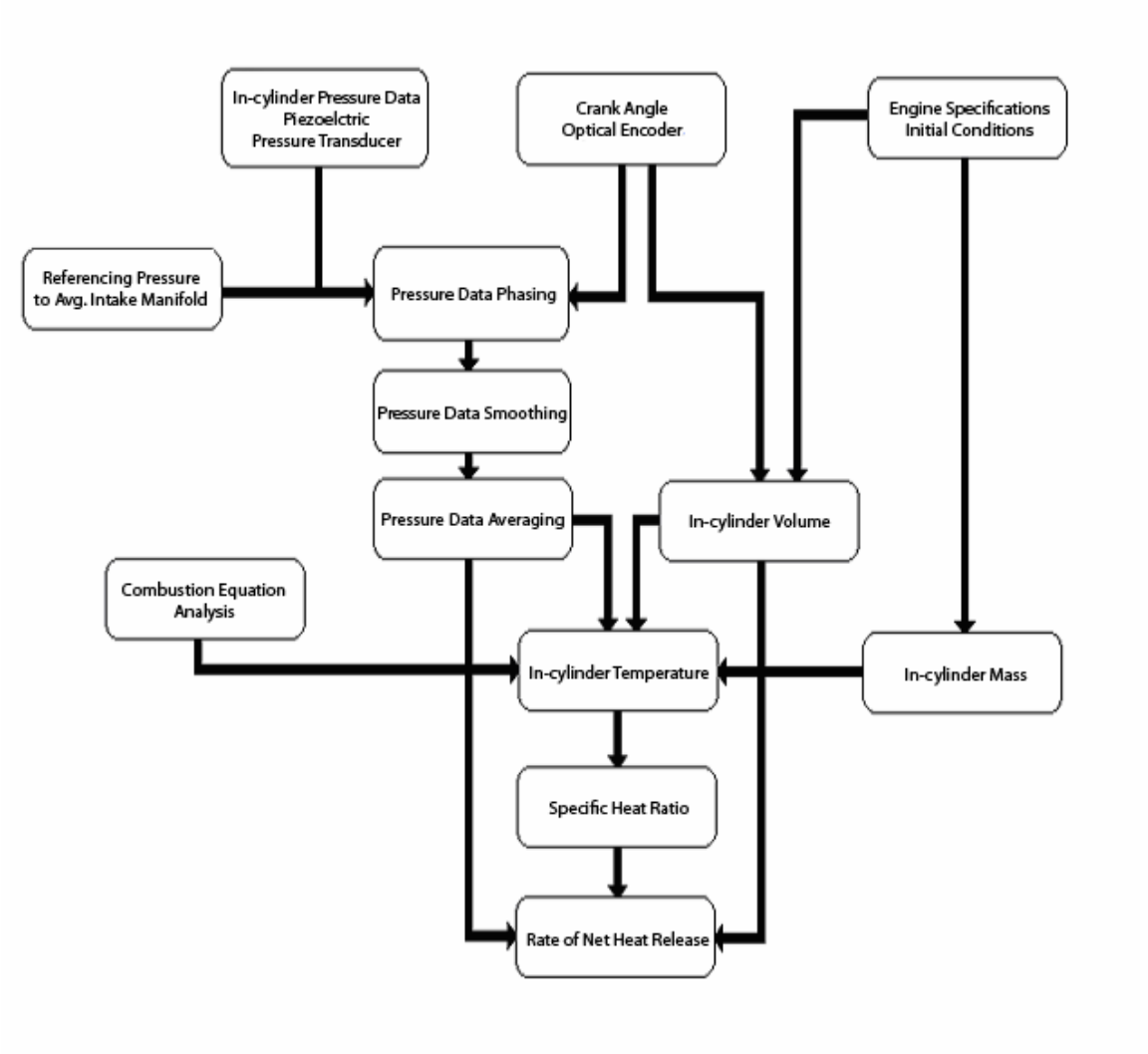

Figure 3.3 Flow Chart for Heat Release Analysis

3.4 Net Heat Release Model

The first law of thermodynamics states that the internal energy of combustion is equal to the heat released through the chemical process of combustion minus the heat transferred by convection across the walls of the cylinder and the work done on the piston. This equation can be written as

$$\frac{d}{d\theta}U = \frac{d}{d\theta}Q_{chemical} - \frac{d}{d\theta}Q_{convection} - \frac{d}{d\theta}W \tag{3.4}$$

where U is the internal energy within the cylinder, $Q_{chemical}$ is the heat produced by combustion, $Q_{convection}$ is the heat transferred across the cylinder walls by convection, W is the work transmitted to the drive shaft and θ is the crank angle measured in degrees. Since the net heat released (the difference between the heat of combustion and the heat by convection) is of interest we can group $Q_{chemical}$ and $Q_{convection}$, using the substitution variable of Q_{net} instead. This equation is given as

$$\frac{d}{d\theta}Q_{net} = \frac{d}{d\theta}U + \frac{d}{d\theta}W \tag{3.5}$$

The internal energy within the combustion chamber can be defined as

$$\frac{d}{d\theta}U = m \cdot C_v \cdot \left(\frac{d}{d\theta}T\right) \tag{3.6}$$

where m is the mass of the fuel air mixture, Cv is the specific heat of the fuel at constant volume and T is the temperature within the cylinder. The work done by the piston during combustion is written as

$$\frac{d}{d\theta}W = P\cdot\left(\frac{d}{d\theta}V\right) \tag{3.7}$$

where P is the instantaneous pressure within the cylinder and $dV/d\theta$ is the first derivative of in-cylinder volume with respect to crank angle. Substituting Equations (3.6) and (3.7) in Equation (3.5) yields

$$\frac{d}{d\theta}Q_{net} = m\cdot C_V\cdot\left(\frac{d}{d\theta}T\right) + P\cdot\left(\frac{d}{d\theta}V\right) \tag{3.8}$$

In the engine testing procedure, the only measured variables will be the crank angle (θ) and the pressure (P). Therefore, manipulating the equation for the net heat release rate so that it is solely a function of crank angle and pressure is necessary. Taking the first derivative of Equation (3.3) gives $dV/d\theta$ as

$$\frac{d}{d\theta}V = \frac{\pi\cdot bore^2}{4}\cdot\left[\frac{a^2\cdot\sin(\theta)\cdot\cos(\theta)}{\left(l^2 - a^2\cdot\sin(\theta)^2\right)^{.5}} + a\cdot\sin(\theta)\right] \tag{3.9}$$

The derivative of temperature with respect to crank angle can be determined by assuming the working fluid during combustion behaves similar to an ideal gas. With this assumption, temperature can be written as

$$T(\theta) = \frac{P\cdot V(\theta)}{m_{fuel}\cdot R_{reactants}} \tag{3.10}$$

and the derivative of temperature with respect to crank angle expressed as

$$\frac{d}{d\theta}T(\theta) = \frac{P\cdot\left(\frac{d}{d\theta}V(\theta)\right) + V(\theta)\cdot\left(\frac{d}{d\theta}P\right)}{m_{fuel}\cdot R_{reactants}} \tag{3.11}$$

The derivative of pressure with respect to crank angle ($dP/d\theta$) was determined by using the algorithm provided by Stone (1999, p. 544) given as

$$\frac{d}{d\theta}P = \frac{P_j - 8P_{j+1} + 8\cdot P_{j+3} - P_{j+4}}{12\cdot\Delta\theta} \tag{3.12}$$

Substituting Equations (3.10), (3.11) and (3.12) into Equation (3.8), the net heat release of the system can be written as

$$\frac{d}{d\theta}Q_{net} = \frac{P\cdot\pi\cdot bore^2}{4}\cdot\left[\frac{a^2\cdot\sin(\theta)\cdot\cos(\theta)}{\left(l^2 - a^2\cdot\sin(\theta)^2\right)^{.5}} + a\cdot\sin(\theta)\right]\cdot\frac{\gamma}{\gamma - 1} \ldots$$
$$+\left[V_c + \frac{\pi}{4}\cdot bore^2\cdot\left[l + a - \left[\left(l^2 - a^2\cdot\sin(\theta)^2\right)^{.5}\right] + a\cdot\cos(\theta)\right]\right]\cdot\frac{1}{\gamma - 1}\cdot\left(\frac{P_j - 8P_{j+1} + 8\cdot P_{j+3} - P_{j+4}}{12\cdot\Delta\theta}\right) \tag{3.13}$$

where γ is the ratio of specific heat at constant pressure over specific heat at constant volume. In Equation (3.12), only the variables θ and P are measured variables from the optical encoder and the pressure transducer respectively. The variables *a*, *l*, and *bore* are geometric givens of the engine (generally specified by the manufacturer) and are assumed to be constants. Finally, for simplicity Equation (3.12) can be expressed in the more common form as

$$\frac{d}{d\theta}Q_{net} = \frac{\gamma}{\gamma - 1}\cdot P\cdot\left(\frac{d}{d\theta}V\right) + \frac{1}{\gamma - 1}\cdot V\cdot\left(\frac{d}{d\theta}P\right) \tag{3.14}$$

3.5 Analysis of the Combustion Equation

The combustion of natural gas or methane can be represented as

$$CH_4 + \frac{As}{\Phi_{actual}}\cdot\left(O_2 + 3.76\cdot N_2\right) = n_1\cdot CO_2 + n_2\cdot H_2O + n_3\cdot N_2 + n_4\cdot O_2 \tag{3.15}$$

where *As* is the stoichiometric molar air-fuel ratio, Φ_{actual} is the actual equivalence ratio during combustion and *n* is the number of moles of the respective product. The equivalence ratio during combustion was determined by using

$$\Phi_{actual} := \left[\frac{Air_{dot} \cdot MW_{methane}}{Gas_{dot} \cdot As \cdot \left(2 \cdot MW_{oxygen} + 2 \cdot 3.76 \cdot MW_{nitrogen}\right)} \right]^{-1} \tag{3.16}$$

where Air_{dot} and Gas_{dot} are the respective flow rates determined by Srinivasan et al. (2004) and *MW* is the molecular weight of the respective molecule.

With the actual equivalence ratio determined, a carbon, hydrogen, nitrogen and oxygen balance was performed to determine the magnitude of each *n* in Equation (3.4). Once the number of moles for each product was determined the mass of each product molecule was determined in order to compute the gas constant of the product mixture. Determining the gas constant of the products was accomplished by the following steps:

1.) Determination of the total number of moles of the products.

$$N_{products} := n_1 + n_2 + n_3 + n_4 \tag{3.17}$$

2.) Determination of the mass of each product molecule.

$$m_{CO2} = n_1 \cdot MW_{carbondioxide} \tag{3.18}$$

$$m_{H2O} = n_2 \cdot MW_{water} \tag{3.19}$$

$$m_{N2} = n_3 \cdot MW_{nitrogen} \tag{3.20}$$

$$m_{O2} = n_4 \cdot MW_{oxygen} \tag{3.21}$$

3.) Determination of the molar weight of the products.

$$m_{products} = m_{CO2} + m_{H2O} + m_{N2} + m_{O2} \tag{3.22}$$

$$M_{products} = m_{products} \cdot \left(N_{products} \right)^{-1} \tag{3.23}$$

4.) Determination of the gas constant of the products.

$$R_{products} = R_{universal} \left(M_{products} \right)^{-1} \tag{3.24}$$

3.6 Evaluation of In-Cylinder Temperature

In this study the authors evaluated the effects of using a temperature dependent specific heat ratio [$\gamma(T)$] in comparison to a constant specific heat ratio (γ_{air}); which is normally equal to the specific heat ratio of air. In effort to compute a temperature dependent specific heat ratio, the temperature profile for the pressure data was needed. The temperature at a given crank angle and pressure was determined by using the ideal gas law, given as

$$T(\theta) = \frac{P \cdot V(\theta)}{m_{fuel} \cdot R_{reactants}} \tag{3.25}$$

where P is the in-cylinder pressure, $V(\theta)$ is the in-cylinder volume, m_{fuel} is the mass of the fuel and $R_{reactants}$ is the gas constant for the reaction between methane and air. The gas constant for the reactants is given as

$$R_{reactants} = \frac{R_{methane} + \frac{AF_{stoichiometric}}{\Phi_{actual}} \cdot R_{air}}{1 + \frac{AF_{stoichiometric}}{\Phi_{actual}}} \tag{3.26}$$

where $R_{methane}$ and R_{air} are the gas constants of methane and air given by Ferguson and Kirkpatrick (2001, p. 355). The stoichiometric air to fuel ratio is represented by $AF_{stoichiometric}$. With the gas constant of the reactants determined, the mass of the fuel air mixture was evaluated by

$$m_{fuel} = \frac{P_{IVC} V_{IVC}}{R_{reactants} \cdot T_{IVC}} \tag{3.27}$$

where the subscript *IVC* indicates the pressure, volume and temperature at inlet valve closure. The pressure at inlet valve closure was determined by Srinivasan et al. (2004). The in-cylinder volume was determined by using Equation (3.3) with the respective crank angle at which P_{IVC} occurred. The temperature at inlet valve closure was evaluated using the polytropic process, given as

$$T_{IVC} = T_o \cdot \left(\frac{V_o}{V_{IVC}} \right)^{n-1} \tag{3.28}$$

where the subscript *naught* indicates the temperature and volume at the inlet manifold and *n* is the polytropic index of 1.35 for methane combustion.

3.7 Specific Heat Ratio

Quite often in engine research, the specific heat ratio is approximated as a linear function of temperature to reduce model complexity. The simplest assumption is that gamma – the specific heat ratio – is constant value throughout the cycle (Depcik et al., 2007). It has been suggested, that the most accurate determinations of the specific heat occur when the model incorporates detailed temperature dependent correlations for each species in the combustion mixture (Depcik, 2000; Depcik et al., 2007) since the ROHR is largely determined by changes within the internal energy of the combustion mixture. In order to determine the specific heat ratio of the combustion species, the specific heat at constant pressure was needed for each component of the products. The equations for the specific heats at constant pressure as a function of temperature were given by Turns

(2000, p. 646). The specific heat at constant pressure of the products as a mixture is given as

$$Cp_{products} = mf_{CO2} \cdot Cp_{CO2} + mf_{H2O} \cdot Cp_{H2O} + mf_{N2} \cdot Cp_{N2} + mf_{O2} \cdot Cp_{O2} \quad (3.29)$$

where *mf* is the mass fraction of each molecule and *Cp* is the specific heat at constant pressure for each molecule. The mass fraction of a single product is simply the mass of the product divided by the total mass of the products. The specific heat at constant volume is given as

$$Cv_{products} = Cp_{products} - R_{products} \quad (3.30)$$

With both specific heats (constant pressure and volume) as a function of temperature, the specific heat ratio [$\gamma(T)$] can now be determined by evaluating the fraction given by

$$\gamma = \frac{Cp_{products}}{Cv_{products}} \quad (3.31)$$

Equation (3.14) can now be solved as a function of in-cylinder pressure and crank angle.

3.8 Determination of Work and IMEP

The work done upon the piston at each step in crank angle can be represented as the pressure at that crank angle multiplied by the change in volume per crank angle step. The indicated work transmitted to the piston due to combustion, neglecting all frictional losses, can be represented as

$$W = \int P \cdot \left(\frac{d}{d\theta} V(\theta) \right) d\theta \quad (3.32)$$

The imep of the engine as given by Ferguson and Kirkpatrick (2001, p. 86) is the indicated work over the displaced volume of the piston and is written as

$$IMEP = \frac{W}{V_d} \tag{3.33}$$

3.9 Uncertainty Analysis

Literature in the field of engine testing has failed to accurately address the uncertainty associated with the net heat release rate. This failure is primarily due to the authors' attempt to compare two or more models for the evaluation of the ROHR. Though sensitivity analysis – the approach most often used by previous literature – is useful in comparing two models it does not describe the inherent error within the models due to their assumptions. Uncertainty analysis provides researchers with the numerical tools to quantify the errors associated with each model thereby yielding useful interpretations of the results. It is the focus of this study to implement uncertainty analysis to compare four different approaches to evaluating the ROHR. The first of these models will use the correlations provided by Turns (2000) to determine the specific heat ratios of each species in the combustion product. The second model assumes that the specific heat ratio throughout the combustion cycle is constant and equal to the specific heat ratio of air. The last two models use the correlations for the specific heat ratio of the combustion mixture proposed by Brunt in 1998 and then modified in 1999. It is important to note here that this study only examines the uncertainty in the net heat release rate. Because the gross heat release rate involves estimating the heat transfer across the cylinder walls, – a process which involves empirically derived correlations – it makes sense to estimate the coupled effect of the chemical and heat transfer effects by estimating the net heat release rate.

The uncertainty associated within any determined experimental results, *r*, can be written as (Coleman & Steele, 1999, p. 49)

$$U_r^2 = \left(\frac{d}{dX_1} r\right)^2 \cdot U_{X1}^2 + \left(\frac{d}{dX_2} r\right)^2 \cdot U_{X2}^2 .. \left(\frac{d}{dX_n} r\right)^2 \cdot U_{Xn}^2 \tag{3.34}$$

where Ux_i are the uncertainties in the measure variables X_i. Hence, from Equation (3.34), the uncertainty equation of the net heat release rate [Equation (3.14)] can be written as

$$\begin{aligned} U_{dQnet}^2 = &\left(\frac{d}{d\gamma} dQ_{net}\right)^2 \cdot U_\gamma^2 + \left(\frac{d}{dP} dQ_{net}\right)^2 \cdot U_P^2 \ldots \\ &+ \left(\frac{d}{ddV} dQ_{net}\right)^2 \cdot U_{dV}^2 + \left(\frac{d}{ddP} dQ_{net}\right)^2 \cdot U_{dP}^2 \ldots \\ &+ \left(\frac{d}{dV} dQ_{net}\right)^2 \cdot U_V^2 \end{aligned} \tag{3.35}$$

The uncertainty equations for the indicated work and imep are written as

$$UW^2 = \left(\frac{d}{dP} W\right)^2 \cdot U_P^2 + \left(\frac{d}{ddV} W\right)^2 \cdot U_{dV}^2 \tag{3.36}$$

$$U_{IMEP}^2 = \left(\frac{d}{dW} IMEP\right)^2 \cdot U_W^2 + \left(\frac{d}{dV_d} IMEP\right)^2 \cdot U_{Vd}^2 \tag{3.37}$$

If all the uncertainty values for pressure, volume, their respective derivatives and the specific heat ratio were known then solving for the uncertainties in the net heat release rate, indicated work, and imep estimates would be relatively straight forward. However, since the only measured variables are in-cylinder pressure and crank angle, the expressions for volume, in-cylinder mass, temperature and specific heat ratio must be expressed in terms of crank angle and pressure.

As with all measurement devices there is a degree in which the experimenter is uncertain of the accuracy of the device. Coleman and Steele (1999) name this inherent uncertainty as bias or systematic uncertainty. The bias uncertainty is typically given by the manufacturer of the measuring device as some percentage of the device full scale value. The other uncertainty associated with measurement device is the precision error or random uncertainty; the ability of the device to record the same measurement at the same conditions over time. The precision error is calculated by determining the precision limit such that the probability of the sample mean plus or minus the precision limit is 0.95. The precision limit is determined by assuming the sample population comes from a Gaussian parent population such that a t-distribution is implemented at the 0.05 significance level. The equation for the precision limit is expressed as

$$P_X = \frac{t \cdot S_X}{\sqrt{N}} \tag{3.38}$$

where P_x is the random uncertainty, S_x is the sample standard deviation, N is the number of observations in the sample and t is the t-value at the 0.05 significance level for N-1 degrees of freedom.

3.10 Uncertainty Calculations

To determine the uncertainties within the net heat release rate, indicated work and imep the systematic and random errors associated within the measure variables were needed. The systematic and random error estimates were obtained from the device's respective manufacturer and are given in Table 3.1.

Table 3.1 Systematic and Random Errors

Source	Systematic Error	Random Error
Optical Encoder (θ)	0.5 c.a. degrees	0.1 c.a. degrees
Piezoelectric Pressure Transducer (P)	.4% of the FSV	**
Intake Manifold Temperature (T_o)	1% of the FSV	1 Kelvin
Intake Manifold Pressure (P_o)	1% of the FSV	.01 bar
** The random error of the pressure data is determined for each injection timing.		

The total uncertainty in each of the variables listed in Table 3.1 can be determined using the expression given as (Coleman & Steele, 1999, p. 42)

$$U_i = (B_i^2 + P_i^2)^{1/2} \tag{3.39}$$

where B_i is the systematic error and P_i is the random error listed in Table 3.1. It is important to note that the geometric properties of the engine were not included in the uncertainty calculation. The bore, crank radius, stroke length and compression ratio were assumed to be constants thereby having no uncertainty associated with their given values.

The scope of this study was to determine the uncertainty associated within the net heat release rate, indicated work and imep. The analysis was done by computing the net heat release rates for different injection timings by using the pressure data provided by

Srinivasan et al. (2004). Two analyses of the injection timings were performed for both a temperature dependent specific heat ratio and a constant specific heat ratio. The constant specific heat ratio analysis was conducted under the assumption that air would be the only working fluid within the system. The uncertainties within the net heat release rates, indicated work and imep were calculated by implementing a detailed uncertainty analysis on the system. The systematic and random uncertainties for the optical encoder and piezoelectric pressure transducer were determined from manufacturer specifications (systematic) and statistical analyses (random). The uncertainty within the initial conditions for pressure and temperature were estimated as the data for these averaged values was not available.

CHAPTER 4

RESULTS AND DISCUSSION

4.1 Summary

In-cylinder pressure data for various injection timings of a single-cylinder direct-injection pilot-ignited natural gas compression ignition engine, obtained from Srinivasan et al. (2004, 2006a, & 2006b), was used by the author to construct a zero dimensional single zone model to evaluate the net heat release rate. Following the determination of the net heat release rate, indicated work, and imep, a detailed uncertainty analysis was conducted to determine the engine measurements that most significantly influence the uncertainty in combustion analysis. The results of these analyses are discussed in this chapter.

A detailed uncertainty analysis for each of the injection timings (15° BTDC - 60° BTDC with incremental steps of 5°) was performed to determine uncertainty in the net heat release rate, indicated work and imep in addition to the uncertainty percentage contributions (UPCs) and uncertainty magnification factors (UMFs) of the net heat release with respect to pressure, volume and specific heat ratio (gamma). Furthermore, a comparison of the uncertainty contribution at constant value gamma versus a temperature dependent gamma on the net heat release was performed on all injection timings. Finally, as presented in Depcik's and Jacobs' study (2007, p. 16) two correlations for a

temperature dependent gamma were compared against the specific heat at constant pressure correlation (Turns, 2000, p. 646) for only the 60° injection timing, as a representative case study.

4.2 Experimental Setup

The pressure data used in this analysis was obtained from a single-cylinder direct-injection pilot-ignited natural gas compression ignition engine at half load (Srinivasan et al., 2004, 2006a & 2006b). The geometric attributes of the engine are given in Table 4.1.

Table 4.1 Engine Properties

Single Cylinder Four Stroke Engine Specifications	
Bore	.1371 m
Stroke Length	.1651 m
Connecting Rod Length	.2612 m
Crank Radius	.0830 m
Compression Ratio	14.5

4.3 Initial Conditions

Table 4.2 lists the measured flow rates for air, natural gas (NG) and diesel. The engine speed for all injection timings was held constant at 1700 revolutions per minute. The initial temperature at the intake manifold was estimated to be 348 Kelvin. Lastly, the inlet manifold pressure was measure to be equal to 1.41 bars for all injection timings. As discussed in Chapter 3, the air flow rates were used by the author to determine the actual air to fuel ratio of the combustion mixture in addition to the equivalence ratio during combustion. The initial temperature and pressure conditions were implemented in the

equation for a polytropic process to determine the pressure and temperature at inlet valve closure.

Table 4.2 Initial Conditions

	Flow Rates and Initial Conditions					
Injection Timing	Air Flow	Diesel Flow	NG Flow	Eng. Spd.	To	Po
15 degrees BTDC	2860 g/min	3.3 g/min	82.2 g/min	1700 rev/min	348 K	1.41 bar
20 degrees BTDC	2880 g/min	3.3 g/min	77.8 g/min	1700 rev/min	348 K	1.41 bar
25 degrees BTDC	2880 g/min	3.3 g/min	75.0 g/min	1700 rev/min	348 K	1.41 bar
30 degrees BTDC	2910 g/min	3.3 g/min	73.5 g/min	1700 rev/min	348 K	1.41 bar
35 degrees BTDC	2900 g/min	3.3 g/min	71.8 g/min	1700 rev/min	348 K	1.41 bar
40 degrees BTDC	2910 g/min	3.3 g/min	69.8 g/min	1700 rev/min	348 K	1.41 bar
45 degrees BTDC	2930 g/min	3.3 g/min	68.5 g/min	1700 rev/min	348 K	1.41 bar
50 degrees BTDC	2940 g/min	3.3 g/min	68.8 g/min	1700 rev/min	348 K	1.41 bar
55 degrees BTDC	2880 g/min	3.3 g/min	69.5 g/min	1700 rev/min	348 K	1.41 bar
60 degrees BTDC	2850 g/min	3.3 g/min	72.2 g/min	1700 rev/min	348 K	1.41 bar

4.4 Determination of the Rate of Net Heat Release

The rate of net heat release during combustion was determined from using a zero dimensional single zone combustion model. The correctly phased pressure data, crank angle, air/fuel flow rates, initial conditions and molecular weights of the combustion reactants and products were used to determine the in-cylinder volume, mass fractions, temperature profile and the specific heat ratio of combustion. Finally, the pressure data, in-cylinder volume and specific heat ratio along with the appropriate first derivatives of pressure and volume were used to determine the rate of net heat release rate for a given injection timing by evaluating Equation (4.1). By integrating the values of Equation (4.1) over all crank angles the net heat release per cycle can be determined and is categorized in Table 4.3.

$$\frac{d}{d\theta}Q_{net} = \frac{\gamma}{\gamma - 1}\cdot P\cdot\left(\frac{d}{d\theta}V\right) + \frac{1}{\gamma - 1}\cdot V\cdot\left(\frac{d}{d\theta}P\right) \tag{4.1}$$

Table 4.3 Net Heat Release per Cycle Values at a Given Injection Timing

	Net Heat Release Per Cycle	
	Temperature Dependent Gamma	Constant Gamma
15 degrees BTDC	2.04 kJ	1.98 kJ
20 degrees BTDC	2.03 kJ	1.97 kJ
25 degrees BTDC	2.10 kJ	2.05 kJ
30 degrees BTDC	2.14 kJ	2.09 kJ
35 degrees BTDC	2.19 kJ	2.13 kJ
40 degrees BTDC	2.23 kJ	2.17 kJ
45 degrees BTDC	2.14 kJ	2.09 kJ
50 degrees BTDC	2.05 kJ	2.01 kJ
55 degrees BTDC	2.05 kJ	2.00 kJ
60 degrees BTDC	2.00 kJ	1.95 kJ
*Brunt 1998 Correlation	2.06 kJ	--
*Brunt 1999 Correlation	2.04 kJ	--

*Correlations were analyzed using 60 degree injection timing pressure data.

Figure 4.1 is a graphical portrayal of the rate of heat release rate as a function of crank angle for an injection timing of 60 degrees BTDC. The heat release, Q_{smooth}, is in units of joules per crank angle degree. The most noticeable trend within Figure 4.1 is the truncation of the ROHR that occurs when implementing the constant gamma assumption – as seen by the dashed line. The difference between the 1998 and 1999 Brunt correlations to the Turns 2000 correlations on the ROHR appears to be relatively small and may not seem significant in glancing, however an uncertainty analysis – discussed in the next section – reveals that uncertainty associated with the correlations differ significantly.

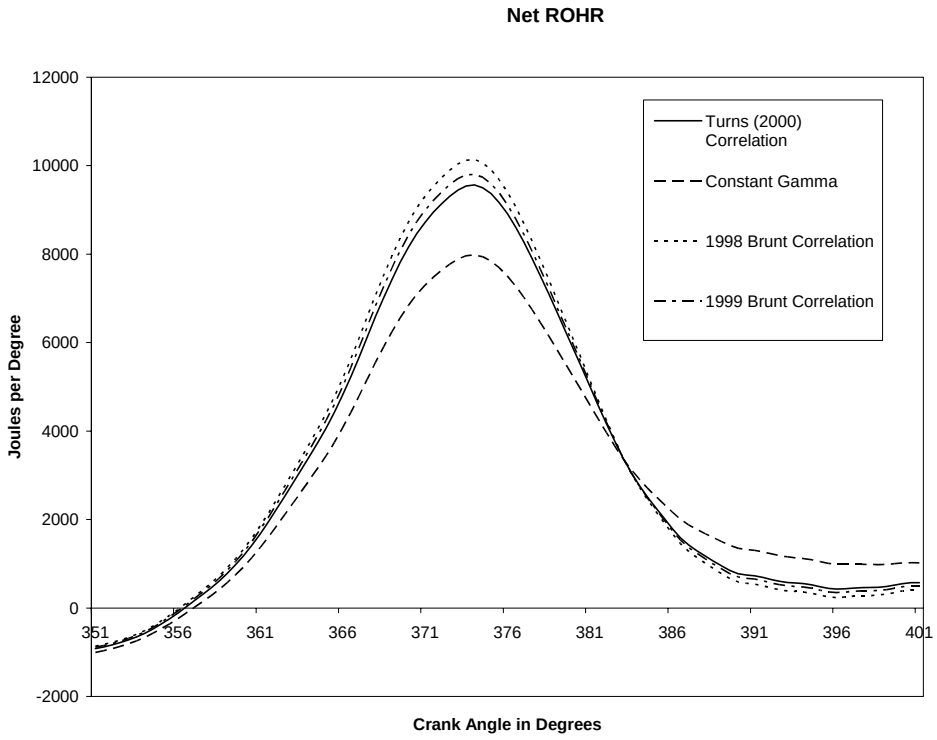

Figure 4.1 ROHR as a Function of Crank Angle with a 60 Degree BTDC Injection Timing

4.5 Uncertainty Analysis of the Net Heat Release

A detailed uncertainty analysis was conducted on the rate of net heat release. The initial systematic and random uncertainty estimates for the pressure transducer, initial temperature, initial pressure and optical encoder are given in Table 3.1. With the fundamental systematic and random errors estimated a detailed uncertainty analysis could be performed on the underlying elements (volume, air/fuel ratio, temperature etc.) within the net heat release. The detailed analysis of determining the uncertainty in the net heat release rate for both a temperature dependent and constant specific heat ratio can be

found in Appendix A. The value of uncertainty for the net heat release on a cycle by cycle basis was determined by integrating the uncertainty in the net heat release rate over all crank angles and is presented Table 4.4 and Figure 4.2. Only the 60 degree injection timing pressure data was used in the analysis of Brunt's 1998 and 1999 correlations.

Table 4.4 Values of Uncertainty for the Net Heat Release Rate

	Uncertainty in the Net Heat Release	
Injection Timing	Temperature Dependent Specific Heat Ratio	Constant Specific Heat Ratio
15 degrees BTDC	.464 kJ	.755 kJ
20 degrees BTDC	.466 kJ	.769 kJ
25 degrees BTDC	.491 kJ	.804 kJ
30 degrees BTDC	.516 kJ	.837 kJ
35 degrees BTDC	.534 kJ	.862 kJ
40 degrees BTDC	.554 kJ	.883 kJ
45 degrees BTDC	.565 kJ	.882 kJ
50 degrees BTDC	.527 kJ	.853 kJ
55 degrees BTDC	.531 kJ	.845 kJ
60 degrees BTDC	.525 kJ	.811 kJ
*Brunt 1998 Correlation	.668 kJ	--
*Brunt 1999 Correlation	.634 kJ	--

*Correlations were analyzed using 60 degree injection timing pressure data.

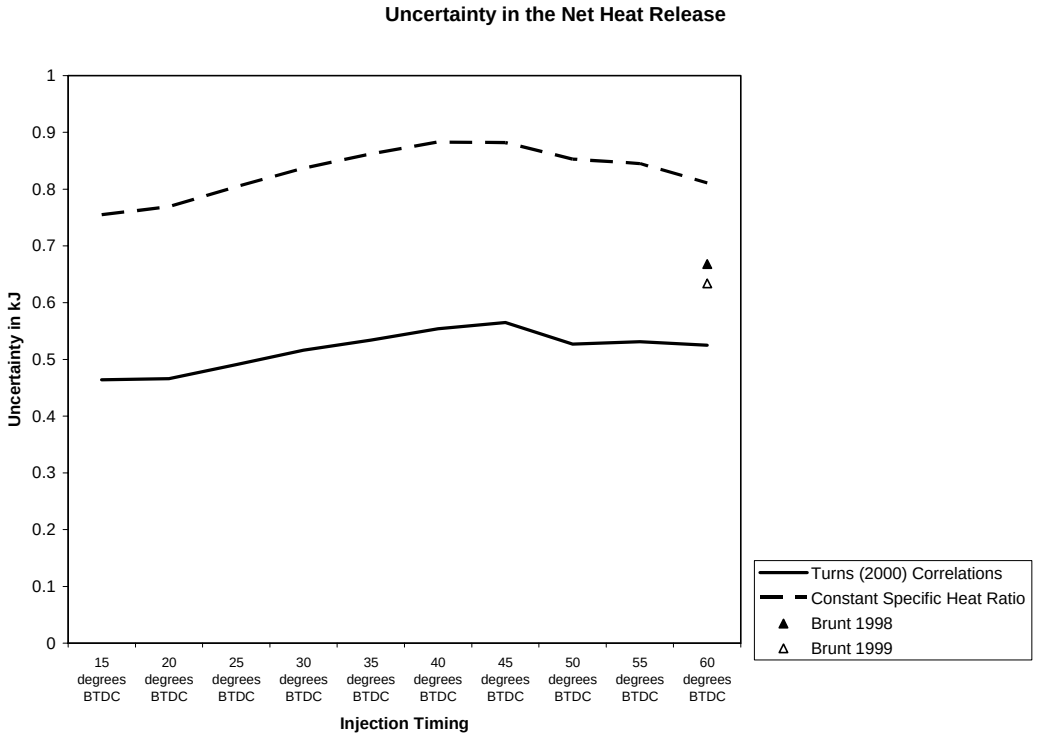

Figure 4.2 Plot of the Uncertainty in the Net Heat Release

The net heat release plus/minus its uncertainty at the respective crank angle for an injection timing of 60 degrees is portrayed in Figure 4.3. The area between the two dotted bands is the 95% confidence interval in which the true value of the rate of heat release lies. Plots of the net heat release with uncertainty bands for all injection timings can be found in Appendix B.

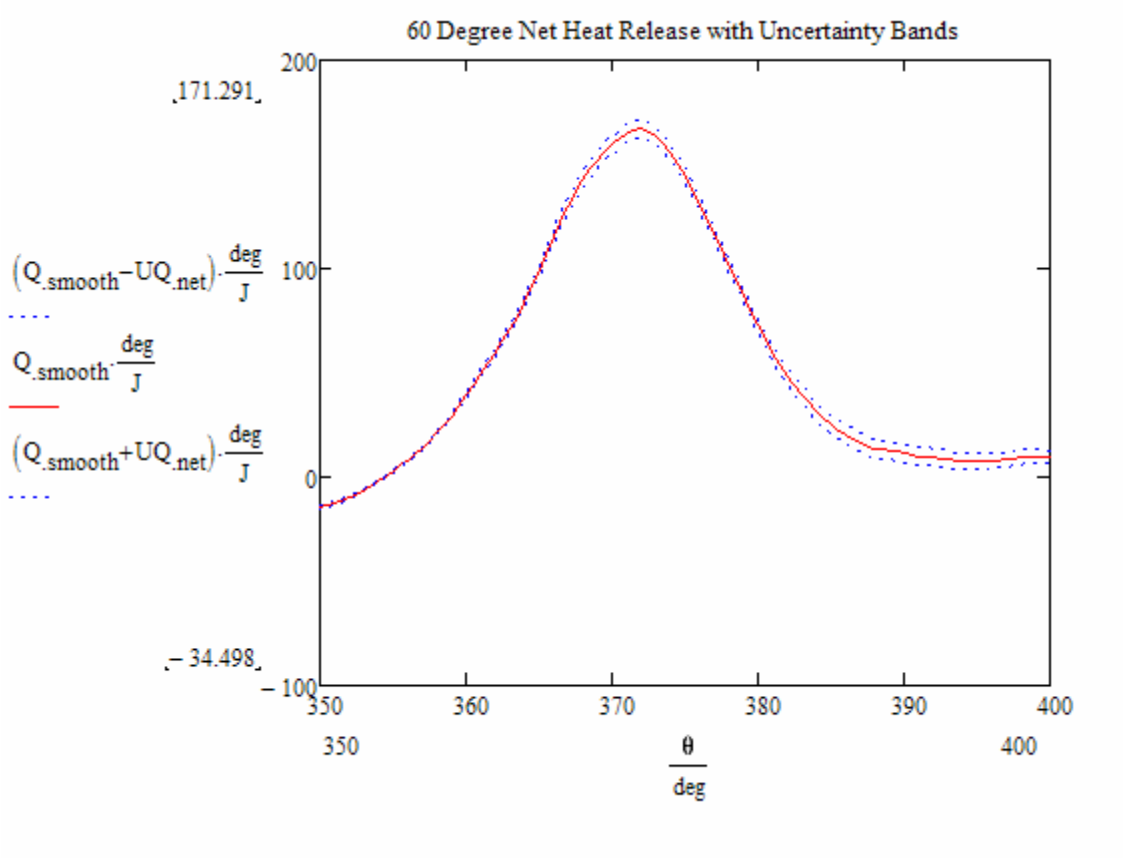

Figure 4.3 Net Heat Release Rate with Uncertainty Bands at a 60 Degree Injection Timing

4.6 Net Heat Release Discussion

The general trend in net heat release rates as a function of injection timing and a temperature dependent gamma is that of a parabolic distribution. Extremely early and late injection timings yield the smaller amount of heat release with the early injection timings being a bit more fruitful. The maximum net heat release from the tested injection timings was found to be 2.23 kJ per cycle corresponding to 40° injection timing. Similar trends were found in the constant gamma net heat release rates. However, assuming gamma to be constant throughout combustion truncated the net heat release by an average of 2.19% for all injection timings. The 1998 and 1999 Brunt correlations, also temperature

dependent gamma correlations, overestimate the net heat release when compared to the correlations provided by Turns (2000). The overshoot of the Brunt correlations (when compared to Turns') at a 60° injection timing are about 3.10% and 2.05% for the 1998 and 1999 correlations.

Between two and three percent of an overestimate or underestimate may not seem like a noteworthy error to most researchers; however, calculating the deviation of a correlation or method from the accepted normal does not capture measurement uncertainty. Unfortunately engine research models have quantified error through sensitivity analysis. The results of the detailed uncertainty analysis, provided in Table 4.4, illustrates the true error (given the experimental setup and initial conditions) in measuring the net heat release. The full scale value (FSV) percentage of uncertainty in the net heat release with an injection timing of 60º BTDC using the Turns' (2000) specific heat correlations is 26.3%. Assuming gamma to be constant increases the FSV uncertainty 42.40%. Brunt's correlations fair a little better than the constant gamma assumption with FSV uncertainties of 32.4% using the 1998 correlation and 31.1% using the 1999 correlation at an injection timing of 60 degrees.

Classifying a model's error by evaluating a percentage difference between the model's FSV and the accepted norm FSV grossly underestimates the error within the model. With a 40% FSV uncertainty on average, assuming the specific heat ratio of the fuel-air mixture to be equal to the specific heat ratio of air and constant throughout combustion is not an acceptable assumption when modeling engine combustion. Though Brunt's 1998 and 1999 correlations fair better than the constant gamma assumption, it would be best to implement Turns' correlations to achieve smaller FSV uncertainties for

nearly equal amount of modeling effort. Even with the increased accuracy of Turns' equations, the true value of the net heat release can only be determined with an accuracy of roughly 80 percent. With such high degree of uncertainty in the net heat release calculation, understanding which of the measured variables contributes the most to the total uncertainty is essential. Uncertainty percentage contributions and magnification factors provide such insight and are discussed in the next section.

4.7 Evaluation of the UPCs and UMFs

The uncertainty percentage contributions and uncertainty magnification factors are perhaps the most important aspects of uncertainty analysis. An uncertainty percentage contribution identifies the percentage contribution of each variable to the total uncertainty. Uncertainty magnification values express the degree a respective uncertainty will increase or decrease as it propagates through the data reduction equations. A positive UMF demonstrates growth in an uncertainty while a negative UMF indicates a decrease in magnitude. Figure 4.4 describes the UPC values for pressure, volume and gamma for an injection timing of 60 degrees while Figure 4.5 reveals the UMF trends of pressure, volume and gamma during combustion. Plots of UPC and UMF values for all injection timings can be found in Appendix C.

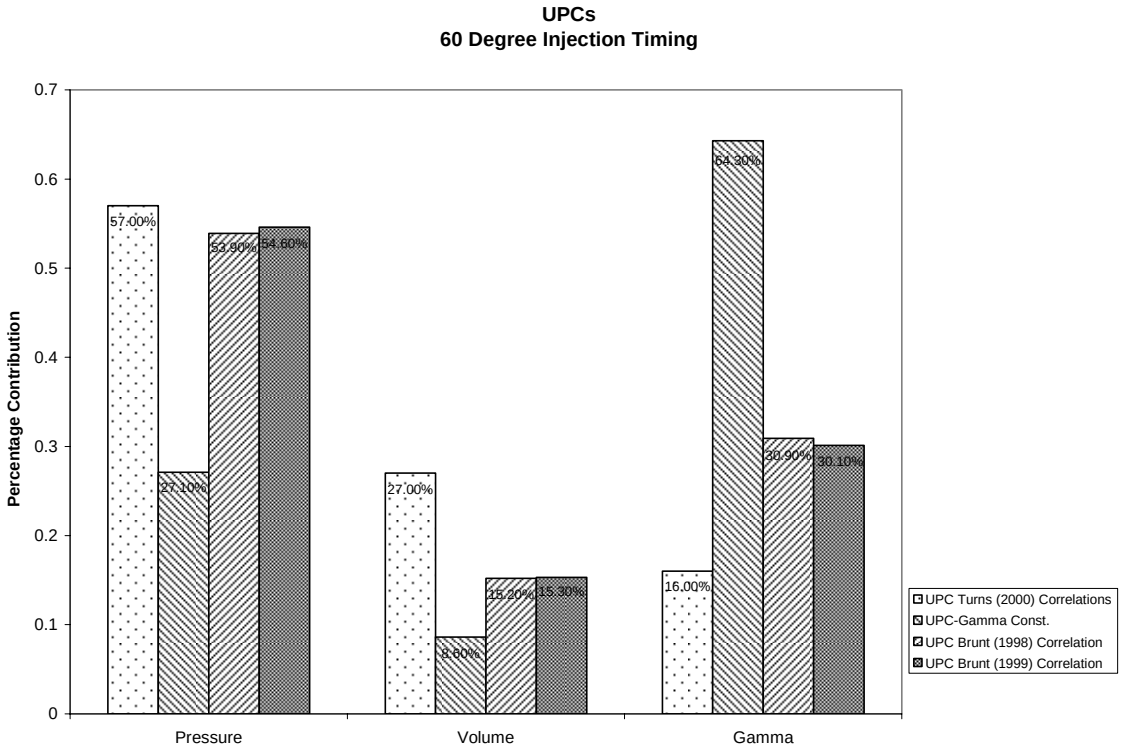

Figure 4.4 UPC Values of the Net Heat Release for an Injection Timing of 60 Degrees BTDC

The uncertainty percentage contributions (indicated by the bar graphs in Figure 4.4) provide important information to the researcher. Using the specific heat correlations provided by Turns, the greatest contribution to the total uncertainty in the net heat release is from the piezoelectric pressure transducer (57.00 %) followed by the instantaneous volume (27.00 %) and the specific heat ratio (16.00 %). The most striking result is the increase in uncertainty contribution of gamma when assumed to be constant and equal to air. From Table 4.4 one can deduce that there is a 35.21% increase in total uncertainty associated with the net heat release when implementing this assumption; more importantly, gamma contributes to 64.30% of the total uncertainty in the net heat release

under the constant-equal-to-air specific heat ratio assumption. The increase in percentage contribution from 16.00% to 64.30% simply by assuming gamma to be constant and equal to air demonstrates the impracticality of using such an assumption. Though the increases in total uncertainty using Brunt's correlations versus Turns' is not as extreme [60.175 kJ (Turns) to 76.545 kJ (1998 correlation) and 72.682 kJ (1999 correlation)], the increase is due to the change in equations used to model the specific heat ratio of the air-to-fuel mixture.

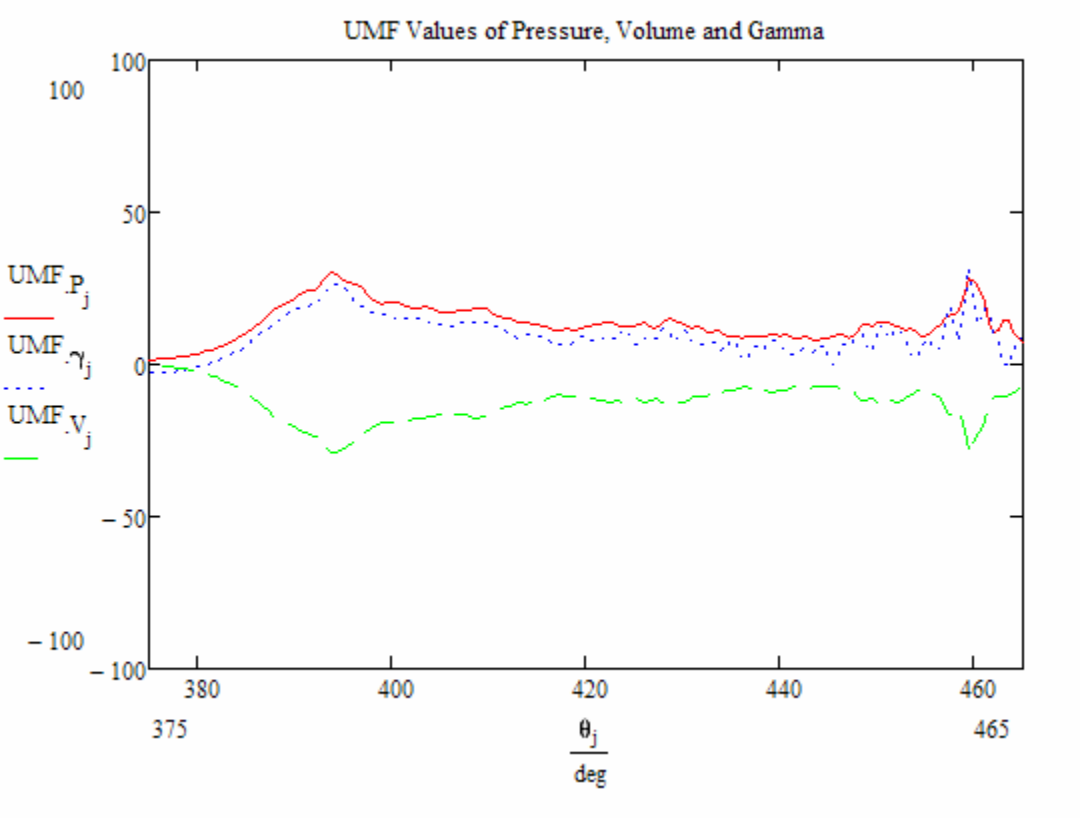

Figure 4.5 UMF Values for Pressure, Volume and Gamma using Turns (2000) Correlations

While the uncertainty percentage contribution is a useful means in comparing two methods of evaluation, uncertainty magnification factors provide researchers information as to which measured variable requires the greatest amount of measurement accuracy for a given experimental model. The analysis using Turns' equations of specific heat at constant pressure was most sensitive to the pressure and specific heat ratio as shown by the solid and dotted lines in Figure 4.5. The uncertainty in the instantaneous volume due to crank angle resolution decreased in magnitude as it propagated through the net heat release rate equation as demonstrated by the dashed line in Figure 4.5.

4.8 Evaluation of Indicated Work and IMEP

The evaluation of the indicated work (IW) and imep were relatively straightforward calculations. The equation for IW is the integration of pressure and the first derivative of volume, Equation (4.2), while the imep can be determined by dividing the IW by the displacement volume, Equation (4.3).

$$IW := \sum_{i} \left[\left(Pf60_{mean_i} \right) \cdot dV\left(\theta_i \right) \cdot \Delta\theta \right] \tag{4.2}$$

$$IMEP := \frac{IW}{V_d} \tag{4.3}$$

It is important to note that the effects of a constant specific heat ratio did not propagate into these equations. As a result, the engine work and imep was determined only for the

Turns' correlations for all injection. Figure 4.6 demonstrates the effect of injection timing on the engine work and imep.

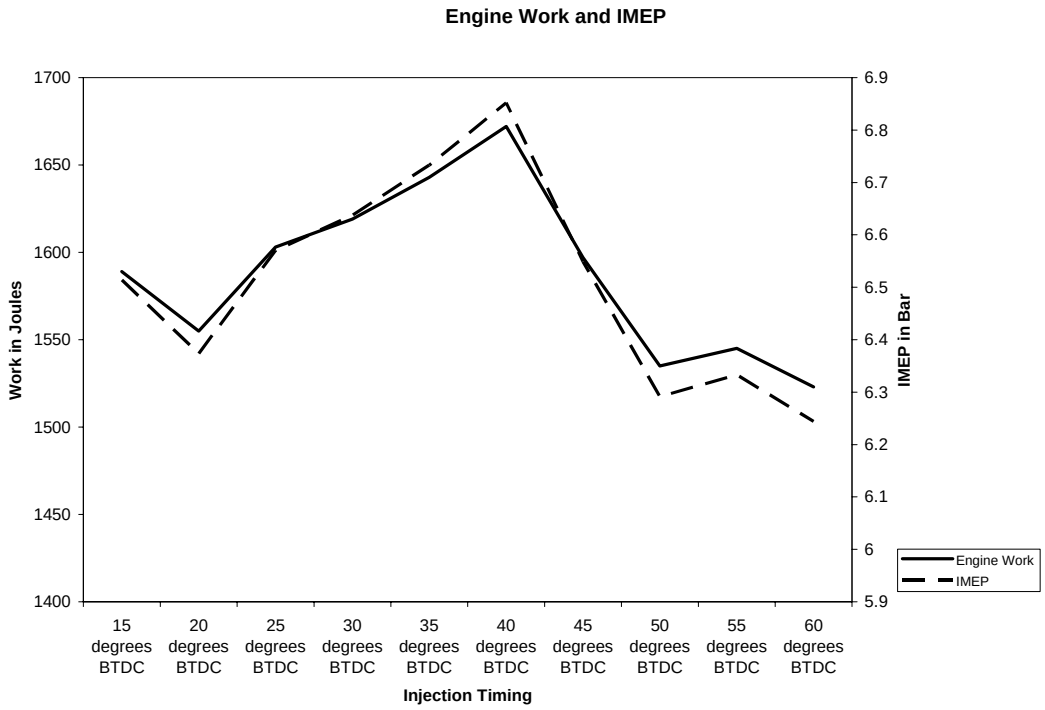

Figure 4.6 Indicated Work and IMEP Values for all Injection Timings

4.9 Uncertainty in Engine Work and IMEP

A general uncertainty analysis was performed on both the engine work and imep. However, percentage contributions and magnification factors of these uncertainties were neglected due to the simplicity of the equations. Nevertheless, the author did note the effects on the imep and engine work when a small error in accuracy of the assumed crank angle resolution (1.0% FSV) was introduced to the 60 degree injection timing analysis. Figure 4.6 represents the uncertainty associated with engine work and imep for all

injections timings with the inclusion of the 1.0% crank angle resolution error for the 60 degree injection timing.

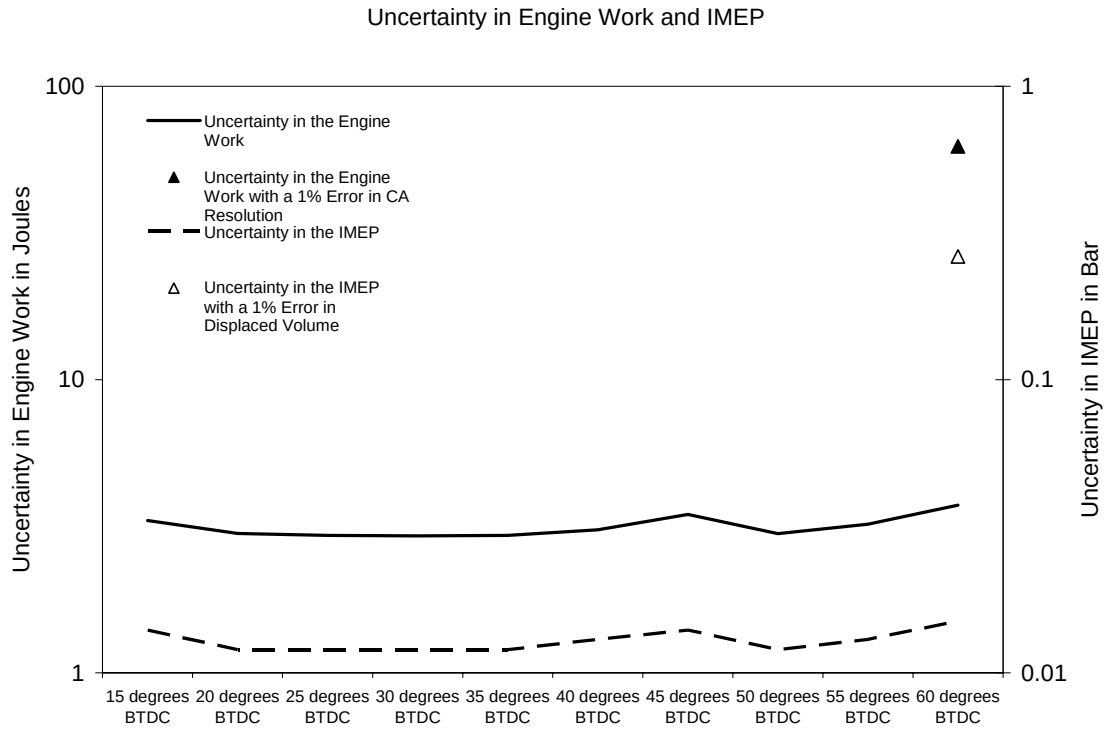

Figure 4.7 Uncertainty in Engine Work and IMEP

It is important to note that the uncertainties in both the indicated work and imep are relatively insensitive to changes in the in-cylinder pressure caused by injection timing advancement. However, the indicated work and imep are sensitive to coarser crank angle resolutions and uncertainty in compression ratio calculations. For the 60 degree BTDC injection timing, a one-percent error was introduced in the assumed constant crank angle resolution ($\Delta\theta$) – as demonstrated by the solid triangle in Figure 4.7. The effect was a significant increase the uncertainty in the indicated work. The determination of the imep is sensitive to not only the crank angle resolution but also the compression ratio of the

engine. A one-percent error was introduced to the assumed constant displacement volume and the effects on the imep are shown by the outlined triangle in Figure 4.7. Brunt et al. (1991 & 1996) concluded similar results from their research on the effects of crank angle resolution in engine testing.

CHAPTER V

CONCLUSIONS AND FUTURE WORK

5.1. Conclusions

The results from the analyses demonstrate that there is noteworthy difference in the uncertainty of the net heat release based upon the evaluation method of the specific heat ratio. The assumption that gamma is constant and equal to the specific heat ratio of air throughout combustion is an impractical assumption because:

1. The heat release rate during combustion is underestimated.
2. The uncertainty within the heat release is 42% of the full scale value.
3. The uncertainty percentage contribution of gamma significantly outweighs the contributions from pressure and volume.

Brunt et al. (1998, 1999) presented two correlations for evaluating the specific heat ratio of the combustion mixture that were temperature dependent and which proved to be a better assumption than holding gamma to be constant. However, Brunt's correlations slightly overestimated the net heat release when compared to Turns' correlations, but more importantly was the FSV percentage uncertainty of the net heat release, 32.4% for the 1998 correlation and 31.1% for the 1999 correlation.

The analyses demonstrated that the uncertainty in the net heat release can be minimized by determining the specific heats of the combustion products as a function of temperature and then using the individual specific heats in conjunction with their respective mass fraction to determine the combustion gamma. Even with such precision, the uncertainty in the net heat release was found to be between 22% and 26% of the full scale value. However, more control is given to the experimenter using this method because the majority of the uncertainty stems from the pressure measurements rather than the specific heat ratio.

Though the focus of this analysis was not to optimize the combustion of natural gas, the net heat release rate schedule for multiple injection timings were evaluated as a comparison to previous research. It was determined that the uncertainty of the net heat release rates for the different injection timings was not significantly different. Each injection timing was evaluated separately from the others and therefore was not a variable in performing the uncertainty analysis.

Lastly, the results of this analysis were supported by literature within the discipline of engine testing. It was determined that the pressure measurements play a crucial role in the accuracy of the net heat release rate. In addition, the evaluation of the engine work and imep demonstrated that the resolution of the optical encoder is a key component in these evaluations – coarser resolutions increase the inaccuracy in both work and imep.

5.2. Future Work

It was the hope of the author to demonstrate the importance and need for detailed uncertainty analyses in experimentation, especially in engine testing. While precision and thoroughness was a goal in this analysis some assumptions were made and due to time constraints and practicality not all aspects of combustion were taken into account. In summary the following recommendations are proposed for future analyses.

- *Variability in Engine Attributes:* As mentioned before, the geometric properties of the engine were assumed to be constant. Uncertainties within these measurements were neglected and thereby did not influence the total uncertainty in the net heat release rate. Compression ratio, bore and stroke length, for example, are values with inherent uncertainty that would drive the uncertainty in the instantaneous volume up. In this analysis, the uncertainty in the volume was very small since the aforementioned values were assumed to be constant.
- *Reference Pressure:* In this analysis, due to the lack of raw data, the intake manifold pressure, P_o, was assumed to have minimal bias uncertainty and no precision uncertainty. In actuality, the pressure transducer would have minor fluctuations which would introduce a random uncertainty into the equation.
- *Heat Transfer Across the Cylinder Walls:* Only the net heat release rate was determined in this analysis. One important aspect of engine testing is the determination of the gross heat transfer.
- *Pegging Techniques:* This analysis did not incorporate different pegging techniques for the reference pressure. Uncertainty contributions due to pegging

techniques would be a quantitative means to reinforce the studies conducted by previous researchers.

REFERENCES

Amann, C.A. (1985). Cylinder-pressure measurement and its use in engine research. *SAE 852067.*

Bell, M.L., McDermott, A., Zeger, S.L., Samet, J.M. & Dominici, F. (2004). Ozone and short-term mortality in 95 US urban communities, 1987-2000. *JAMA, 292, No. 19,* 292-311.

Brown, W.L. (1967). Methods for evaluating requirements and errors in cylinder pressure measurement. *SAE 670008*.

Brunt, M.F.J. & Lucas, G.G. (1991). The effect of crank angle resolution on cylinder pressure analysis. *SAE 910041.*

Brunt, M.F.J. & Emtage, A.L. (1996). Evaluation of IMEP routines and analysis errors. *SAE 960609*.

Brunt, M.F.J. & Pond, C.R. (1997). Evaluation of techniques for absolute cylinder pressure correction. *SAE 970036.*

Brunt, M.F.J. & Emtage, A.L. (1997). Evaluation of burn rate routines and analysis errors. *SAE 970037.*

Coleman, H.W & Steele, W.G. (1999). *Experimentation and Uncertainty Analysis for Engineers, 2nd Edition.* New York: John Wiley & Sons, Inc.

Depcik, C. (2000). *Open-ended thermodynamic cycle simulation.* Unpublished master thesis, University of Michigan, Ann Arbor.

Depcik, C., Jacobs, T, Hagena, J., & Assanis, D. (2007). Instructional use of a single-zone, premixed charge, spark-ignition engine heat release simulation. *International Journal of Mechanical Engineering Education,* 35(1), 1-31.

Ferguson, C.R. & Kirkpatrick, A.T. (2001). *Internal combustion engines.* New York: John Wiley & Sons, Inc.

Freeman, L.A., Carpenter, M.C., Rosenberry, D.O., Rousseau, J.P., Unger, R. & McLean, J.S. (2004). *Use of submersible pressure transducer in water-resources investigations.* Retrieved June 5, 2008 from U.S. Geological Survey Web site: http://pubs.usgs.gov/twri/twri8a3/

Hayes, T.K. & Savage, L.D. (1986). Cylinder pressure data acquisition and heat release analysis on a personal computer. *SAE 860029.*

Heywood, J.B. (1988). *Internal Combustion Engine Fundamentals.* New York: McGraw-Hill Book Company.

Hribernik, A. (1998). Statisitical determination of correlation between pressure and crankshaft angle during indication of combustion engines. *SAE 982541.*

Karim, G.A. (1968). "Combustion in dual fuel engines – A status report," Eighth International Conference on Combustion Engines, Congress Palace, Brussels, 6^{th} – 10^{th} May 1968.

Krieger, R.B. & Borman, G.L. (1967). The computation of apparent heat release for internal combustion engines. *ASME.*

Krishnan, S.R. (2001). *Heat release analysis of dual fuel combustion in a direct injection compression ignition engine.* Unpublished master thesis, University of Alabama, Tuscaloosa.

Lancaster, D.R., Krieger, R.B. & Lienesch, J.H. (1975). Measurement and analysis of engine pressure data. *SAE 750026.*

Lapuerta, M., Armas, O. & Bermudez, V. (2000). Sensitivity of diesel engine thermodynamic cycle to measurement errors and estimated parameters. *Applied Thermal Engineering, 20,* 843-861.

Muzio, L.J. & Quartucy, G.C. (1997). Implementing NOx control: research to application. *Progress in Energy and Combustion Science*, *23,* 233-266.

National Instruments (2006). *Encoders*. Retrieved November 12, 2007, from National Instruments: NI Developer Zone Web site: http://zone.ni.com/devzone/cda/tut/p/id/3321

Randolph, A.L. (1990a). Methods of processing cylinder-pressure transducer signal to maximize data accuracy. *SAE 900170.*

Randolph, A.L. (1990b). Cylinder-pressure-transducer mounting techniques to maximize data accuracy. *SAE 900171.*

Shayler, P.J. & Wiseman, M.W. (1990). Improving the determination of mass fraction burnt. *SAE 900351*.

Srinivasan, K.K., Krishnan, S.R., Singh, S., Bell, S.R. & Midkiff, K.C. (2004). Strategies for reduced NOx emissions in pilot-ignited natural gas engines. *Journal of Engineering for Gas Turbines and Power, 126,* 665-671.

Srinivasan, K.K., Krishnan, S.R., Singh, S. & Midkiff, K.C. (2006a). The advancement injection low pilot ignited natural gas engine: a combustion analysis. *Journal of Engineering for Gas Turbines and Power, 128,* 213-218.

Srinivasan, K.K., Krishnan, S.R. & Midkiff, K.C. (2006b). Improving low load combustion, stability, and emissions in pilot-ignited natural gas engines. *Proc. IMechE, 220, Part D,* 229-239.

Stone, R. (1999). *Introduction to Internal Combustion Engines.* SAE International; 3 edition.

Turns, S.R. (2000). *An Introduction to Combustion 2nd Edition*. Boston: McGraw-Hill Book Company.

APPENDIX A

DETAILED UNCERTAINTY ANALYSIS

Detailed Uncertainty Analysis for 60 Degree Injection Timing Implementing Turns (2000) Correlations for Combustion Species Specific Heat Ratios.

Common Conversions:

$bar := 100000 \cdot Pa$ $kmol := 1000 \cdot mol$ $kJ := 1000 \cdot J$ $kPa := 1000 \cdot Pa$

$Rev := 2 \cdot \pi \cdot rad$

Engine Specifications:

$Gas_{dot} := 72.2 \cdot \frac{gm}{min}$ $Air_{dot} := 2850 \cdot \frac{gm}{min}$ $Diesel_{dot} := 3.3 \cdot \frac{gm}{min}$

$T_o := 348 \cdot K$ $P_o := 1.41 \cdot bar$ $\Delta\theta := .5 \cdot deg$ $N := 1700 \cdot \frac{Rev}{min}$

$\theta_{inj} := 60 \cdot deg$ $\theta_{IVO} := 685 \cdot deg$ $\theta_{IVC} := 217 \cdot deg$ $\theta_{EVO} := 506 \cdot deg$ $\theta_{EVC} := 10 \cdot deg$

$b := .13716 \cdot m$ $s_c := .1651 \cdot m$ $l := .2612 \cdot m$ $a := \frac{s_c}{2}$ $r := 14.5$

The above values are the engine specifications and flow rates as given by Srinivasan. The flow rate of methane was represented as Gas dot. To and Po are the average intake manifold conditions. The resolution of the optical encoder is expressed as Δθ. The speed of the engine, N, was 1700 revolutions per minute. θinj is the crank angle that fuel injection occurs. The subscripts IVO, IVC, EVO and EVC stand for inlet valve opening, inlet valve closure, exhaust valve opening and exhaust valve closure respectively. Lastly, the geometric properties of the engine as determined by Srinivasan et al. (2004) are given as b (bore), sc (stroke length), l (connecting rod length), a (crank radius) and r (compression ratio).

Smoothing the Pressure Data (Motoring and Firing)

$Motoring :=$

	0
0	-5.371
1	...

$kk := 1, 2 .. 1438$ $y := 0 .. 1$ $N := 50$

$i := 1, 2 .. 1437$ $x := 0, 1 .. 49$

$$Pmsmooth1_{kk} := \frac{Motoring_{kk-1} + 2 \cdot Motoring_{kk} + Motoring_{kk+1}}{4}$$

(Stone, 1999, pp. 543)

$$Pmsmooth_i := \frac{Pmsmooth1_{i-1} + 2 \cdot Pmsmooth1_i + Pmsmooth1_{i+1}}{4}$$

$\theta_i := .5 \cdot i \cdot deg$ The motoring pressure data was used to determine if the pressure data was correctly phased with the optical encoder. The logarithmic plot of pressure versus volume was used to determine if cross-over was present.

$Firing_{60deg} :=$

	0
0	-6.934

$xx := 0, 1 .. 149 \quad NN := 150$

$$Pfsmooth1_{kk,xx} := \frac{Firing_{60deg_{kk-1,xx}} + 2 \cdot Firing_{60deg_{kk,xx}} + Firing_{60deg_{kk+1,xx}}}{4}$$

$$Pfsmooth_{i,xx} := \frac{Pfsmooth1_{i-1,xx} + 2 \cdot Pfsmooth1_{i,xx} + Pfsmooth1_{i+1,xx}}{4}$$

$$P_{f60}(i, xx) := Pfsmooth_{i,xx} \cdot bar$$

$$Pf60_{mean_i} := \sum_{xx=0}^{149} \frac{P_{f60}(i, xx}{150} \quad Sx60_i := \left[\frac{1}{149} \sum_{xx=0}^{149} \left(P_{f60}(i, xx) - Pf60_{mean_i} \right)^2 \right]^{.5}$$

$$Pf60_{mean} := Pf60_{mean} + 8.266 \cdot bar$$

$$P := Pf60_{mean}$$

With the pressure data appropriately phased, the mean pressure at a given crank angle over 150 cycles was determined. The mean cyclic pressure is represented by $Pf60_{mean}$. The standard deviation across the the cycles was determined and is given by Sx. The standard deviation would later be used in determining the random error in the pressure data. Lastly the pressure data was referenced to the average inlet manifold pressure. The 8.266 bar added onto the pressure data was the difference between the recorded pressure data at bottom dead center and Po.

Volume Calculations:

$$V_d := \frac{\pi}{4} \cdot b^2 \cdot s_c \qquad V_d = 2.439 \times 10^3 \cdot cm^3 \qquad V_c := \frac{V_d}{r - 1}$$

$$V(\theta) := V_c + \frac{\pi}{4} \cdot b^2 \cdot \left[l + a - \left[\left(l^2 - a^2 \sin(\theta)^2 \right)^{.5} + a \cdot \cos(\theta) \right] \right]$$

$$dV(\theta) := \frac{d}{d\theta} V(\theta) \qquad ddV(\theta) := \frac{d}{d\theta} dV(\theta)$$

The above calculations determined the displacement volume, Vd, and the clearance volume, Vc. With the clearance volume known the in-cylinder volume as a function of crank angle could be determined and is given as V(θ). The first and second derivatives of volume were evaluated here as they would be used later in determining the heat release rate and the uncertainty in the heat

release rate.

Molecular Weights of Reactants and Products:

$MW_{air} := 28.97 \cdot \frac{kg}{kmol}$ $MW_{carbondioxide} := 44 \cdot \frac{kg}{kmol}$ $MW_{methane} := 16 \cdot \frac{kg}{kmol}$

$MW_{nitrogen} := 14 \cdot \frac{kg}{kmol}$ $MW_{oxygen} := 16 \cdot \frac{kg}{kmol}$ $MW_{water} := 18 \cdot \frac{kg}{kmol}$

Gas Constants of Reactants and Products:

$R_{universal} := 8.3145 \cdot \frac{J}{mol \cdot K}$

$R_{air} := \frac{R_{universal}}{MW_{air}}$ $R_{carbondioxide} := \frac{R_{universal}}{MW_{carbondioxide}}$ $R_{methane} := \frac{R_{universal}}{MW_{methane}}$

$R_{nitrogen} := \frac{R_{universal}}{MW_{nitrogen}}$ $R_{oxygen} := \frac{R_{universal}}{MW_{oxygen}}$ $R_{water} := \frac{R_{universal}}{MW_{water}}$

The lean combustion equation is as follows:

$$CH_4 + \frac{As}{\Phi_{lean}} \cdot \left(O_2 + 3.76 \cdot N_2\right) = n_1 \cdot CO_2 + n_2 \cdot H_2O + n_3 \cdot N_2 + n_4 \cdot O_2$$

Carbon Balance:

$1 = n_1$

Hydrogen Balance:

$4 = 2 \cdot n_2$

Oxygen Balance:

$$\frac{2 \cdot As}{\Phi_{actual}} = 2 \cdot n_1 + n_2 + 2 \cdot n_4$$

Stoichiometric Combustion Analysis:

$\Phi_{stoichiometric} := 1.0$

$\alpha_1 := 1 \qquad \alpha_2 := 2 \qquad As := \frac{(2\cdot\alpha_1 + \alpha_2)\cdot\Phi_{stoichiometric}}{2} \qquad \alpha_3 := \frac{7.52\cdot As}{2\cdot\Phi_{stoichiometric}}$

Air to Fuel Ratios:

$AF_{stoic} := \frac{As\cdot(2\cdot MW_{oxygen} + 2\cdot 3.76\cdot MW_{nitrogen})}{MW_{methane}} \qquad AF_{stoic} = 17.16$

$AF_{actual} := \frac{Air_{dot}}{Diesel_{dot} + Gas_{dot}} \qquad \Phi_{actual} := \frac{AF_{stoic}}{AF_{actual}} = 0.455$

Lean Combustion Analysis:

$n_1 := 1\cdot mol \qquad n_2 := 2\cdot mol \qquad n_4 := \frac{\frac{2\cdot As}{\Phi_{actual}}\cdot mol - 2\cdot n_1 - n_2}{2} \qquad n_3 := \frac{7.52\cdot As}{2\cdot\Phi_{actual}}\cdot mol$

Mass Fractions of Products:

$N_{products} := n_1 + n_2 + n_3 + n_4$

$m_{CO2} := n_1\cdot MW_{carbondioxide} \qquad m_{H2O} := n_2\cdot MW_{water}$

$m_{N2} := n_3\cdot MW_{nitrogen} \qquad m_{O2} := n_4\cdot MW_{oxygen}$

$m_{products} := m_{CO2} + m_{H2O} + m_{N2} + m_{O2}$

$mf_{CO2} := \frac{m_{CO2}}{m_{products}} \qquad mf_{H2O} := \frac{m_{H2O}}{m_{products}}$

$mf_{N2} := \frac{m_{N2}}{m_{products}} \qquad mf_{O2} := \frac{m_{O2}}{m_{products}}$

Molecular Weight and Gas Constant of the Products:

$MW_{products} := \frac{m_{products}}{N_{products}} \qquad R_{products} := \frac{R_{universal}}{MW_{products}}$

Gas Constant and mass of the Reactants:

$$R_{reactants} := \frac{R_{methane} + \frac{AF_{stoic}}{\Phi_{actual}} \cdot R_{air}}{1 + \frac{AF_{stoic}}{\Phi_{actual}}}$$

$\theta_{IVC} = 217 \cdot deg$ $\quad P_{IVC} := Pf60_{mean_{436}}$

$P_{IVC} = 1.616 \cdot bar$ $\quad n := 1.35$ $\quad V_{IVC} := V(\theta_{436})$

$$T_{IVC} := T_o \cdot \left(\frac{V_o}{V_{IVC}} \right)^{n-1} \qquad V_o := V(\theta_{361})$$

$$m_{reactants} := \frac{(P_{IVC}) \cdot (V_{IVC})}{R_{reactants} \cdot (T_{IVC})}$$

The temperature at inlet valve closure was determined using the polytropic process. The array index of 436 was used because the crank angle step is equal to 0.5 crank angle degrees and due to the smoothing algorithm implemented above 1 crank angle degree was lost on each end of the pressure data. Hence the average firing data runs from 1 crank angle degree to 719 crank angle degrees rather than 0 to 720 crank angle degrees. The polytropic index for methane combustion is given as n.

Temperature of the In-Cylinder Gas using the Firing Pressure Data:

$i := 0, 1 .. 1437$

$$T_i := \begin{cases} \frac{Pf60_{mean_i} \cdot V(\theta_i)}{m_{reactants} \cdot R_{reactants}} & \text{if } 575deg \geq \theta_i \geq 217 \cdot deg \\ T_o & \text{otherwise} \end{cases}$$

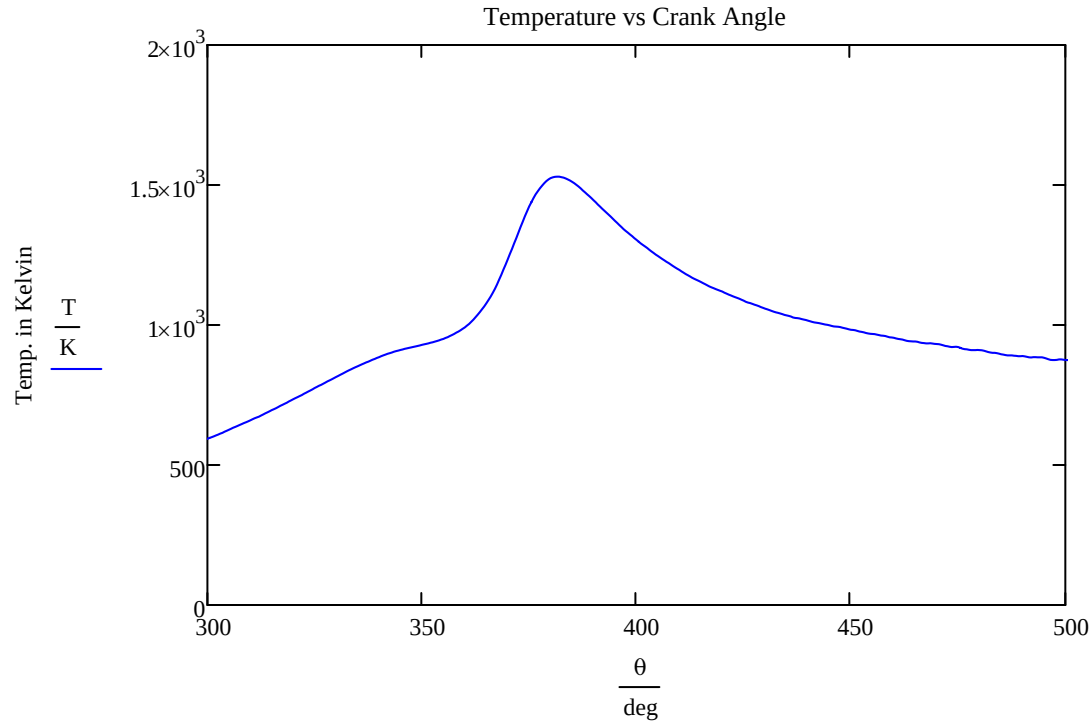

Specific Heat of Fuel Mixture as a Function of Temperature:

$$Cp_{carbondioxide_i} := \begin{cases} \left(\frac{R_{universal}}{MW_{carbondioxide}}\right)\cdot\left[2.28 + .0099\cdot\left(\frac{T_i}{K}\right) - .1041\cdot10^{-4}\cdot\frac{\left(T_i\right)^2}{K^2} + .06867\cdot10^{-7}\cdot\left(\right.\right. \\ \left(\frac{R_{universal}}{MW_{carbondioxide}}\right)\cdot\left[4.454 + .00314\cdot\left(\frac{T_i}{K}\right) - .1278\cdot10^{-5}\cdot\frac{\left(T_i\right)^2}{K^2} + .002394\cdot10^{-}\right. \end{cases}$$

$$Cp_{water_i} := \begin{cases} \frac{R_{universal}}{MW_{water}}\cdot\left[3.387 + .003475\cdot\frac{T_i}{K} - .0635\cdot10^{-4}\cdot\left(\frac{T_i}{K}\right)^2 + .06968\cdot10^{-7}\cdot\left(\frac{T_i}{K}\right)^3 - .02506\cdot1\right. \\ \frac{R_{universal}}{MW_{water}}\cdot\left[2.672 + .00305\cdot\frac{T_i}{K} - .0873\cdot10^{-5}\cdot\left(\frac{T_i}{K}\right)^2 + .1201\cdot10^{-9}\cdot\left(\frac{T_i}{K}\right)^3 - .06392\cdot10^{-}\right. \end{cases}$$

$$Cp_{nitrogen_i} := \begin{cases} \frac{R_{universal}}{MW_{nitrogen}}\cdot\left[3.2986 + .001408\cdot\frac{T_i}{K} - .03963\cdot10^{-4}\cdot\left(\frac{T_i}{K}\right)^2 + .05641\cdot10^{-7}\cdot\left(\frac{T_i}{K}\right)^3 - .0\right. \\ \frac{R_{universal}}{MW_{nitrogen}}\cdot\left[2.9266 + .001488\cdot\frac{T_i}{K} - .05685\cdot10^{-5}\cdot\left(\frac{T_i}{K}\right)^2 + .10097\cdot10^{-9}\cdot\left(\frac{T_i}{K}\right)^3 - .0\right. \end{cases}$$

$$Cp_{oxygen_i} := \begin{cases} \frac{R_{universal}}{MW_{oxygen}}\cdot\left[3.2129 + .001127\cdot\frac{T_i}{K} - .05756\cdot10^{-5}\cdot\left(\frac{T_i}{K}\right)^2 + .13139\cdot10^{-8}\cdot\left(\frac{T_i}{K}\right)^3 - .087\right. \\ \frac{R_{universal}}{MW_{oxygen}}\cdot\left[3.6976 + .0006135\cdot\frac{T_i}{K} - .12588\cdot10^{-6}\cdot\left(\frac{T_i}{K}\right)^2 + .01775\cdot10^{-9}\cdot\left(\frac{T_i}{K}\right)^3 - .11\right. \end{cases}$$

The above equations for the individual product components was given by Turns (2000).

$$Cp_{products_i} := \left(mf_{CO2}\cdot Cp_{carbondioxide_i}\right) + \left(mf_{H2O}\cdot Cp_{water_i}\right) \cdots + \left(mf_{N2}\cdot Cp_{nitrogen_i}\right) + \left(mf_{O2}\cdot Cp_{oxygen_i}\right)$$

$$Cv_{products_i} := mf_{CO2}\cdot\left(Cp_{carbondioxide_i} - R_{carbondioxide}\right) + mf_{H2O}\cdot\left(Cp_{water_i} - R_{water}\right) \ldots$$
$$+ mf_{N2}\cdot\left(Cp_{nitrogen_i} - R_{nitrogen}\right) + mf_{O2}\cdot\left(Cp_{oxygen_i} - R_{oxygen}\right)$$

$$\gamma_i := \frac{Cp_{products_i}}{Cv_{products_i}}$$

Pressure Derivative using the Pressure Smoothing Algorithm:

$$j := 0, 1 .. 1433$$

$$dP_j := \frac{P_j - 8\cdot P_{j+1} + 8\cdot P_{j+3} - P_{j+4}}{12\cdot\Delta\theta}$$ (Stone, 1999, pp. 543)

Calculating the Net Heat Release Rate: $jj := 4, 5 .. 1429$

$$dQ_{net_j} := \frac{\gamma_j}{\gamma_j - 1}\cdot P_j\cdot\left(dV\left(\theta_j\right)\right) \ldots$$
$$+ \frac{1}{\gamma_j - 1}\cdot V\left(\theta_j\right)\cdot\left(dP_j\right)$$

$$Q_{smooth_{jj}} := \frac{1}{9}\cdot\left(dQ_{net_{jj-4}} + dQ_{net_{jj-3}} + dQ_{net_{jj-2}} + dQ_{net_{jj-1}} \ldots\right.$$
$$\left. + dQ_{net_{jj}} + dQ_{net_{jj+1}} + dQ_{net_{jj+2}} + dQ_{net_{jj+3}} + dQ_{net_{jj+4}}\right)$$

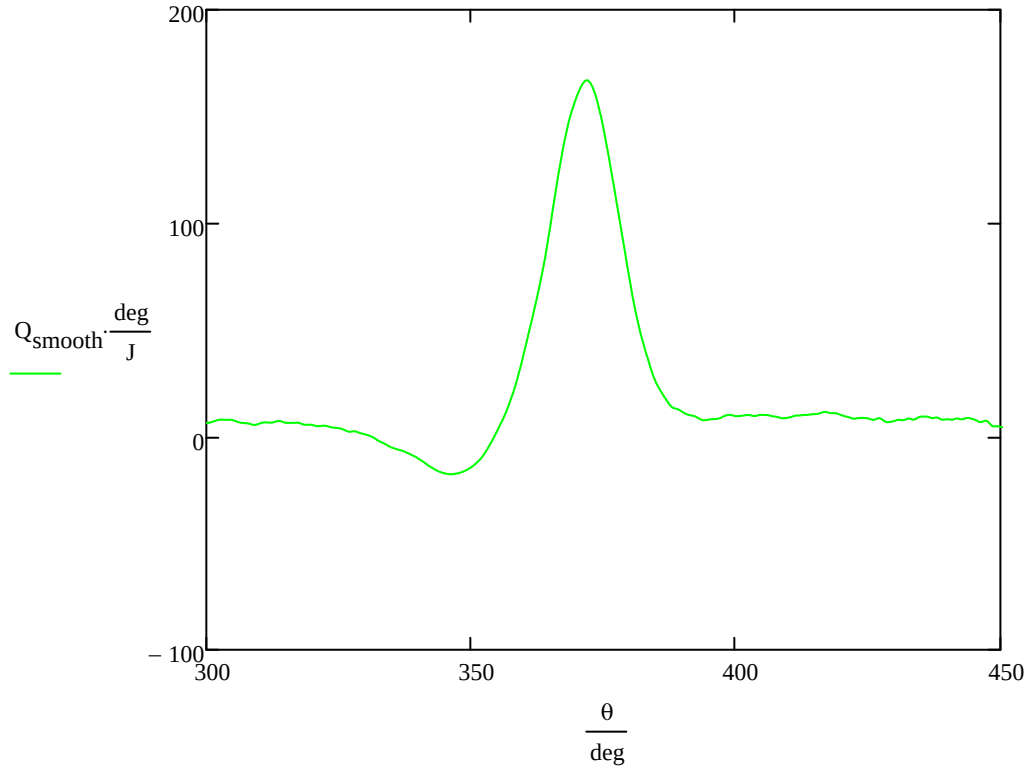

$dQ_{net} := Q_{smooth}$

$\sum_{i=4}^{1429} Q_{smooth_i} \cdot \Delta\theta = 1.999 \cdot kJ$

Uncertainties for each of the measured variables:

$Ub_\theta := 0.5 \cdot deg$ $\quad Up_\theta := 0.1 \cdot deg$ $\quad Ub_{To} := .75\% \cdot T_o$ $\quad Up_{To} := 0 \cdot K$

$Ub_P := .4\% \cdot P$ $\quad Up_P := \sum_{i=0}^{1437} \frac{\left(\frac{2 \cdot Sx60_i}{\sqrt{NN}}\right)}{1440}$ $\quad Ub_{Po} := .15\% \cdot P_o$ $\quad Up_{Po} := 0 \cdot bar$

$U\theta := \left(Ub_\theta^{\,2} + Up_\theta^{\,2}\right)^{.5}$ $\quad U\theta = 0.51 \cdot deg$

$UP := \left(Ub_P^{\,2} + Up_P^{\,2}\right)^{.5}$ $\quad mean(UP) = 0.071 \cdot bar$

$UTo := \left(Ub_{To}^{\,2} + Up_{To}^{\,2}\right)^{.5}$ $\quad UTo = 2.61\,K$

$UPo := \left(Ub_{Po}^{\,2} + Up_{Po}^{\,2}\right)^{.5}$ $\quad UPo = 2.115 \times 10^{-3} \cdot bar$

Uncertainty Calculation in Volume:

$$V = \frac{\pi}{4}\cdot b^2\cdot s_c + \frac{\pi}{4}\cdot b^2\cdot\left[l + a - \left[\left(l^2 - a^2\cdot\sin(\theta)^2\right)^{.5} + a\cdot\cos(\theta)\right]\right]$$

$$Uv^2 = \left(\frac{d}{d\theta}V\right)^2\cdot U\theta^2$$ because engine specifications (bore, stroke length, etc.) are assumed to be constant

$$Uv^2 = \left[\frac{\pi\cdot bore^2}{4}\cdot\left[a\cdot\sin(\theta) + \frac{a^2}{\left(l^2 - a^2\cdot\sin(\theta)^2\right)^{.5}}\cdot\sin(\theta)\cdot\cos(\theta)\right]\right]^2\cdot U\theta^2$$

$$dv_i := \frac{\pi\cdot b^2}{4}\cdot\left[a\cdot\sin\left(\theta_i\right) + \frac{a^2}{\left(l^2 - a^2\cdot\sin\left(\theta_i\right)^2\right)^{.5}}\cdot\sin\left(\theta_i\right)\cdot\cos\left(\theta_i\right)\right]$$

$$Uv_i := \left[\left(dv_i\right)^2\cdot U\theta^2\right]^{.5}$$

Uncertainty in the Air/Fuel Ratio:

$$Uair_{dot} := 2\%\cdot Air_{dot} \qquad Udiesel_{dot} := 0.5\%\cdot Diesel_{dot} \qquad Ugas_{dot} := 0.5\%\cdot Gas_{dot}$$

$$U_{AF} := \sqrt{\left(Uair_{dot}\right)^2\cdot\left(\frac{1}{Diesel_{dot} + Gas_{dot}}\right)^2 + \left(Udiesel_{dot}\right)^2\cdot\left[\frac{Air_{dot}}{\left(Diesel_{dot} + Gas_{dot}\right)^2}\right]^2 ... + \left[\left(Ugas_{dot}\right)^2\cdot\left[\frac{Air_{dot}}{\left(Diesel_{dot} + Gas_{dot}\right)^2}\right]^2\right]}$$

$$U_{AF} = 0.776$$

Uncertainty in the Equivalence Ratio:

$$U_\Phi := \sqrt{U_{AF}^2\cdot\left(\frac{AF_{stoic}}{AF_{actual}^2}\right)^2}$$

Uncertainty in the gas constant of the reactants:

$$Ur_{reactants} := \sqrt{\left(U_{\Phi}\right)^2 \cdot \left[\frac{AF_{stoic}}{\Phi_{actual}^2 \cdot \left(1 + \frac{AF_{stoic}}{\Phi_{actual}}\right)} \cdot \left(\frac{R_{methane} + \frac{AF_{stoic} \cdot R_{air}}{\Phi_{actual}}}{1 + \frac{AF_{stoic}}{\Phi_{actual}}} - R_{air} \right) \right]^2}$$

$$UT_{IVC} := \left[UTo^2 \cdot \left(\frac{d}{dT_o} T_{IVC} \right)^2 + Uv^2 \cdot \left(\frac{d}{dV_o} T_{IVC} \right)^2 + Uv^2 \cdot \left(\frac{d}{dV_{IVC}} T_{IVC} \right)^2 \right]^{.5}$$

Uncertainty in the mass of the fuel:

$$dmT_{IVC} := \frac{-P_{IVC} \cdot V_{IVC}}{R_{reactants} \cdot T_{IVC}^2} \qquad dmP_{IVC} := \frac{V_{IVC}}{R_{reactants} \cdot T_{IVC}}$$

$$dmV_{IVC} := \frac{P_{IVC}}{R_{reactants} \cdot T_{IVC}} \qquad dmR_{reactants} := \frac{-P_{IVC} \cdot V_{IVC}}{R_{reactants}^2 \cdot T_{IVC}}$$

$$Um := \left[dmP_{IVC}^2 \cdot UP^2 + dmT_{IVC}^2 \cdot UT_{IVC}^2 + dmV_{IVC}^2 \cdot (Uv)^2 + dmR_{reactants}^2 \cdot Ur_{reactants}^2 \right]^{.5}$$

Uncertainty in the Temperature:

$$T_i := \begin{cases} \frac{P_i \cdot V(\theta_i)}{m_{reactants} \cdot R_{reactants}} & \text{if } 575deg \geq \theta_i \geq 217 \cdot deg \\ T_o & \text{otherwise} \end{cases}$$

$$dTp_i := \frac{V(\theta_i)}{m_{reactants} \cdot R_{reactants}} \qquad dTv_i := \frac{P_i}{m_{reactants} \cdot R_{reactants}}$$

$$dTm_i := \frac{-\left(P_i \cdot V(\theta_i)\right)}{m_{reactants}^2 \cdot R_{reactants}} \qquad dTr_{reactants_i} := \frac{-P_i \cdot V(\theta_i)}{m_{reactants} \cdot R_{reactants}^2}$$

$$UT_i := \begin{cases} \left[\left(dTp_i\right)^2 \cdot \left(UP_i\right)^2 + \left(dTv_i\right)^2 \cdot \left(Uv_i\right)^2 + \left(dTm_i\right)^2 \cdot \left(Um_i\right)^2 + \left(dTr_{reactants_i}\right)^2 \cdot \left(Ur_{reactants}\right)^2 \right]^{.5} & \text{if } 575 \\ UTo & \text{otherwise} \end{cases}$$

Uncertainty in the Cp of the products:

$$dCp_{cd_i} := \frac{R_{universal}}{MW_{carbondioxide}} \cdot \left\| \begin{array}{l} \left[.0099 - 2 \cdot .1041 \cdot 10^{-4} \cdot \left(\frac{T_i}{K} \right) + 3 \cdot .002394 \cdot 10^{-8} \cdot \left(\frac{T_i}{K} \right)^2 - 4 \cdot .1669 \cdot 10^{-13} \cdot \left(\right. \right. \\ \left[.00314 - 2 \cdot .1278 \cdot 10^{-5} \cdot \left(\frac{T_i}{K} \right) + 3 \cdot .002394 \cdot 10^{-8} \cdot \left(\frac{T_i}{K} \right)^2 - 4 \cdot .1669 \cdot 10^{-13} \right. \end{array} \right.$$

$$UCp_{cd_i} := \left[\left(dCp_{cd_i} \right)^2 \cdot \left(UT_i \right)^2 \right]^{.5}$$

$$dCp_{w_i} := \frac{R_{universal}}{MW_{water}} \cdot \left\| \begin{array}{l} \left[.003475 - 2 \cdot .0635 \cdot 10^{-4} \cdot \left(\frac{T_i}{K} \right) + 3 \cdot .06968 \cdot 10^{-7} \cdot \left(\frac{T_i}{K} \right)^2 - 4 \cdot .02506 \cdot 10^{-10} \cdot \left(\frac{T_i}{K} \right)^3 \right. \\ \left[.00305 - 2 \cdot .0873 \cdot 10^{-5} \cdot \left(\frac{T_i}{K} \right) + 3 \cdot .1201 \cdot 10^{-9} \cdot \left(\frac{T_i}{K} \right)^2 - 4 \cdot .06392 \cdot 10^{-13} \cdot \left(\frac{T_i}{K} \right)^3 \right] \end{array} \right.$$

$$UCp_{w_i} := \left[\left(dCp_{w_i} \right)^2 \cdot \left(UT_i \right)^2 \right]^{.5}$$

$$dCp_{n_i} := \frac{R_{universal}}{MW_{nitrogen}} \cdot \left| \begin{array}{l} .001408 - 2 \cdot .03963 \cdot 10^{-4} \cdot \left(\frac{T_i}{K} \right) + 3 \cdot .05641 \cdot 10^{-7} \cdot \left(\frac{T_i}{K} \right)^2 - 4 \cdot .02445 \cdot 10^{-10} \cdot \left(\frac{T_i}{K} \right) \\ .001488 - 2 \cdot .05685 \cdot 10^{-5} \cdot \left(\frac{T_i}{K} \right) + 3 \cdot .10097 \cdot 10^{-9} \cdot \left(\frac{T_i}{K} \right)^2 - 4 \cdot .06753 \cdot 10^{-13} \cdot \left(\frac{T_i}{K} \right) \end{array} \right.$$

$$UCp_{n_i} := \left[\left(dCp_{n_i} \right)^2 \cdot \left(UT_i \right)^2 \right]^{.5}$$

$$dCp_{o_i} := \frac{R_{universal}}{MW_{oxygen}} \cdot \left| \begin{array}{l} .001127 - 2 \cdot .05756 \cdot 10^{-5} \cdot \left(\frac{T_i}{K} \right) + 3 \cdot .13139 \cdot 10^{-8} \cdot \left(\frac{T_i}{K} \right)^2 - 4 \cdot .08768 \cdot 10^{-11} \cdot \left(\frac{T_i}{K} \right)^3 \\ .0006135 - 2 \cdot .12588 \cdot 10^{-6} \cdot \left(\frac{T_i}{K} \right) + 3 \cdot .01775 \cdot 10^{-9} \cdot \left(\frac{T_i}{K} \right)^2 - 4 \cdot .11364 \cdot 10^{-14} \cdot \left(\frac{T_i}{K} \right) \end{array} \right.$$

$$UCp_{o_i} := \left[\left(dCp_{o_i}\right)^2 \cdot \left(UT_i\right)^2\right]^{.5}$$

$$dCpp_{cd_i} := mf_{CO2} \qquad dCpp_{w_i} := mf_{H2O} \qquad dCpp_{n_i} := mf_{N2} \qquad dCpp_{o_i} := mf_{O2}$$

$$UCpp_i := \frac{1}{K} \cdot \left[\left[\begin{array}{l}\left(dCpp_{cd_i}\right)^2 \cdot \left(UCp_{cd_i}\right)^2 + \left(dCpp_{w_i}\right)^2 \cdot \left(UCp_{w_i}\right)^2 \ldots \\ + \left(dCpp_{n_i}\right)^2 \cdot \left(UCp_{n_i}\right)^2 + \left(dCpp_{o_i}\right)^2 \cdot \left(UCp_{o_i}\right)^2\end{array}\right]\right]^{.5}$$

Uncertainty in the ratio of specific heats:

$$d\gamma_i := \left[\frac{1}{Cp_{products_i} - R_{products}} - \frac{Cp_{products_i}}{\left(Cp_{products_i} - R_{products}\right)^2}\right]$$

$$U\gamma_i := \left[\left(d\gamma_i\right)^2 \cdot \left(UCpp_i\right)^2 + \left(.5\% \cdot \gamma_i\right)^2\right]^{.5}$$

Uncertainty in the Rate of Heat Release:

$$dQnet_{P_{jj}} := \frac{\gamma_{jj}}{\gamma_{jj} - 1} \cdot dV\left(\theta_{jj}\right) \qquad dQnet_{V_{jj}} := \frac{1}{\gamma_{jj} - 1} \cdot dP_{jj}$$

$$dQnet_{\gamma_{jj}} := P_{jj} \cdot dV\left(\theta_{jj}\right) \cdot \left[\frac{1}{\gamma_{jj} - 1} - \frac{\gamma_{jj}}{\left(\gamma_{jj} - 1\right)^2}\right] - \frac{V\left(\theta_{jj}\right) \cdot dP_{jj}}{\left(\gamma_{jj} - 1\right)^2}$$

$$dQnet_{dP_{jj}} := \frac{1}{\gamma_{jj} - 1} \cdot V\left(\theta_{jj}\right)$$

$$UQ_{net_{jj}} := \left[\left(dQnet_{P_{jj}}\right)^2 \cdot \left(UP_{jj}\right)^2 + \left(dQnet_{V_{jj}}\right)^2 \cdot \left(Uv_{jj}\right)^2 + \left(dQnet_{\gamma_{jj}}\right)^2 \cdot \left(U\gamma_{jj}\right)^2\right]^{.5}$$

Note that in the above equation, I left out the contributions that dP and dV make to the uncertainty in UQ. This was done intentionally as when comparing the change in UQ_{net} with the uncertainty assoiciated with dP to UQ_{net} without the uncertainty in dP was negligible. As for dV I made an engineering assumption. When I looked at the uncertainty associated with the volume I noticed that

it was very small. Thus, the uncertainty associated with the change in volume would be even smaller and thereby negligible.

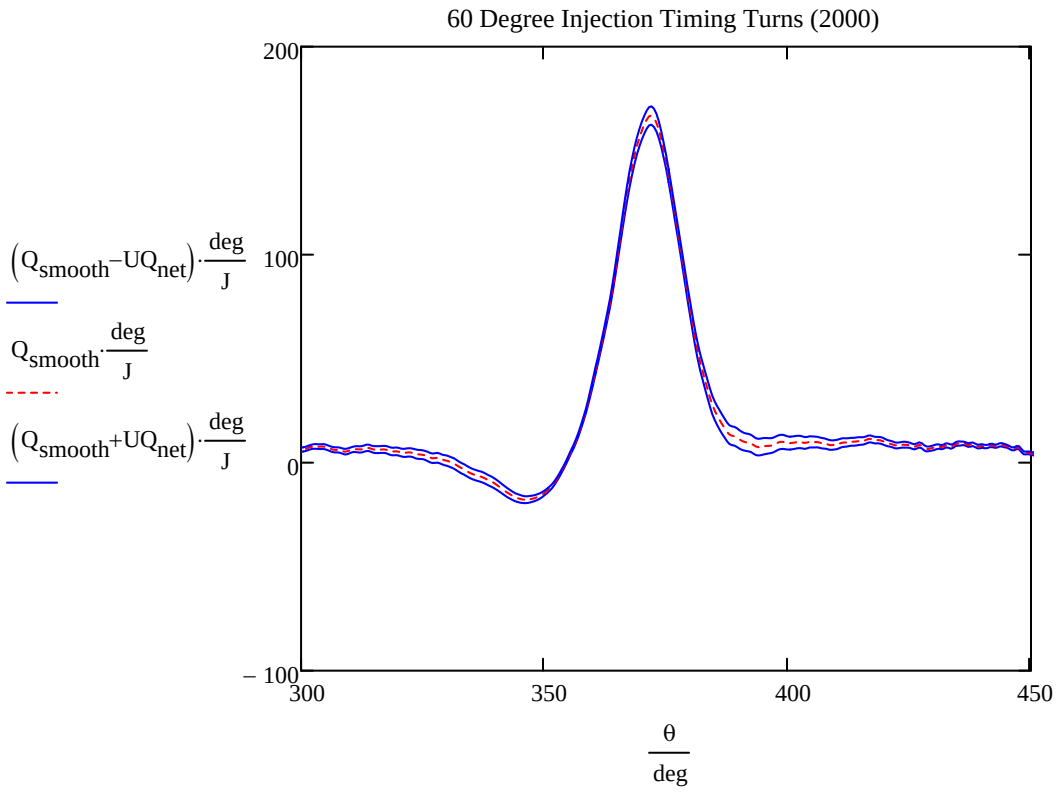

UPC and UMF Calculations:

$$UPC_P := \frac{1}{1426}\cdot\sum_{j=4}^{1429}\frac{\left(\frac{\gamma_j}{\gamma_j - 1}\cdot dV\left(\theta_j\right)\cdot UP_j\right)^2}{\left(UQ_{net_j}\right)^2} = 0.57$$

$$UPC_\gamma := \frac{1}{1426}\cdot\sum_{j=4}^{1429}\frac{\left[\left[\frac{P_j\cdot dV\left(\theta_j\right)}{\gamma_j - 1} - \frac{V\left(\theta_j\right)\cdot dP_j}{\left(\gamma_j - 1\right)^2} - \frac{\gamma_j\cdot P_j\cdot dV\left(\theta_j\right)}{\left(\gamma_j - 1\right)^2}\right]\cdot U\gamma_j\right]^2}{\left(UQ_{net_j}\right)^2} = 0.27$$

$$UPC_V := \frac{1}{1426} \cdot \sum_{j=4}^{1429} \frac{\left(\frac{dP_j}{\gamma_j - 1} \cdot Uv_j \right)^2}{\left(UQ_{net_j} \right)^2} = 0.16$$

$$j := 4, 5 .. 1429$$

$$UMF_{P_j} := \frac{P_j}{dQ_{net_j}} \cdot \left(\frac{\gamma_j}{\gamma_j - 1} \cdot dV\left(\theta_j\right) \right)$$

$$UMF_{\gamma_j} := \frac{\gamma_j}{dQ_{net_j}} \cdot \left[\frac{P_j \cdot dV\left(\theta_j\right)}{\gamma_j - 1} - \frac{V\left(\theta_j\right) \cdot dP_j}{\left(\gamma_j - 1\right)^2} - \frac{\gamma_j \cdot P_j \cdot dV\left(\theta_j\right)}{\left(\gamma_j - 1\right)^2} \right]$$

$$UMF_{V_j} := \frac{V\left(\theta_j\right)}{dQ_{net_j}} \cdot \frac{dP_j}{\gamma_j - 1}$$

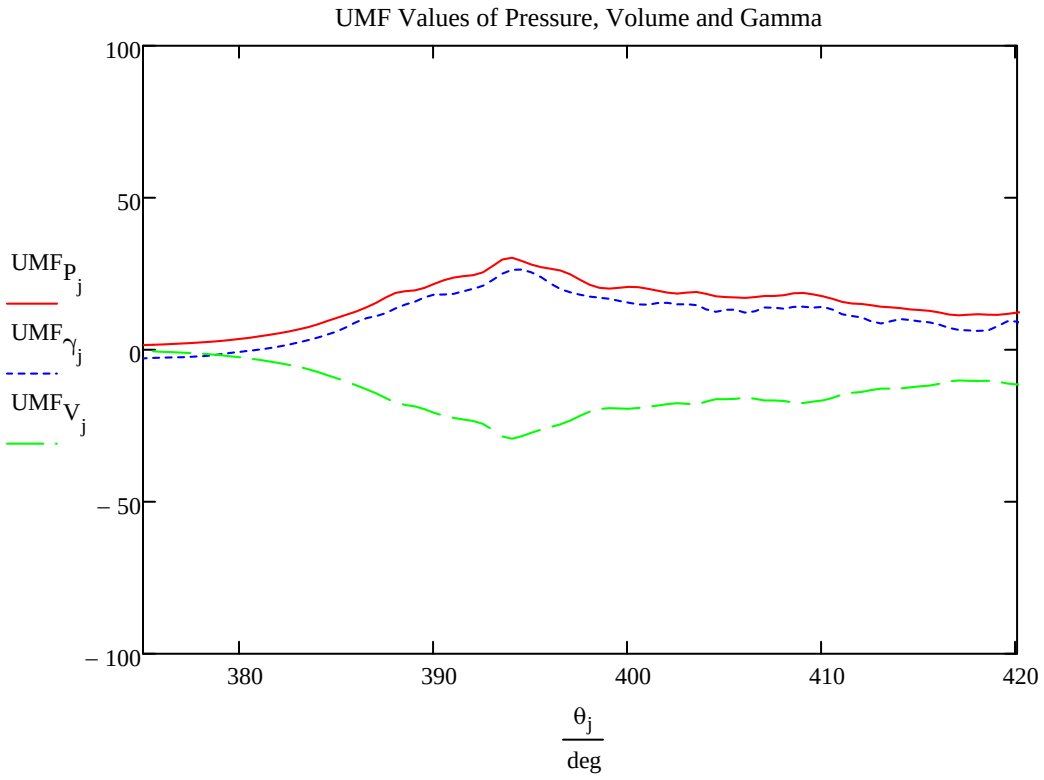

Determination of the Work and IMEP:

$$Work_i := \left(Pf60_{mean_i}\right)\cdot dV\left(\theta_i\right)\cdot \Delta\theta \qquad kW := 1\cdot\frac{kJ}{s}$$

$$IW := \sum_i \left[\left(Pf60_{mean_i}\right)\cdot dV\left(\theta_i\right)\cdot \Delta\theta\right]$$

$$P_b := IW\cdot\frac{1700}{2.0\cdot 60\cdot s} \qquad P_b = 21.58\cdot kW \qquad IMEP := \frac{IW}{V_d}$$

Uncertainty calculation for the Work and IMEP:

$$dW_{dP} := \sum_{i=0}^{1437}\left(dV\left(\theta_i\right)\cdot\Delta\theta\right) \qquad dW_{ddV} := \sum_{i=0}^{1437}\left(Pf60_{mean_i}\cdot\Delta\theta\right)$$

$$UW := \sum_{i=0}^{1437} \sqrt{dW_{dP}{}^2 \cdot \left(UP_i\right)^2} = 3.729\,J$$

$$UIMEP := \left[\left(\frac{1}{V_d}\right)^2 \cdot UW^2\right]^{.5} = 0.015 \cdot bar$$

Uncertainty Percentages of Full Scale Value

$iii := 1, 2 .. 1437 \qquad Pf_{mean_{iii}} := P_{iii}$

$$X_{iii} := \frac{UP_{iii}}{Pf_{mean_{iii}}} \qquad mean(X) = 0.026$$

$$Y_{iii} := \frac{Uv_{iii}}{V\left(\theta_{iii}\right)} \qquad mean(Y) = 7.584 \times 10^{-3}$$

$$Z_{iii} := \frac{U\gamma_{iii}}{\gamma_{iii}} \qquad mean(Z) = 5.318 \times 10^{-3} \qquad mean\left(\frac{UQ_{net}}{Q_{smooth}}\right) = 0.224$$

Uncertainty calculation for the Work and IMEP witha 1.0% error in CA resolution and displacement volume:

$$dW_{dP} := \sum_{i=0}^{1437} \left(dV\left(\theta_i\right) \cdot \Delta\theta\right) \qquad dW_{dV} := \sum_{i=0}^{1437} \left(Pf60_{mean_i} \cdot \Delta\theta\right)$$

$$UW := \sum_{i=0}^{1437} \sqrt{dW_{dP}{}^2 \cdot \left(UP_i\right)^2 + \left(Pf60_{mean_i} \cdot dV\left(\theta_i\right)\right)^2 \cdot (.01 \cdot \Delta\theta)^2} = 62.364\,J$$

$$UIMEP := \left[\left(\frac{1}{V_d}\right)^2 \cdot UW^2\right]^{.5} = 0.256 \cdot bar \qquad \frac{UIMEP}{IMEP} = 4.094 \cdot \%$$

$$\frac{\Delta\theta}{2} \cdot \sum_{i=4}^{1428} \left(Q_{smooth_{i+1}} + Q_{smooth_i}\right) = 2.001 \cdot kJ$$

$$\frac{\Delta\theta}{2} \cdot \sum_{i=4}^{1428} \left(UQ_{net_{i+1}} + UQ_{net_i}\right) = 525.112\,J$$

Detailed Uncertainty Analysis for 60 Degree Injection Timing Implementing a Constant Gamma Assumption.

Common Conversions:

$bar := 100000 \cdot Pa$ $kmol := 1000 \cdot mol$ $kJ := 1000 \cdot J$ $kPa := 1000 \cdot Pa$

$Rev := 2 \cdot \pi \cdot rad$

Engine Specifications:

$Gas_{dot} := 72.2 \cdot \frac{gm}{min}$ $Air_{dot} := 2850 \cdot \frac{gm}{min}$ $Diesel_{dot} := 3.3 \cdot \frac{gm}{min}$

$T_o := 348 \cdot K$ $P_o := 1.41 \cdot bar$ $\Delta\theta := .5 \cdot deg$ $N := 1700 \cdot \frac{Rev}{min}$

$\theta_{inj} := 60 \cdot deg$ $P_{exh} := 13 \cdot bar$ $\theta_{IVO} := 685 \cdot deg$ $\theta_{IVC} := 217 \cdot deg$

$\theta_{EVO} := 506 \cdot deg$ $\theta_{EVC} := 10 \cdot deg$

$b := .13716 \cdot m$ $s_c := .1651 \cdot m$ $l := .2612 \cdot m$ $a := \frac{s_c}{2}$ $r := 14.5$

Smoothing the Pressure Data (Motoring and Firing)

Motoring :=

	0
0	-5.371
1	…

$kk := 1, 2 .. 1438$ $y := 0 .. 1$ $N := 50$

$i := 1, 2 .. 1437$ $x := 0, 1 .. 49$

$$Pmsmooth1_{kk} := \frac{Motoring_{kk-1} + 2 \cdot Motoring_{kk} + Motoring_{kk+1}}{4}$$

$$Pmsmooth_i := \frac{Pmsmooth1_{i-1} + 2 \cdot Pmsmooth1_i + Pmsmooth1_{i+1}}{4}$$

$\theta_i := .5 \cdot i \cdot deg$

$Firing_{60deg} :=$

	0
0	...

$xx := 0, 1 .. 149 \quad NN := 150$

$$Pfsmooth1_{kk,xx} := \frac{Firing_{60deg_{kk-1,xx}} + 2 \cdot Firing_{60deg_{kk,xx}} + Firing_{60deg_{kk+1,xx}}}{4}$$

$$Pfsmooth_{i,xx} := \frac{Pfsmooth1_{i-1,xx} + 2 \cdot Pfsmooth1_{i,xx} + Pfsmooth1_{i+1,xx}}{4}$$

$\theta_i := .5 \cdot i \cdot deg$

$P_{f60}(i, xx) := Pfsmooth_{i,xx} \cdot bar$

$$Pf60_{mean_i} := \sum_{xx=0}^{149} \frac{P_{f60}(i, xx}{150} \quad Sx60_i := \left[\frac{1}{149} \sum_{xx=0}^{149} \left(P_{f60}(i, xx) - Pf60_{mean_i} \right)^2 \right]^{.5}$$

$$Pf60_{precision_{i,y}} := \begin{cases} \left(Pf60_{mean_i} + \frac{2 \cdot Sx60_i}{\sqrt{NN}} \right) & \text{if } y = 1 \\ \left(Pf60_{mean_i} - \frac{2 \cdot Sx60_i}{\sqrt{NN}} \right) & \text{if } y = 0 \end{cases} \qquad P60 := \left[\sum_{i=0}^{1437} \frac{\left(\frac{2 \cdot Sx60_i}{\sqrt{NN}} \right)}{1440} \right]$$

$Pf60_{mean} := Pf60_{mean} + 8.266 \cdot bar$

Volume Calculations:

$$V_d := \frac{\pi}{4} \cdot b^2 \cdot s_c \qquad V_d = 2.439 \times 10^3 \cdot cm^3 \qquad V_c := \frac{V_d}{r - 1}$$

$$V(\theta) := V_c + \frac{\pi}{4} \cdot b^2 \cdot \left[l + a - \left[\left(l^2 - a^2 \sin(\theta)^2 \right)^{.5} + a \cdot \cos(\theta) \right] \right]$$

$$dV(\theta) := \frac{d}{d\theta} V(\theta) \qquad ddV(\theta) := \frac{d}{d\theta} dV(\theta)$$

$\gamma_i := 1.38$ $P := Pf60_{mean}$

Pressure Derivative using the Pressure Smoothing Algorithm:

$j := 0, 1 .. 1433$

$$dP_j := \frac{P_j - 8 \cdot P_{j+1} + 8 \cdot P_{j+3} - P_{j+4}}{12 \cdot \Delta\theta}$$

Calculating the Net Heat Release Rate: $jj := 4, 5 .. 1429$

$$dQ_{net_j} := \frac{\gamma_j}{\gamma_j - 1} \cdot P_j \cdot \left(dV\left(\theta_j\right)\right) \ldots + \frac{1}{\gamma_j - 1} \cdot V\left(\theta_j\right) \cdot \left(dP_j\right)$$

$$Q_{smooth_{jj}} := \frac{1}{9} \cdot \left(\begin{matrix} dQ_{net_{jj-4}} + dQ_{net_{jj-3}} + dQ_{net_{jj-2}} + dQ_{net_{jj-1}} \ldots \\ + dQ_{net_{jj}} + dQ_{net_{jj+1}} + dQ_{net_{jj+2}} + dQ_{net_{jj+3}} + dQ_{net_{jj+4}} \end{matrix} \right)$$

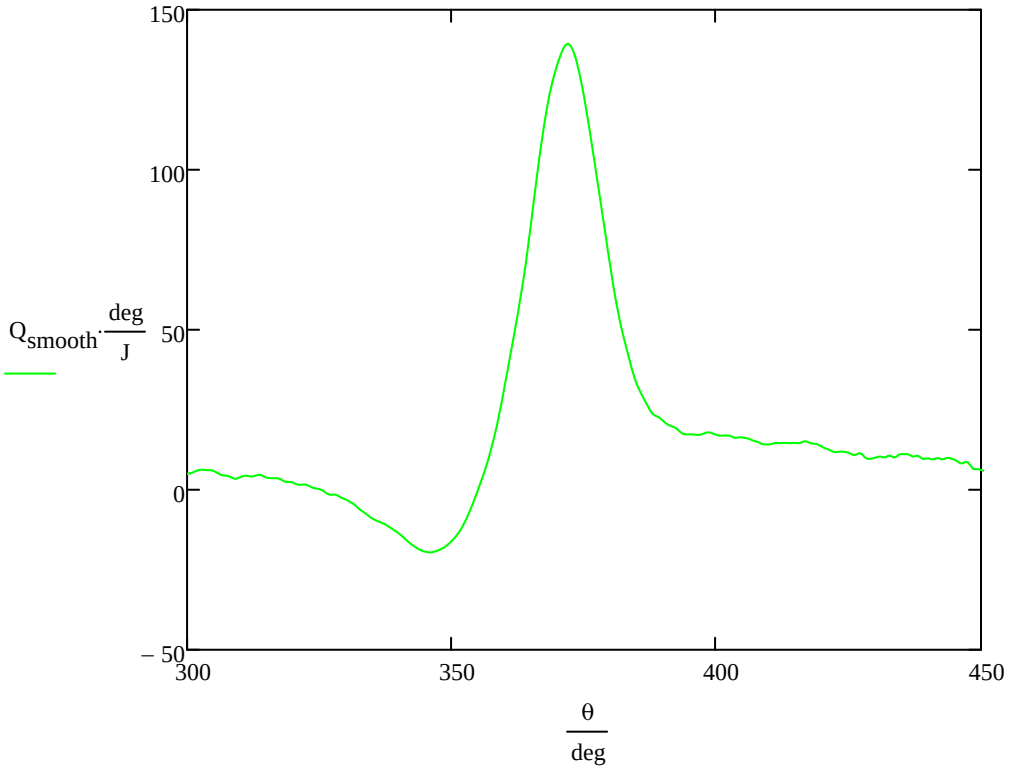

Uncertainties for each of the measured variables:

$Ub_\theta := 0.5 \cdot deg$ $Up_\theta := 0.1 \cdot deg$ $Ub_{To} := .75\% \cdot T_o$ $Up_{To} := 0 \cdot K$

$Ub_P := .4\% \cdot P$ $Up_P := P60$ $Ub_{Po} := .15\% \cdot P_o$ $Up_{Po} := 0 \cdot bar$

$U\theta := \left(Ub_\theta^{\,2} + Up_\theta^{\,2}\right)^{.5}$ $U\theta = 0.51 \cdot deg$

$UP := \left(Ub_P^{\,2} + Up_P^{\,2}\right)^{.5}$

$UTo := \left(Ub_{To}^{\,2} + Up_{To}^{\,2}\right)^{.5}$ $UTo = 2.61\,K$

$UPo := \left(Ub_{Po}^{\,2} + Up_{Po}^{\,2}\right)^{.5}$ $UPo = 2.115 \times 10^{-3} \cdot bar$

Uncertainty Calculation in Volume:

$$V = \frac{\pi}{4} \cdot b^2 \cdot s_c + \frac{\pi}{4} \cdot b^2 \cdot \left[l + a - \left[\left(l^2 - a^2 \cdot \sin(\theta)^2 \right)^{.5} + a \cdot \cos(\theta) \right] \right]$$

$$Uv^2 = \left(\frac{d}{d\theta}V\right)^2 \cdot U\theta^2$$ because engine specifications (bore, stroke length, etc.) are assumed to be constant

$$Uv^2 = \left[\frac{\pi \cdot bore^2}{4} \cdot \left[a \cdot \sin(\theta) + \frac{a^2}{\left(l^2 - a^2 \cdot \sin(\theta)^2\right)^{.5}} \cdot \sin(\theta) \cdot \cos(\theta)\right]\right]^2 \cdot U\theta^2$$

$$dv_i := \frac{\pi \cdot b^2}{4} \cdot \left[a \cdot \sin\left(\theta_i\right) + \frac{a^2}{\left(l^2 - a^2 \cdot \sin\left(\theta_i\right)^2\right)^{.5}} \cdot \sin\left(\theta_i\right) \cdot \cos\left(\theta_i\right)\right]$$

$$Uv_i := \left[\left(dv_i\right)^2 \cdot U\theta^2\right]^{.5}$$

Uncertainty in the ratio of specific heats:

$$U\gamma_i := \left[.028^2 + \left(.5\% \cdot \gamma_i\right)^2\right]^{.5}$$

Uncertainty in the Rate of Heat Release:

$$dQ_{net_{jj}} := \frac{\gamma_{jj}}{\gamma_{jj} - 1} \cdot P_{jj} \cdot \left(dV\left(\theta_{jj}\right)\right) \ldots + \frac{1}{\gamma_{jj} - 1} \cdot V\left(\theta_{jj}\right) \cdot \left(dP_{jj}\right)$$

$$dQnet_{P_{jj}} := \frac{\gamma_{jj}}{\gamma_{jj} - 1} \cdot dV\left(\theta_{jj}\right) \qquad dQnet_{V_{jj}} := \frac{1}{\gamma_{jj} - 1} \cdot dP_{jj}$$

$$dQnet_{dP_{jj}} := \frac{1}{\gamma_{jj} - 1} \cdot V\left(\theta_{jj}\right) \qquad dQnet_{\gamma_{jj}} := P_{jj} \cdot dV\left(\theta_{jj}\right) \cdot \left[\frac{1}{\gamma_{jj} - 1} - \frac{\gamma_{jj}}{\left(\gamma_{jj} - 1\right)^2}\right] - \frac{V\left(\theta_{jj}\right) \cdot dP_{jj}}{\left(\gamma_{jj} - 1\right)^2}$$

$$UQ_{net_{jj}} := \left[\left(dQnet_{P_{jj}}\right)^2 \cdot \left(UP_{jj}\right)^2 + \left(dQnet_{V_{jj}}\right)^2 \cdot \left(Uv_{jj}\right)^2 + \left(dQnet_{\gamma_{jj}}\right)^2 \cdot \left(U\gamma_{jj}\right)^2\right]^{.5}$$

Note that in the above equation, I left out the contributions that dP and dV make to the uncertainty in UQ. This was done intentionally as the calculation for dP is a numerical approximation and thereby has negligible uncertainty. As for dV I made an engineering assumption. When I looked at the uncertainty associated with the volume I noticed that it was very small. Thus, the uncertainty associated with the change in volume would be even smaller and thereby negligible.

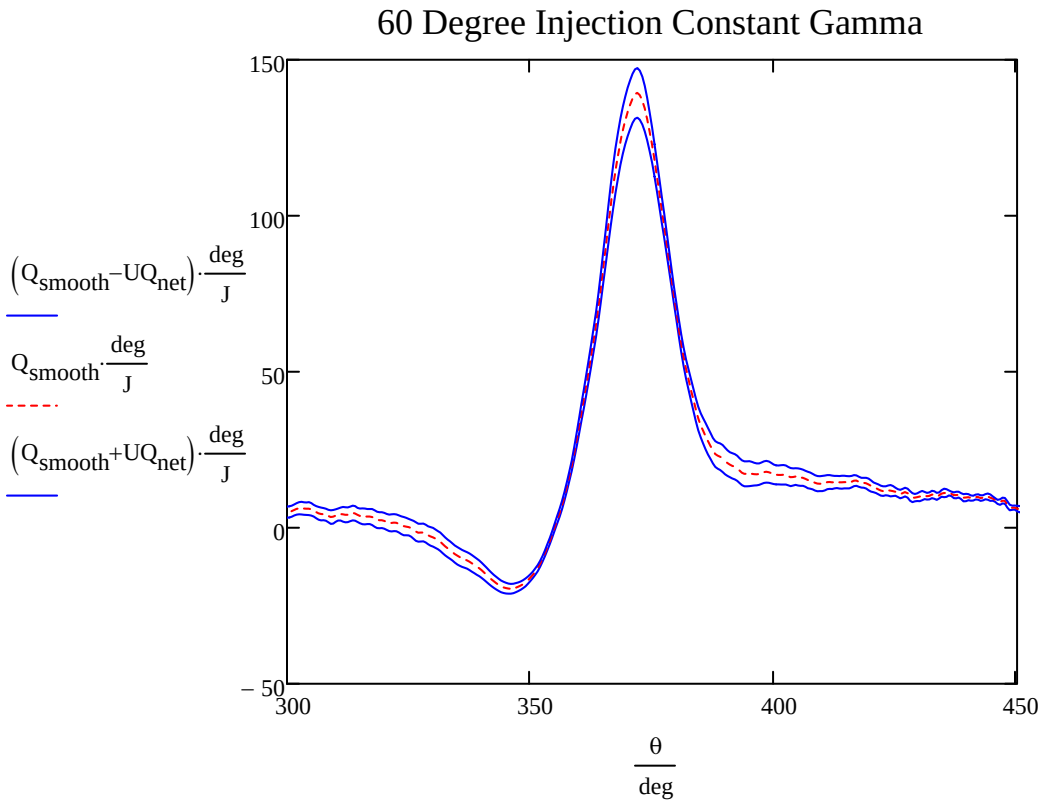
60 Degree Injection Constant Gamma
$\left(Q_{smooth} - UQ_{net}\right) \cdot \frac{deg}{J}$
$Q_{smooth} \cdot \frac{deg}{J}$
$\left(Q_{smooth} + UQ_{net}\right) \cdot \frac{deg}{J}$
150
100
50
0
− 50
300
350
400
450
θ
deg

UPC and UMF Calculations:

$$UPC_P := \frac{1}{1426} \cdot \sum_{j=4}^{1429} \frac{\left(\frac{\gamma_j}{\gamma_j - 1} \cdot dV(\theta_j) \cdot UP_j \right)^2}{\left(UQ_{net_j} \right)^2} = 0.271$$

$$UPC_\gamma := \frac{1}{1426} \cdot \sum_{j=4}^{1429} \frac{\left[\left[\frac{P_j \cdot dV(\theta_j)}{\gamma_j - 1} - \frac{V(\theta_j) \cdot dP_j}{(\gamma_j - 1)^2} - \frac{\gamma_j \cdot P_j \cdot dV(\theta_j)}{(\gamma_j - 1)^2} \right] \cdot U\gamma_j \right]^2}{\left(UQ_{net_j} \right)^2} = 0.643$$

$$UPC_V := \frac{1}{1426} \cdot \sum_{j=4}^{1429} \frac{\left(\frac{dP_j}{\gamma_j - 1} \cdot Uv_j \right)^2}{\left(UQ_{net_j} \right)^2} = 0.086$$

$$j := 4, 5 .. 1429$$

$$UMF_{P_j} := \frac{P_j}{dQ_{net_j}} \cdot \left(\frac{\gamma_j}{\gamma_j - 1} \cdot dV(\theta_j) \right)$$

$$UMF_{\gamma_j} := \frac{\gamma_j}{dQ_{net_j}} \cdot \left[\frac{P_j \cdot dV(\theta_j)}{\gamma_j - 1} - \frac{V(\theta_j) \cdot dP_j}{(\gamma_j - 1)^2} - \frac{\gamma_j \cdot P_j \cdot dV(\theta_j)}{(\gamma_j - 1)^2} \right]$$

$$UMF_{V_j} := \frac{V(\theta_j)}{dQ_{net_j}} \cdot \frac{dP_j}{\gamma_j - 1}$$

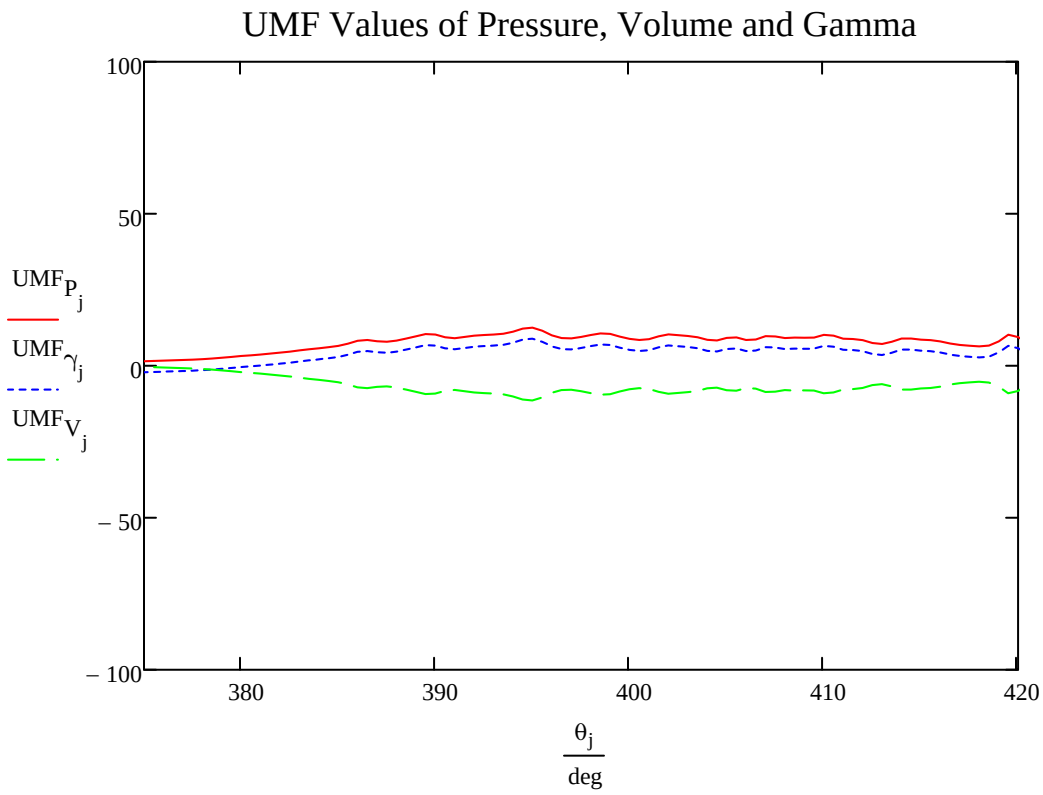

$$\text{Work} := \sum_{i=0}^{1437} \left[\left(\text{Pf60}_{\text{mean}_i} \right) \cdot \text{dV}\left(\theta_i \right) \cdot \Delta\theta \right]$$

$$\text{Work} = 1.523 \cdot \text{kJ}$$

$$P_b := \text{Work} \cdot \frac{1700}{2.0 \cdot 60 \cdot \text{s}} \qquad P_b = 21.58 \cdot \frac{\text{kJ}}{\text{s}} \qquad \text{IMEP} := \frac{\text{Work}}{V_d} = 6.244 \cdot \text{bar}$$

$$\frac{\Delta\theta}{2}\cdot\sum_{i=4}^{1428}\left(Q_{smooth_{i+1}}+Q_{smooth_i}\right)=1.948\cdot kJ$$

$$\frac{\Delta\theta}{2}\cdot\sum_{i=4}^{1428}\left(UQ_{net_{i+1}}+UQ_{net_i}\right)=810.529\,J$$

APPENDIX B

PLOTS OF ROHR UNCERTAINTY BANDS

15 Degree BTDC Injection Timing:

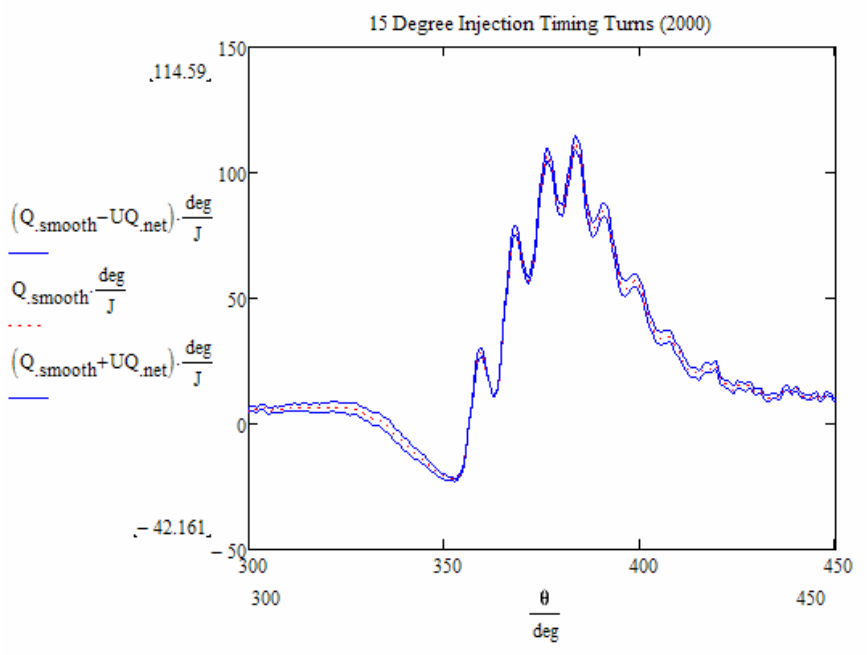

Figure B.1: 15 Degree BTDC Injection Turns (2000) Correlations

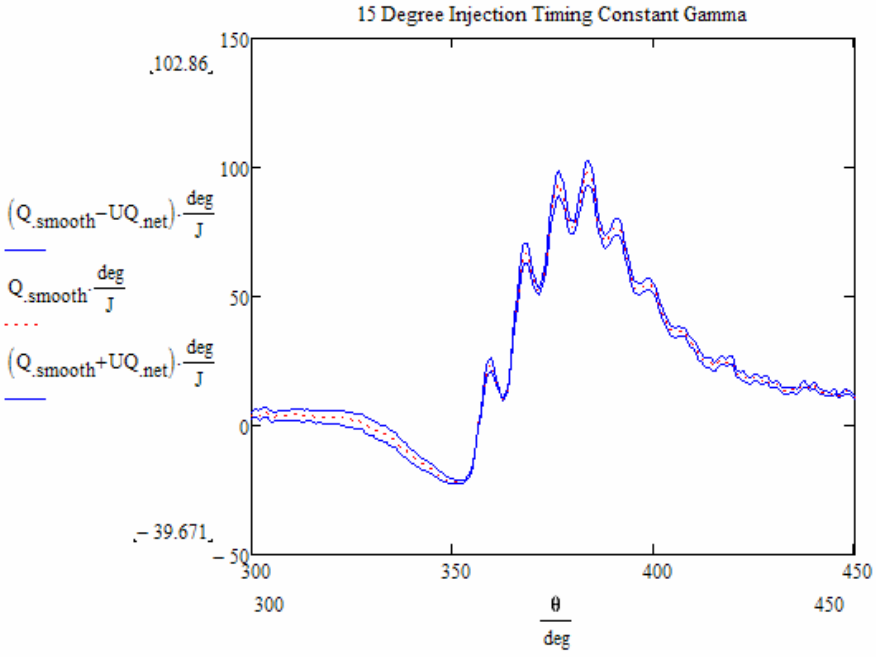

Figure B.2: 15 Degree BTDC Injection Constant Gamma Assumption

20 Degree Injection Timing:

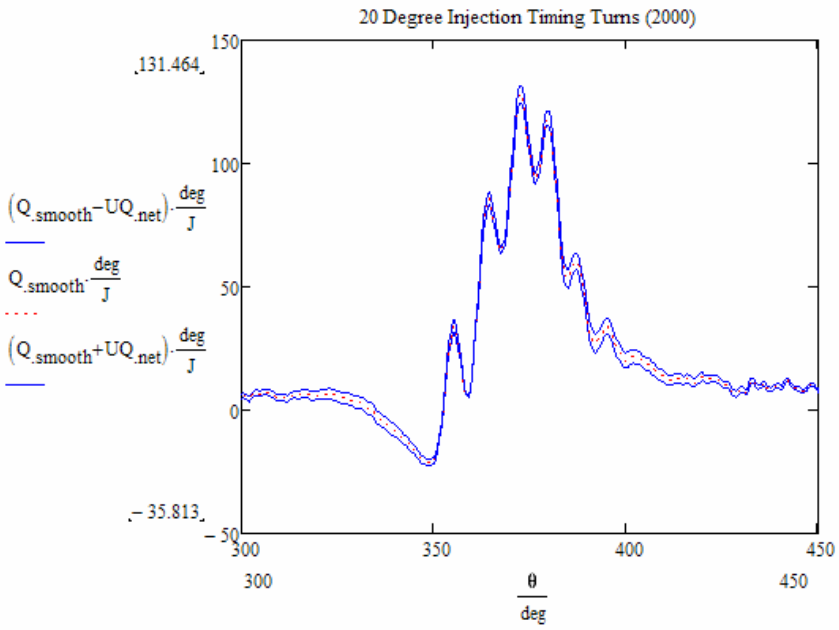

Figure B.3: 20 Degree BTDC Injection Turns (2000) Correlations

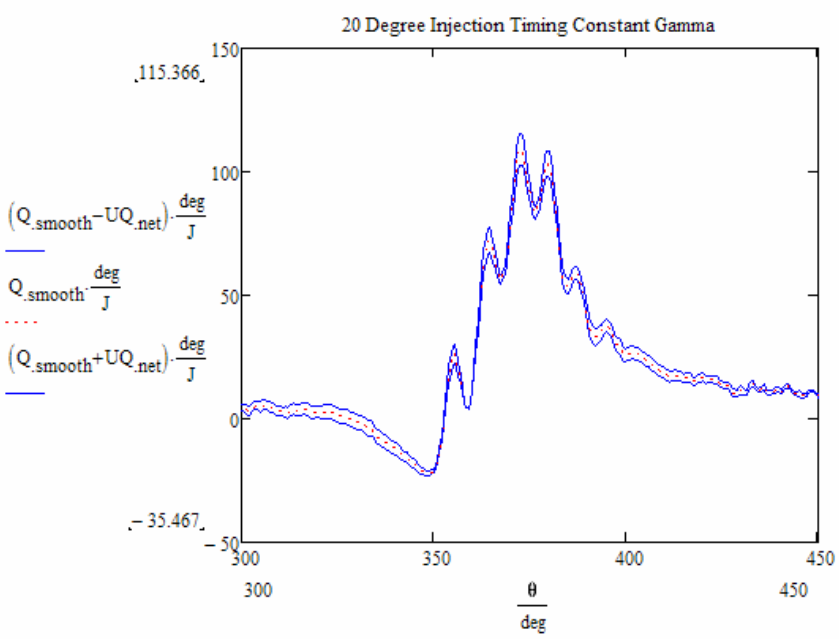

Figure B.4: 20 Degree BTDC Injection Constant Gamma Assumption

25 Degree BTDC Injection Timing:

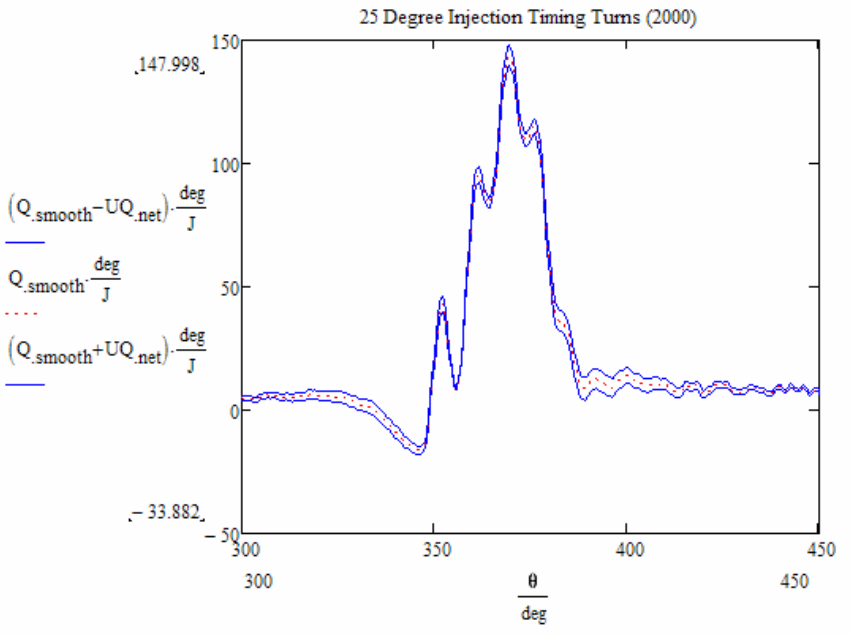

Figure B.5: 25 Degree BTDC Injection Turns (2000) Correlations

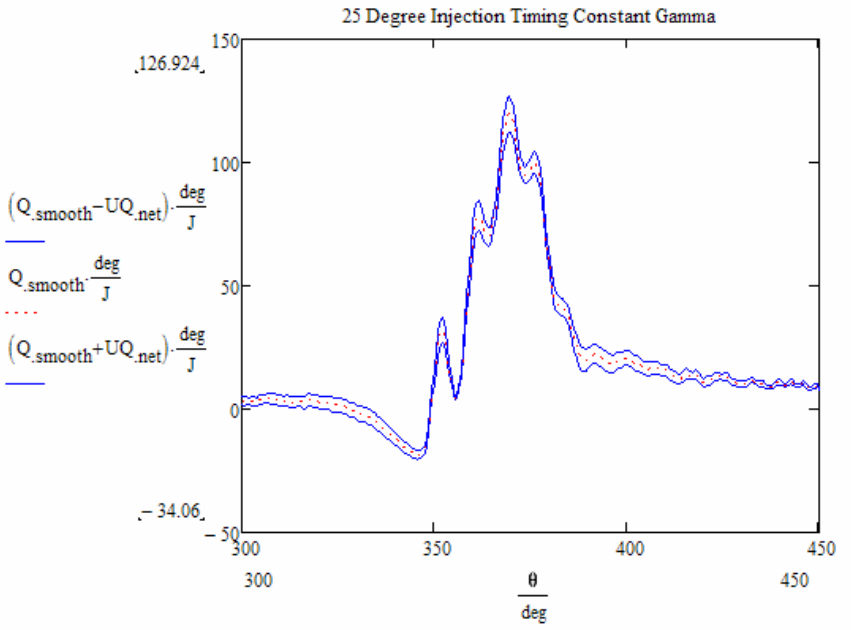

Figure B.6: 25 Degree BTDC Injection Constant Gamma Assumption

30 Degree BTDC Injection Timing:

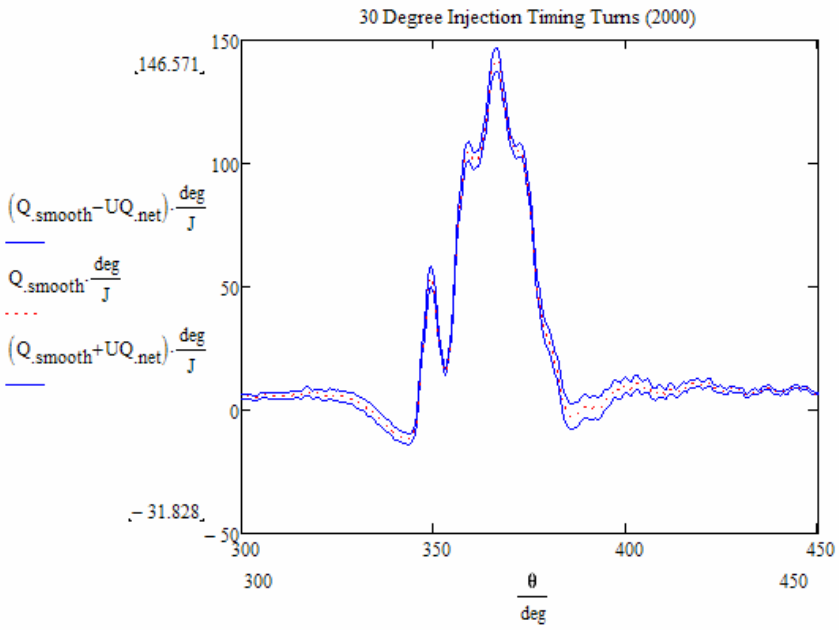

Figure B.7: 30 Degree BTDC Injection Turns (2000) Correlations

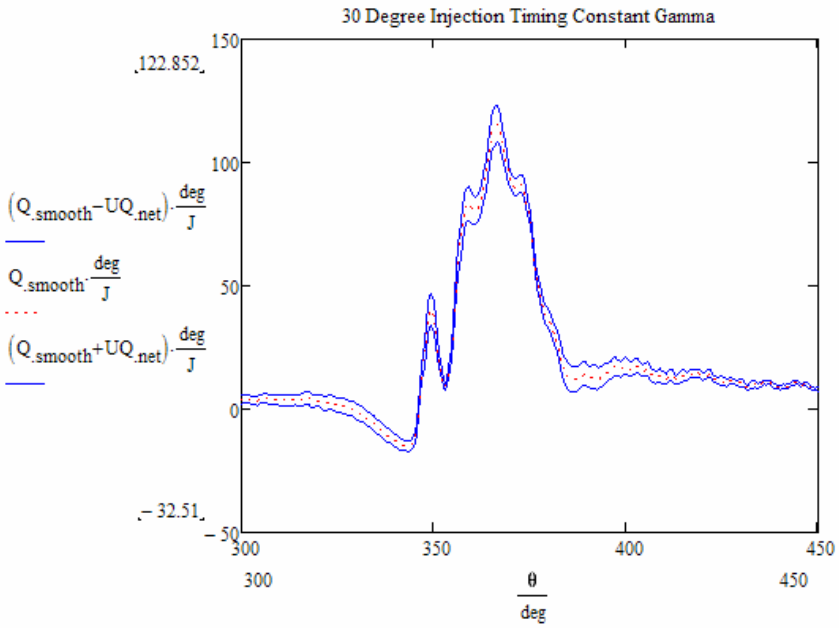

Figure B.8: 30 Degree BTDC Injection Constant Gamma Assumption

35 Degree BTDC Injection Timing:

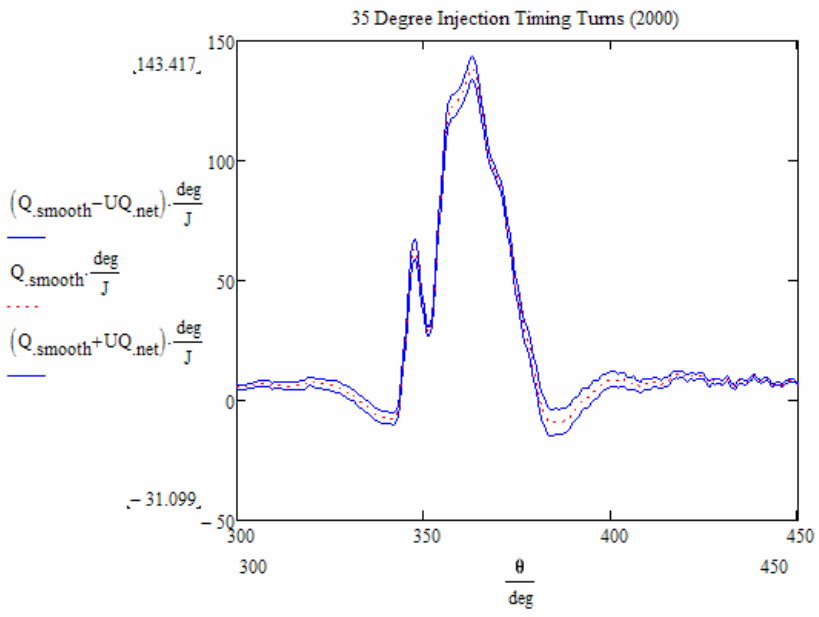

Figure B.9: 35 Degree BTDC Injection Turns (2000) Correlations

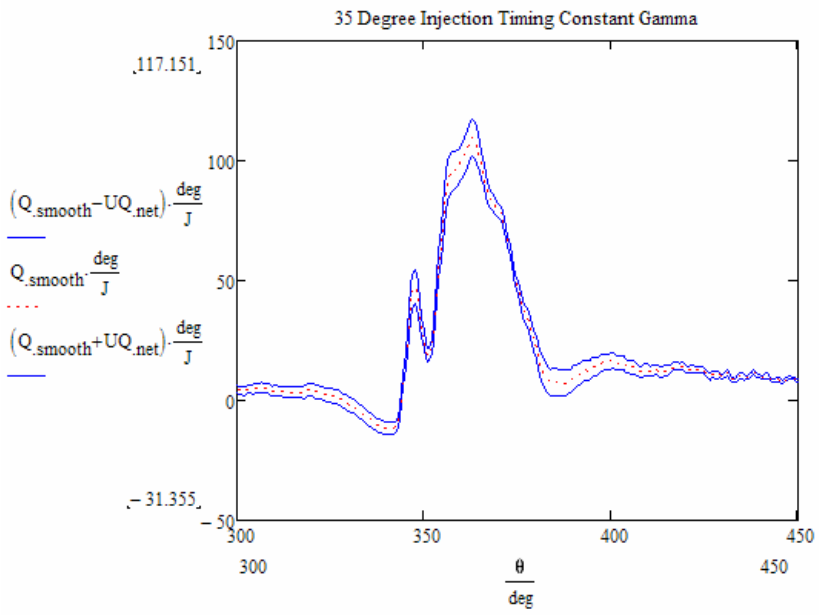

Figure B.10: 35 Degree BTDC Injection Constant Gamma Assumption

40 Degree BTDC Injection Timing:

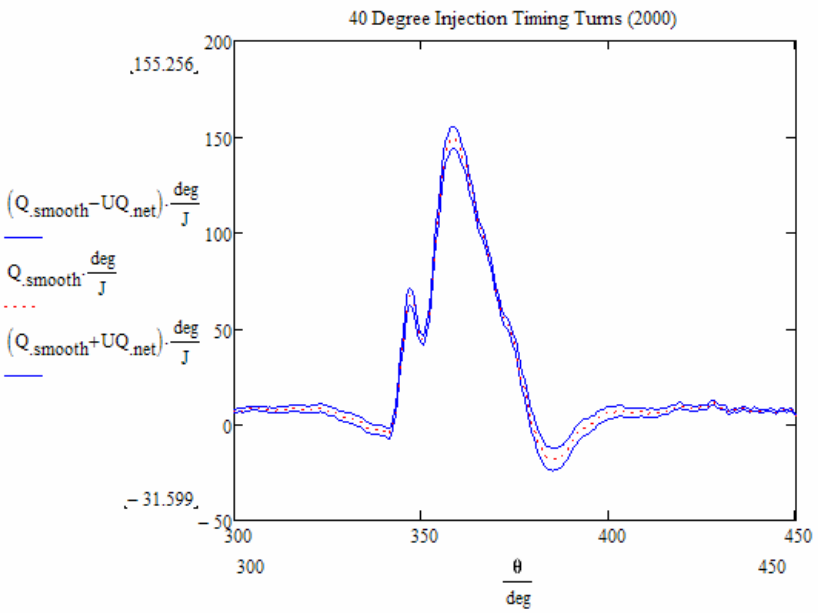

Figure B.11: 40 Degree BTDC Injection Turns (2000) Correlations

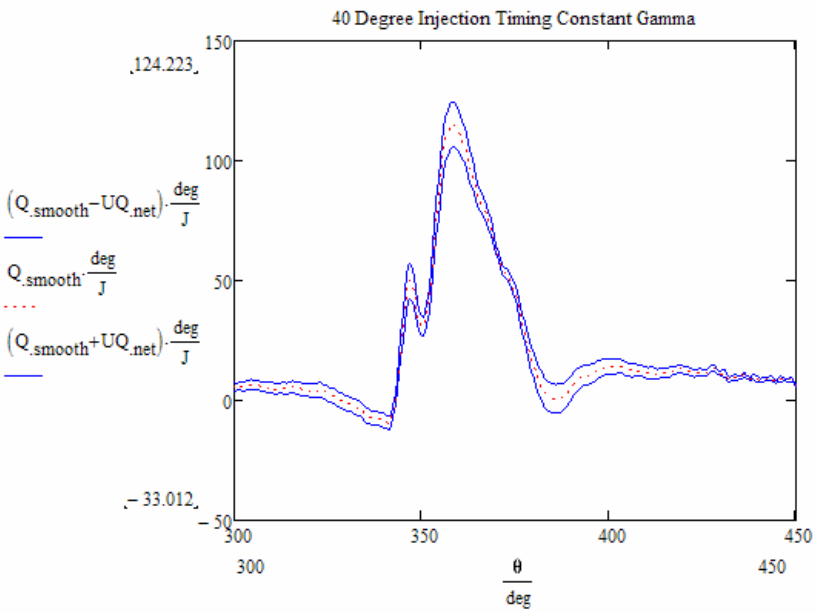

Figure B.12: 40 Degree BTDC Injection Constant Gamma Assumption

45 Degree BTDC Injection Timing:

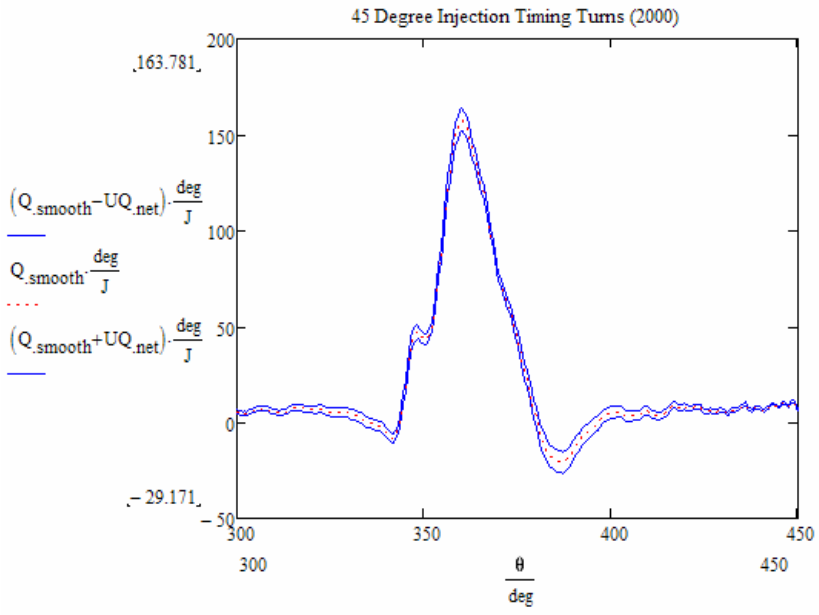

Figure B.13: 45 Degree BTDC Injection Turns (2000) Correlations

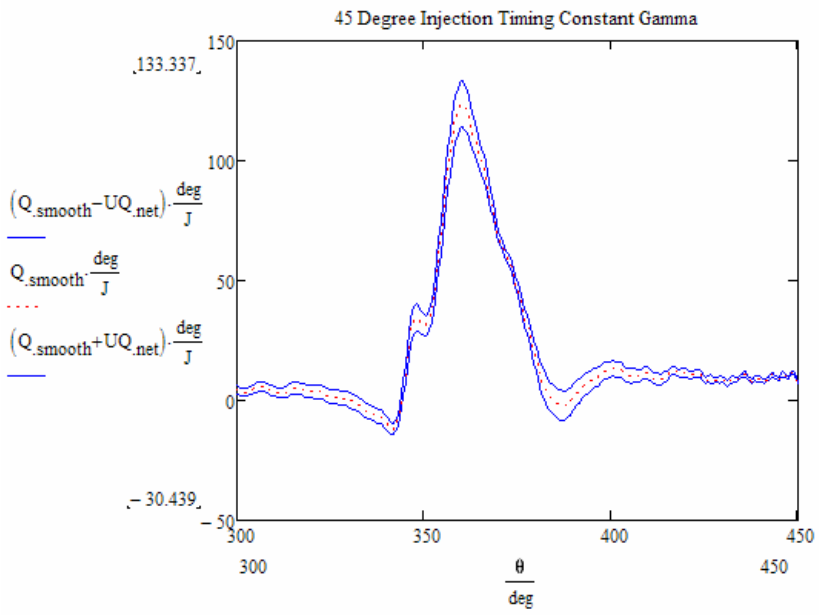

Figure B.14: 45 Degree BTDC Injection Constant Gamma Assumption

50 Degree BTDC Injection Timing:

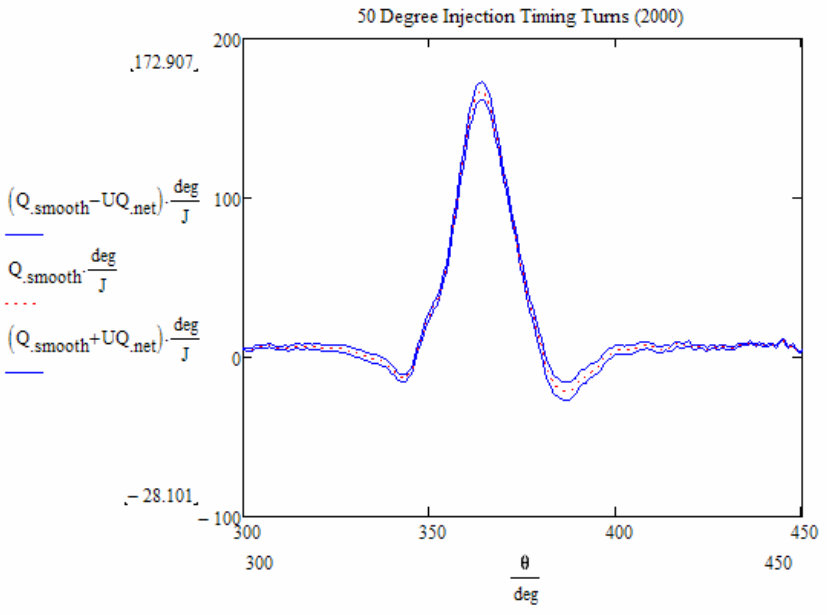

Figure B.15: 50 Degree BTDC Injection Turns (2000) Correlations

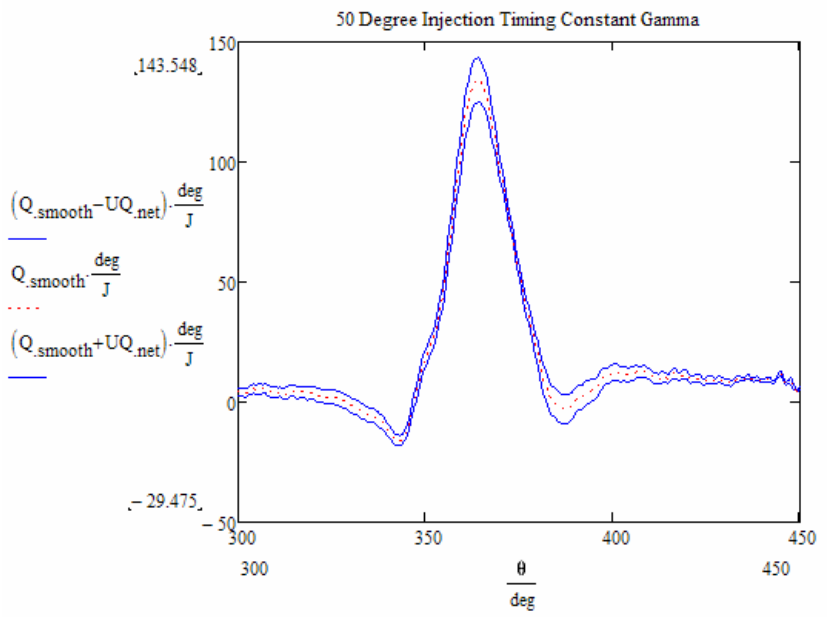

Figure B.16: 50 Degree BTDC Injection Constant Gamma Assumption

55 Degree BTDC Injection Timing:

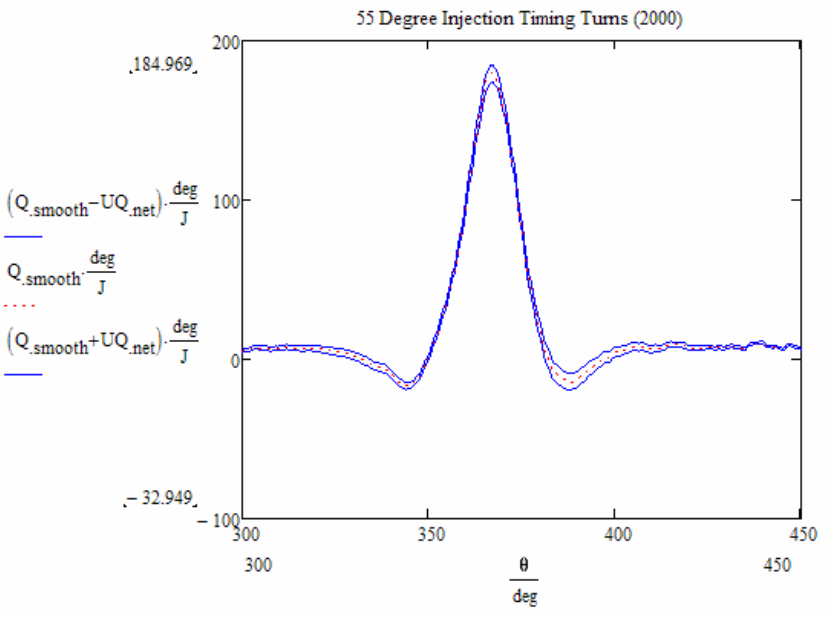

Figure B.17: 55 Degree BTDC Injection Turns (2000) Correlations

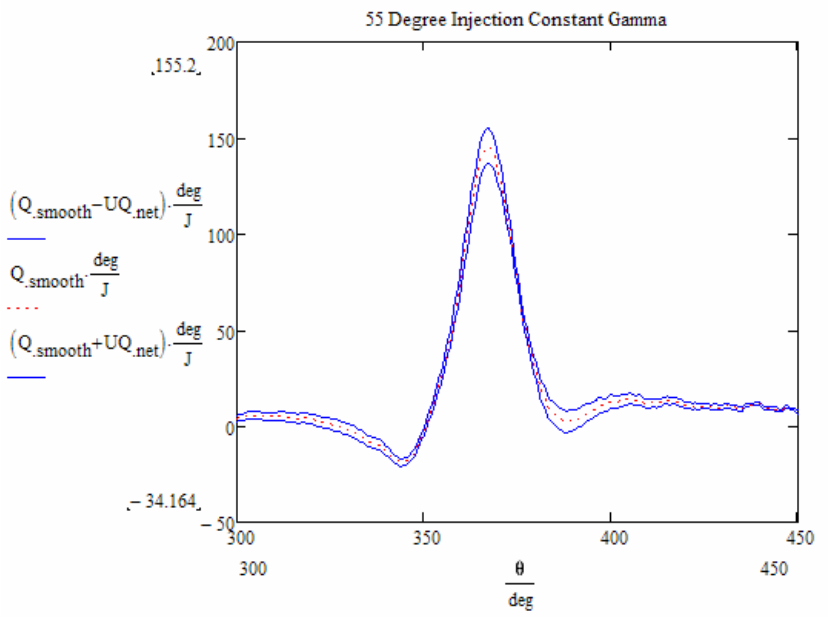

Figure B.18: 55 Degree BTDC Injection Constant Gamma Assumption

60 Degree BTDC Injection Timing:

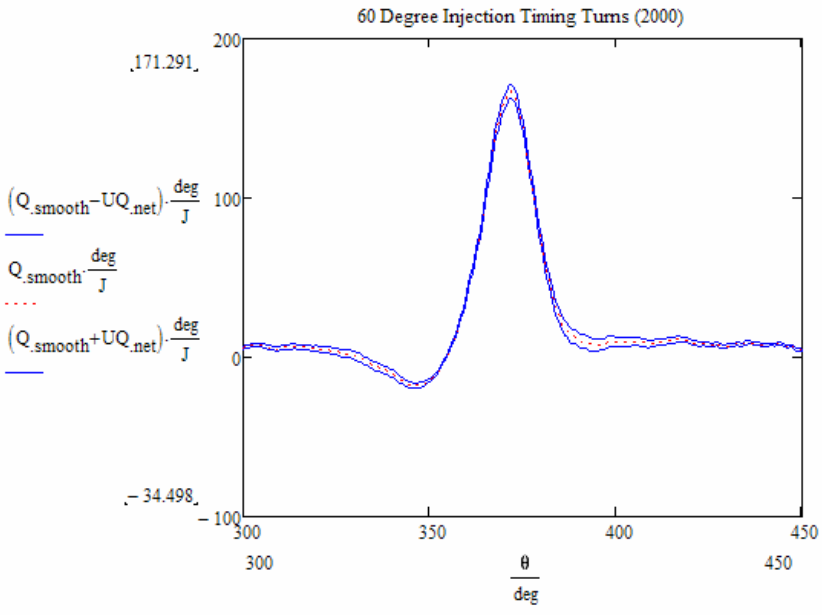

Figure B.19: 60 Degree BTDC Injection Turns (2000) Correlations

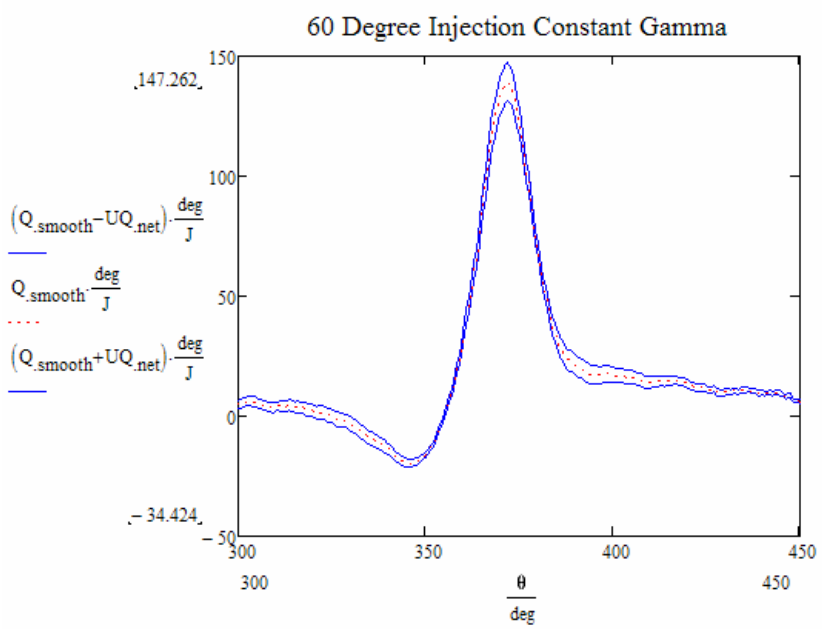

Figure B.20: 60 Degree BTDC Injection Constant Gamma Assumption

60 Degree BTDC Injection Timing Continued:

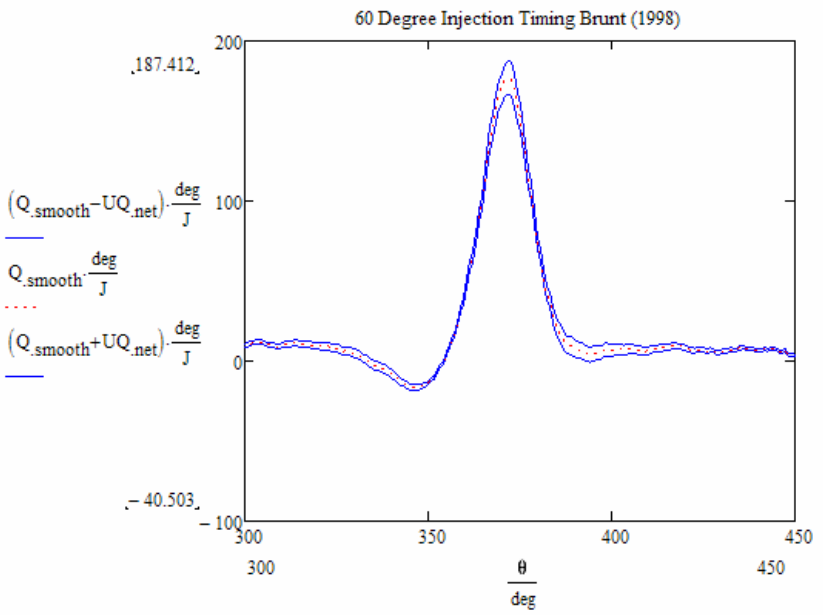

Figure B.21: 60 Degree BTDC Injection Brunt (1998) Correlations

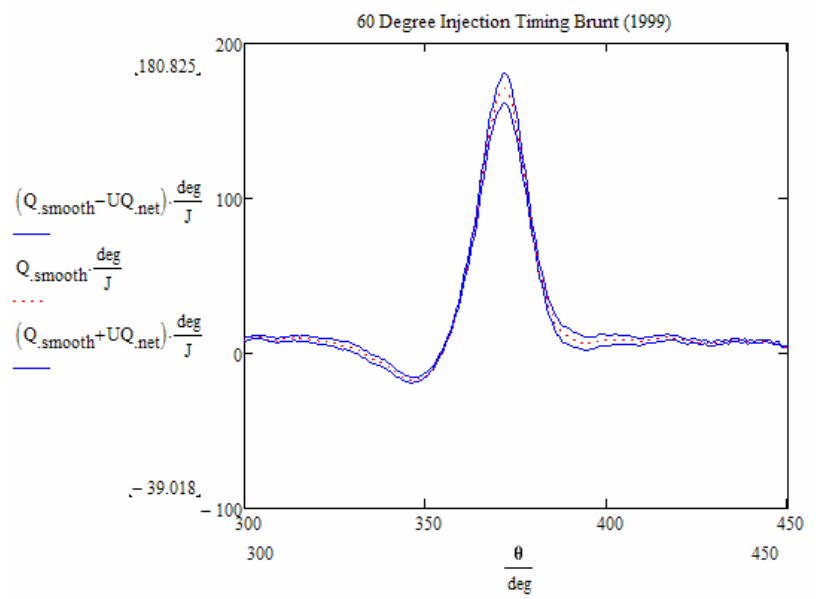

Figure B.22: 60 Degree BTDC Injection Brunt (1999) Correlations

APPENDIX C

ROHR UPC AND UMF PLOTS

15 Degree BTDC Injection Timing:

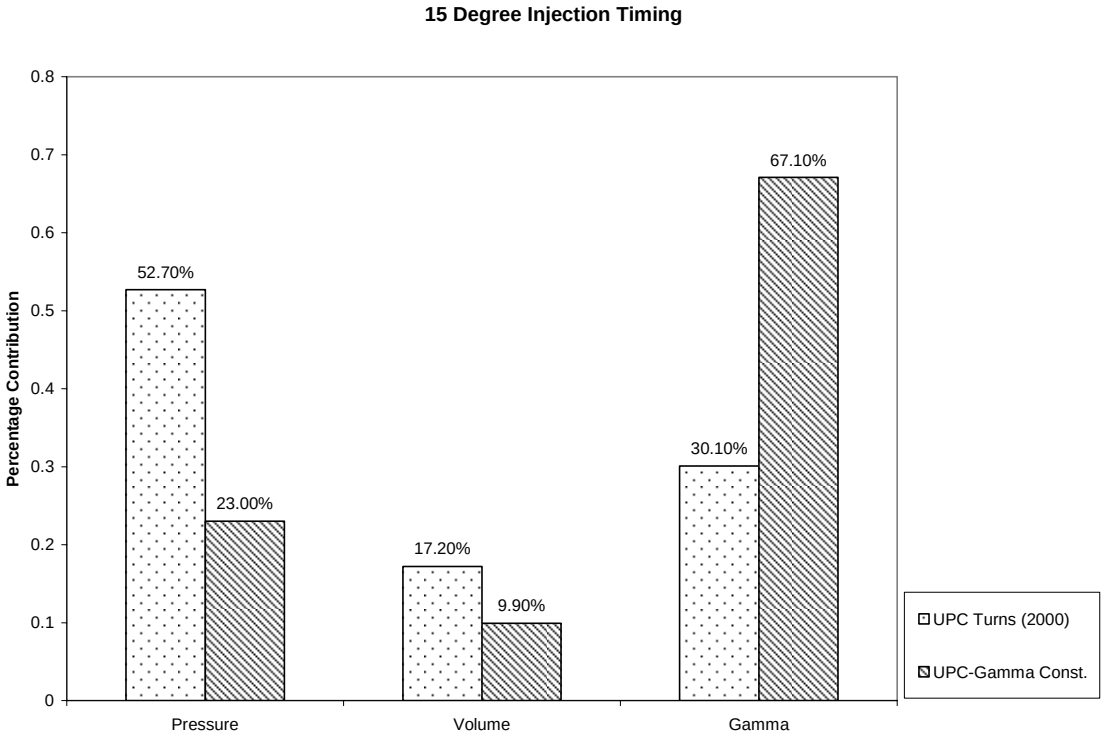

Figure C.1: 15 Degree BTDC Injection UPC Values

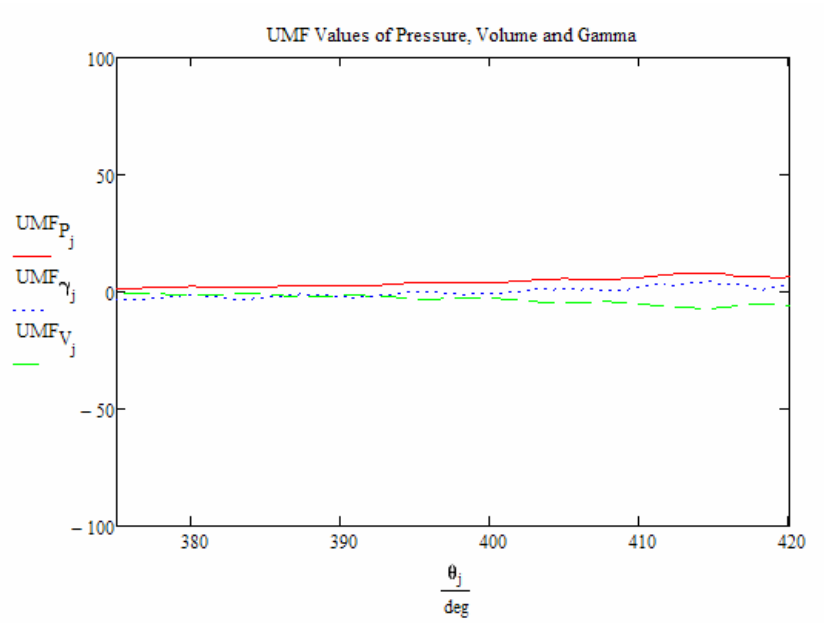

Figure C.2: 15 Degree BTDC Injection Turns (2000) UMF Values

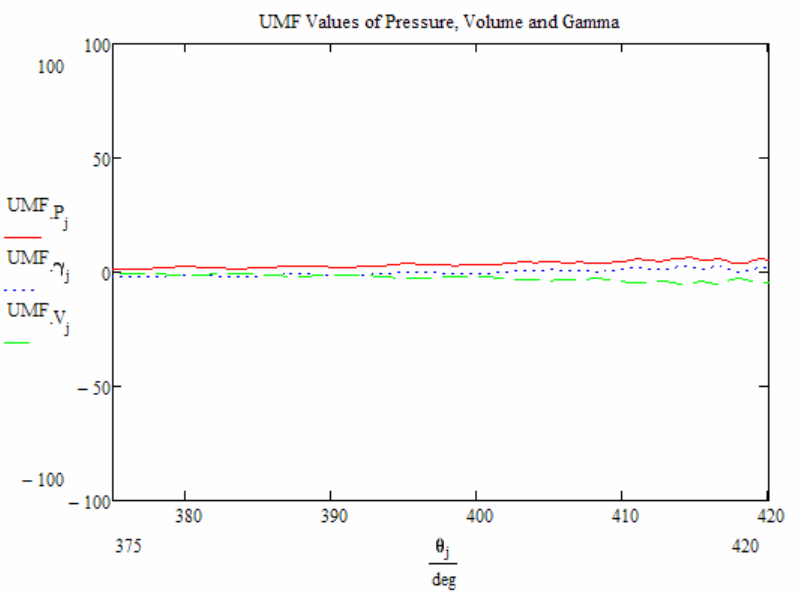

Figure C.3: 15 Degree BTDC Injection
Constant Gamma UMF Values

20 Degree BTDC Injection Timing:

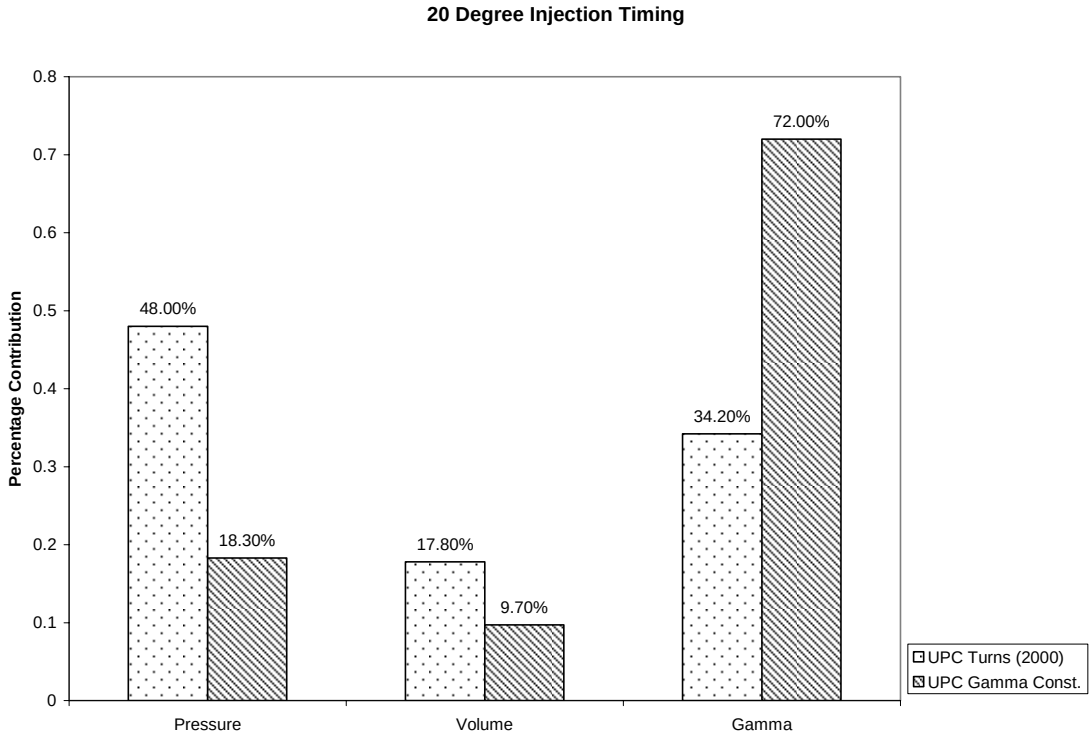

Figure C.4: 20 Degree BTDC Injection UPC Values

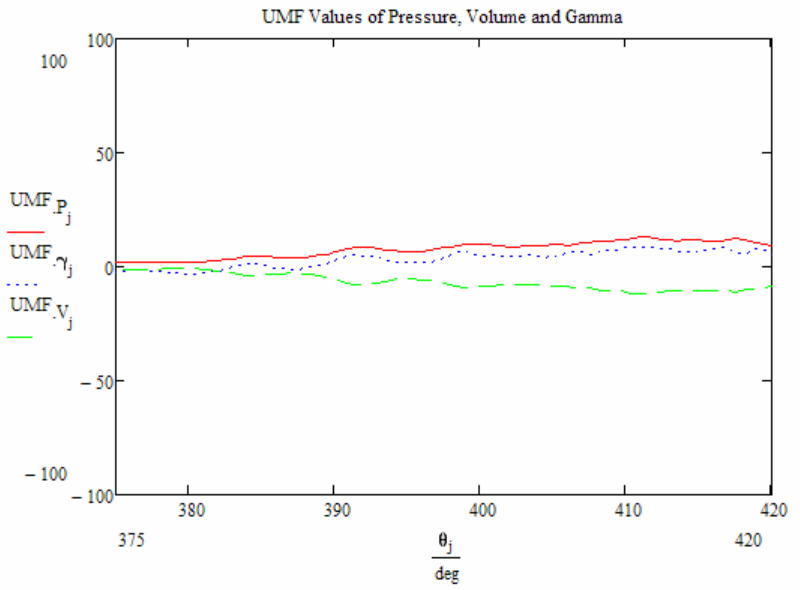

Figure C.5: 20 Degree BTDC Injection Turns (2000) UMF Values

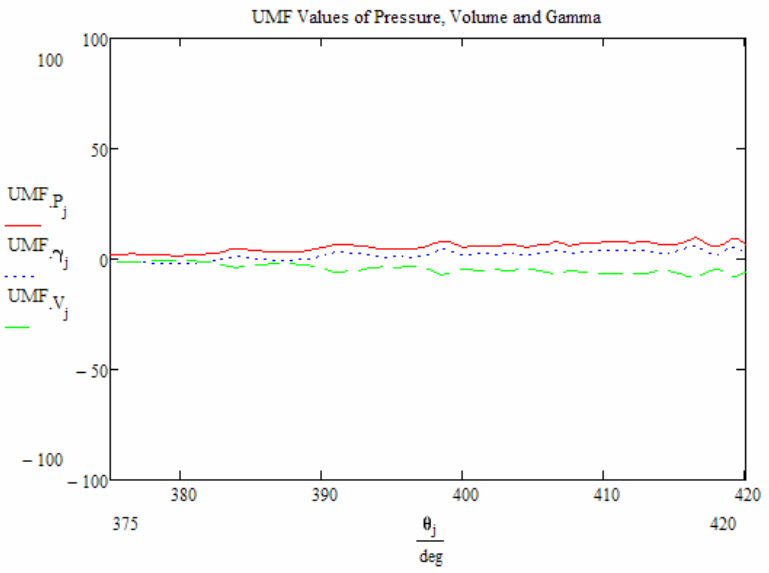

Figure C.6: 20 Degree BTDC Injection
Constant Gamma UMF Values

25 Degree BTDC Injection Timing:

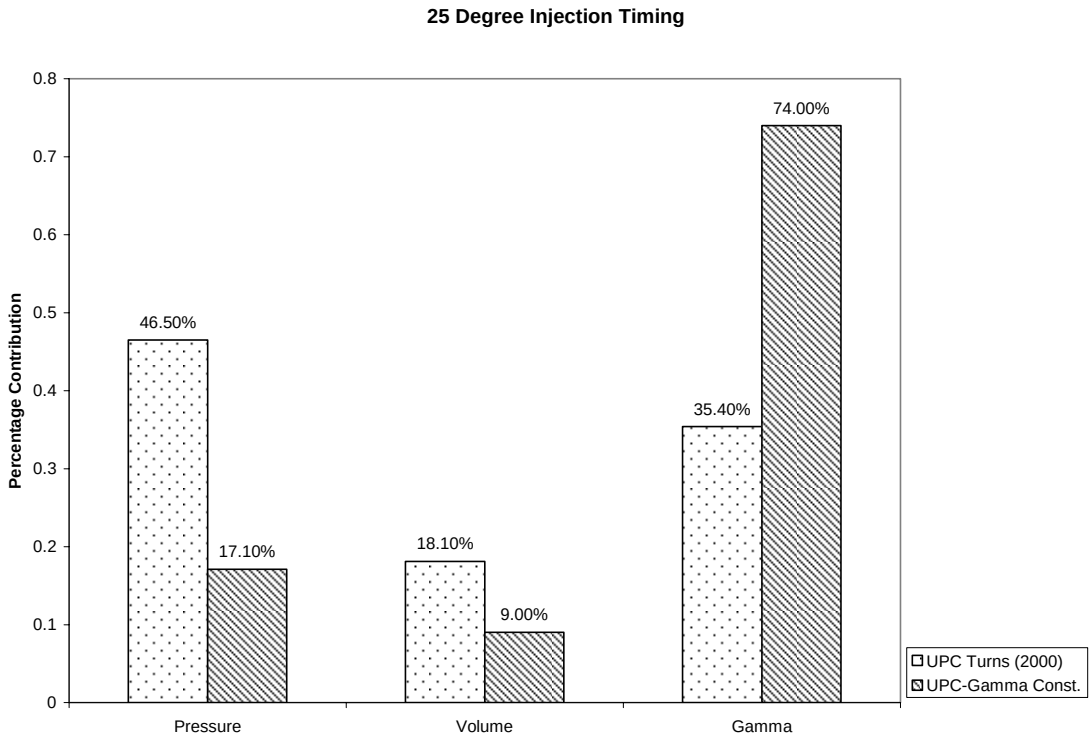

Figure C.7: 25 Degree BTDC Injection UPC Values

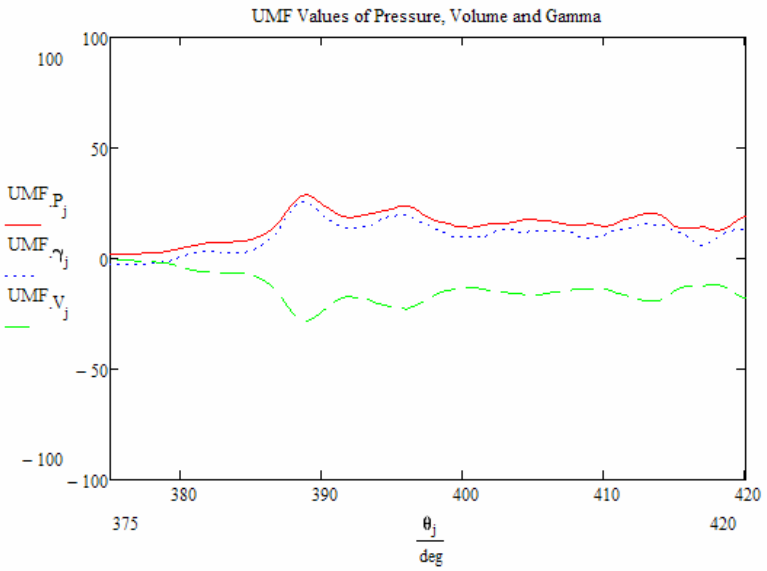

Figure C.8: 25 Degree BTDC Injection Turns (2000) UMF Values

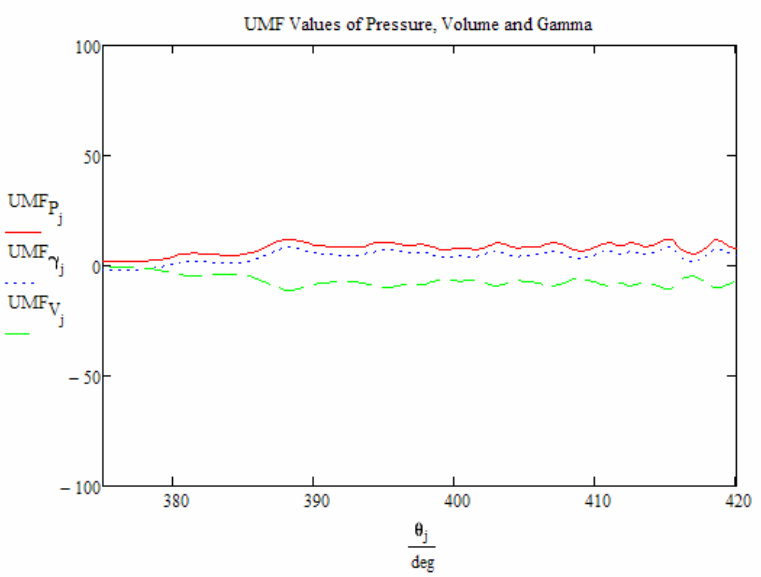

Figure C.9: 25 Degree BTDC Injection
Gamma Constant UMF Values

30 Degree BTDC Injection Timing:

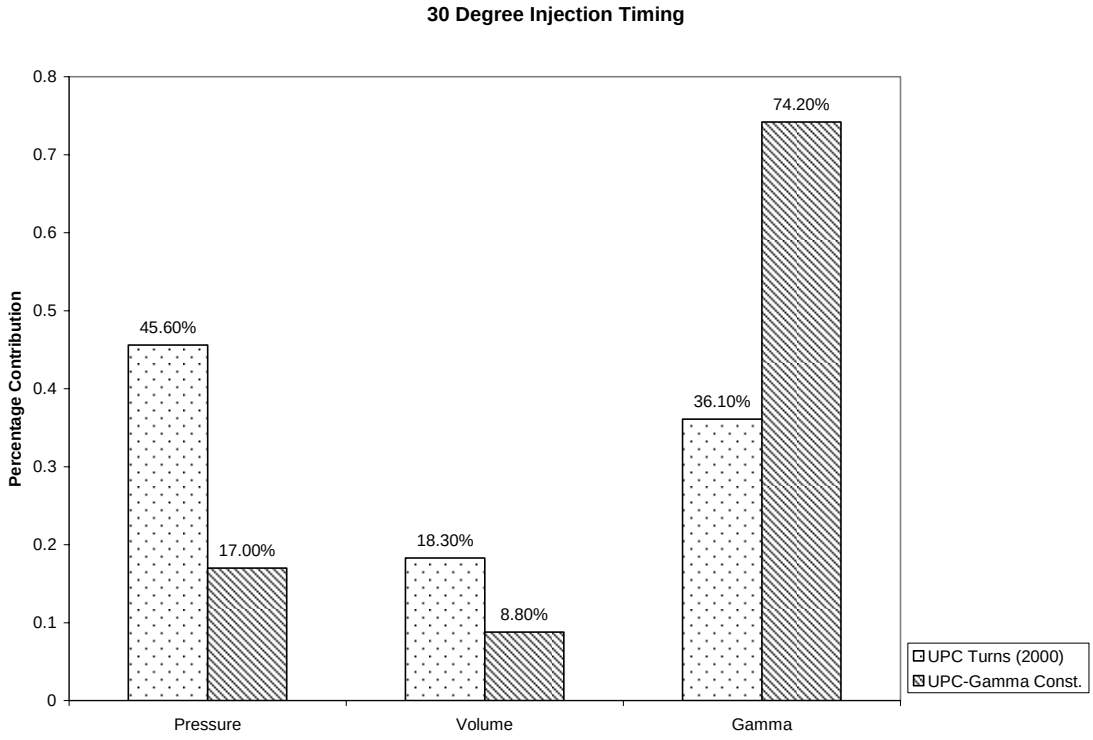

Figure C.10: 30 Degree BTDC Injection
UPC Values

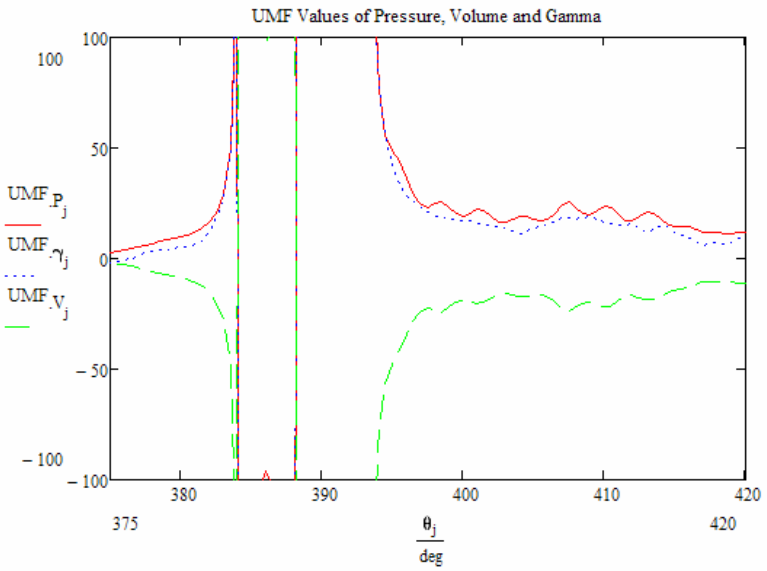

Figure C.11: 30 Degree BTDC Injection
Turns (2000) UMF Values

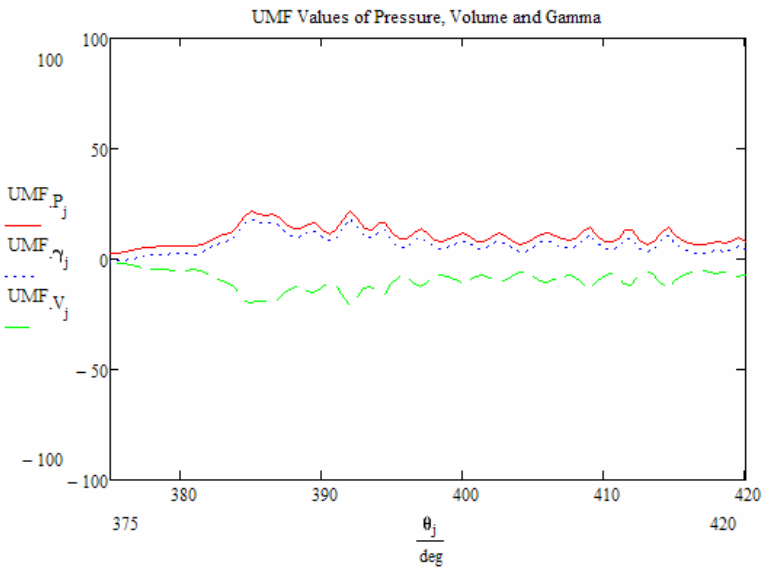

Figure C.12: 30 Degree BTDC Injection
Constant Gamma UMF Values

35 Degree BTDC Injection Timing:

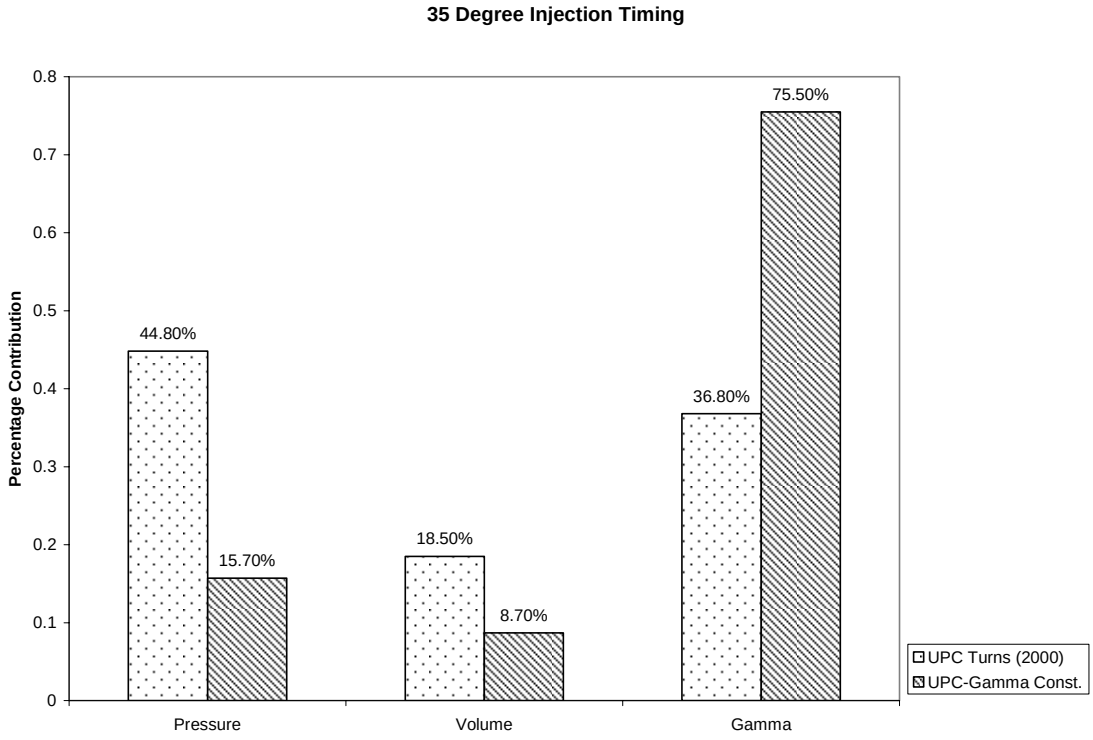

Figure C.13: 35 Degree BTDC Injection
UPC Values

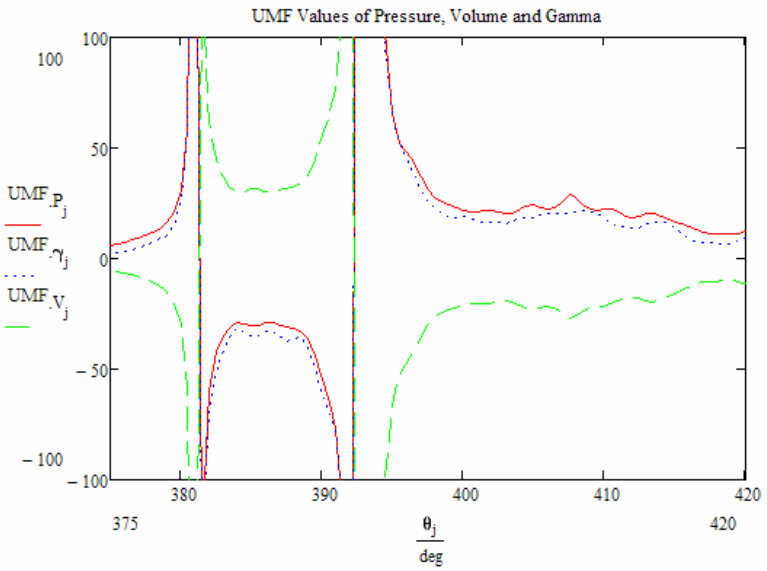

Figure C.14: 35 Degree BTDC Injection
Turns (2000) UMF Values

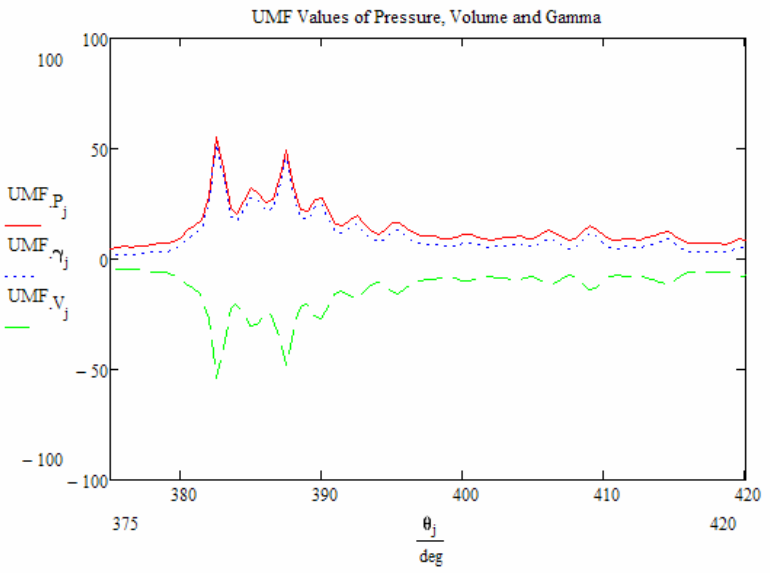

Figure C.15: 35 Degree BTDC Injection
Constant Gamma UMF Values

40 Degree BTDC Injection Timing:

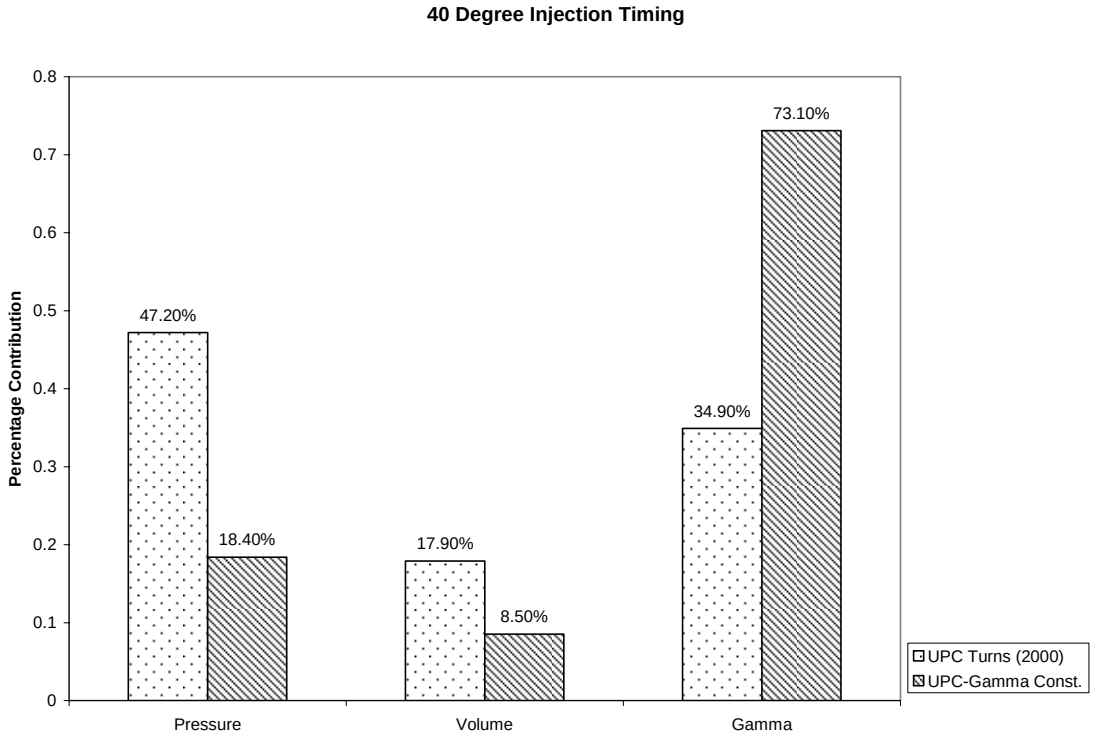

Figure C.16: 40 Degree BTDC Injection UPC Values

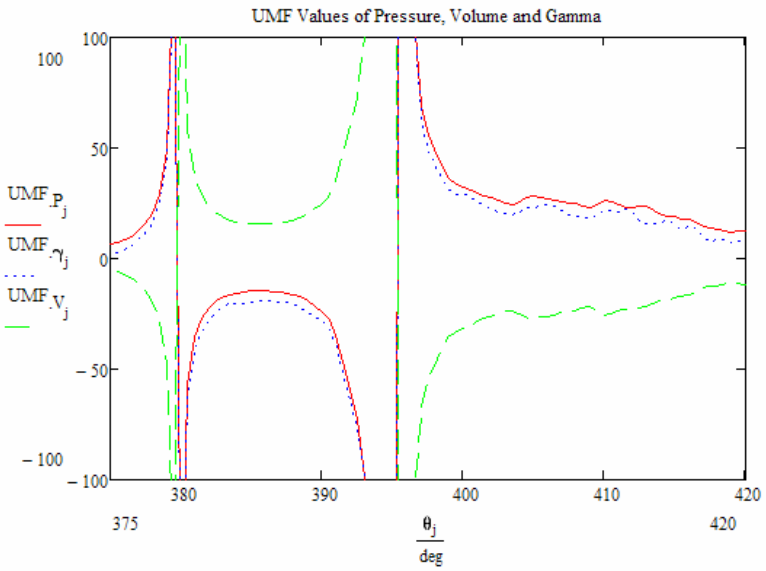

Figure C.17: 40 Degree BTDC Injection Turns (2000) UMF Values

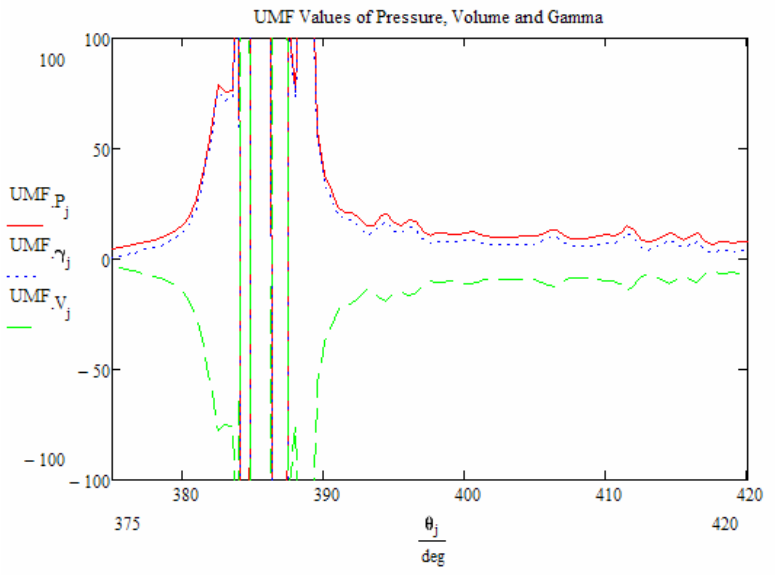

Figure C.18: 40 Degree BTDC Injection
Constant Gamma UMF Values

45 Degree BTDC Injection Timing:

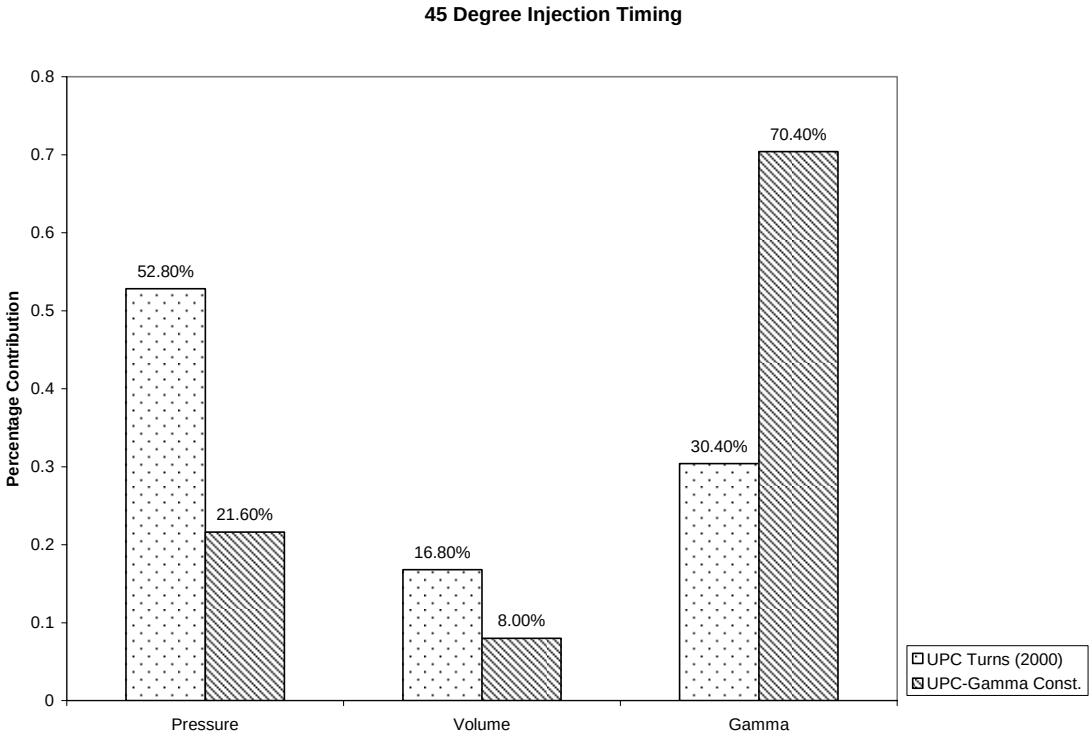

Figure C.19: 45 Degree BTDC Injection UPC Values

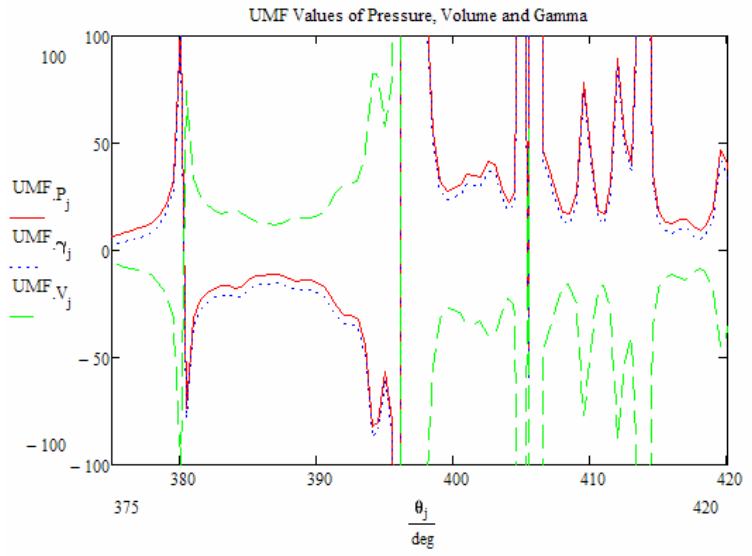

Figure C.20: 45 Degree BTDC Injection Turns (2000) UMF Values

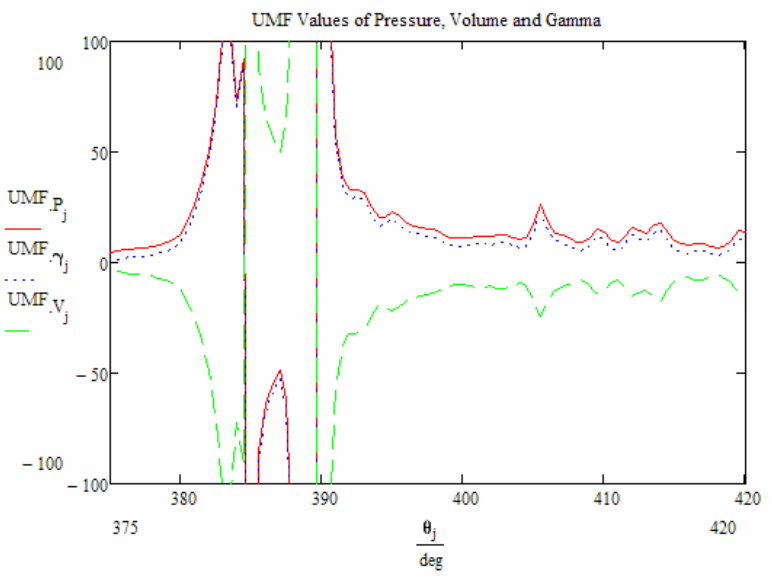

Figure C.21: 45 Degree BTDC Injection
Constant Gamma UMF Values

50 Degree BTDC Injection Timing:

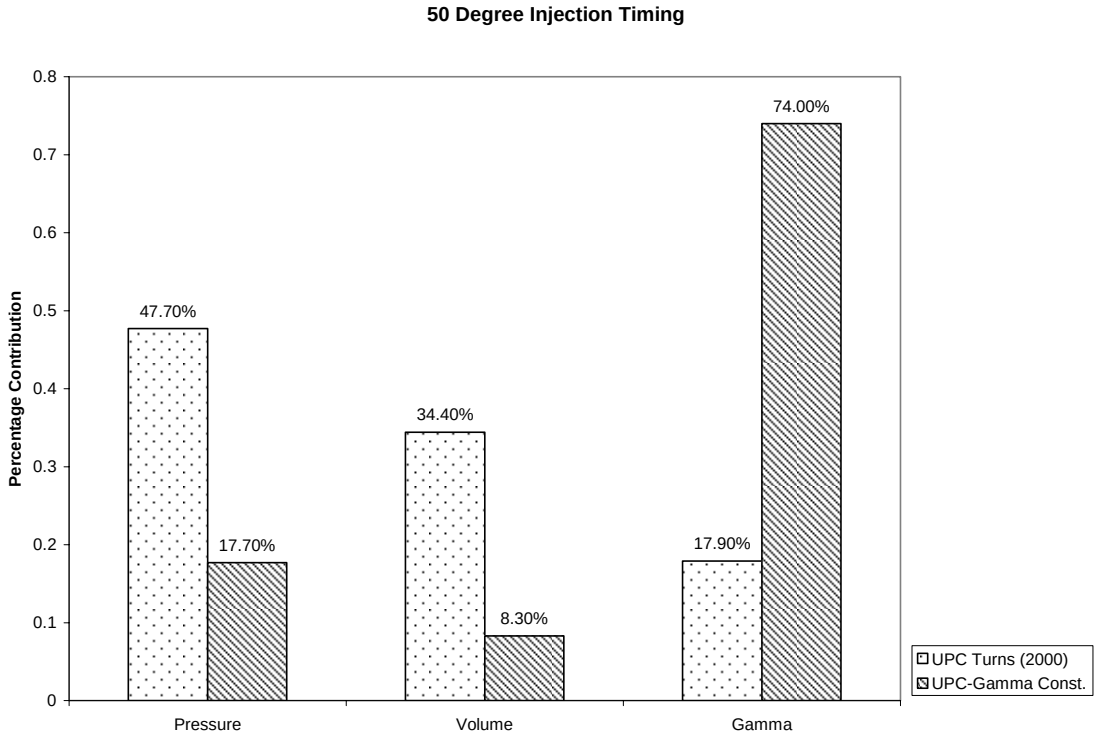

Figure C.22: 50 Degree BTDC Injection UPC Values

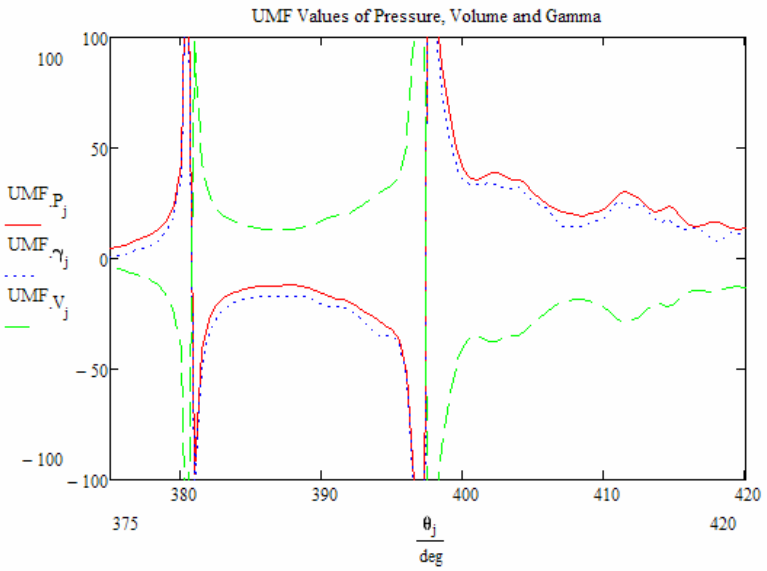

Figure C.23: 50 Degree BTDC Injection Turns (2000) UMF Values

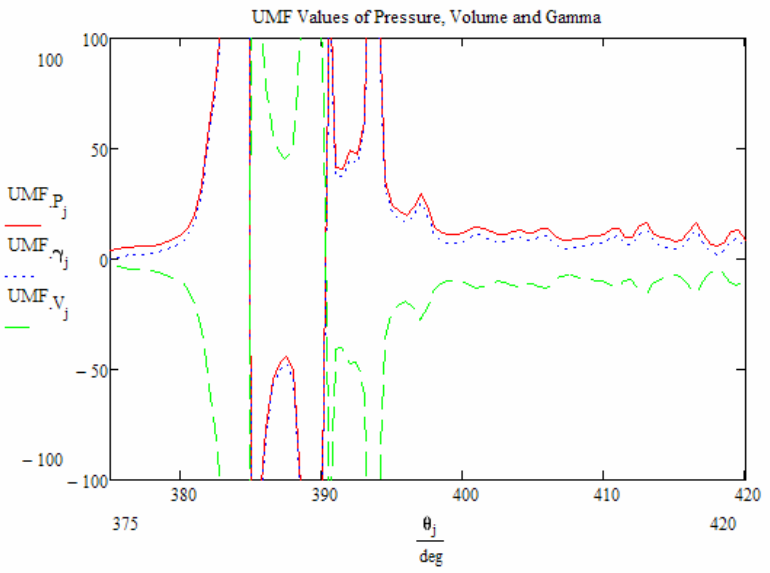

Figure C.24: 50 Degree BTDC Injection
Constant Gamma UMF Values

55 Degree BTDC Injection Timing:

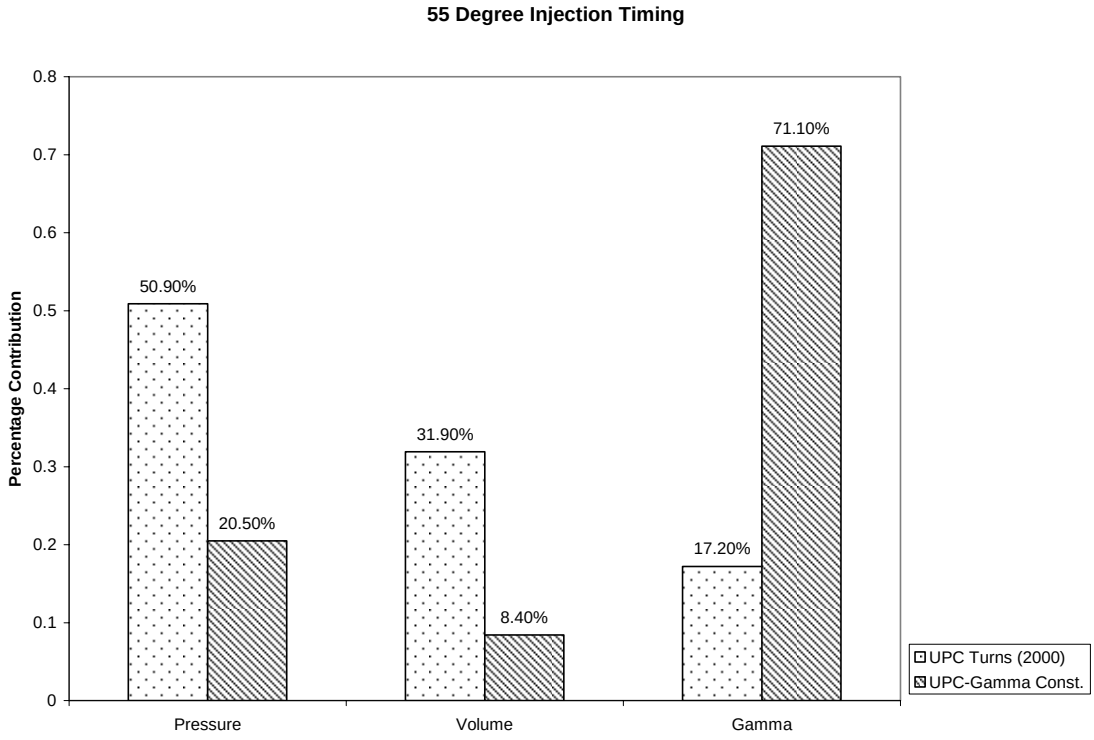

Figure C.25: 55 Degree BTDC Injection UPC Values

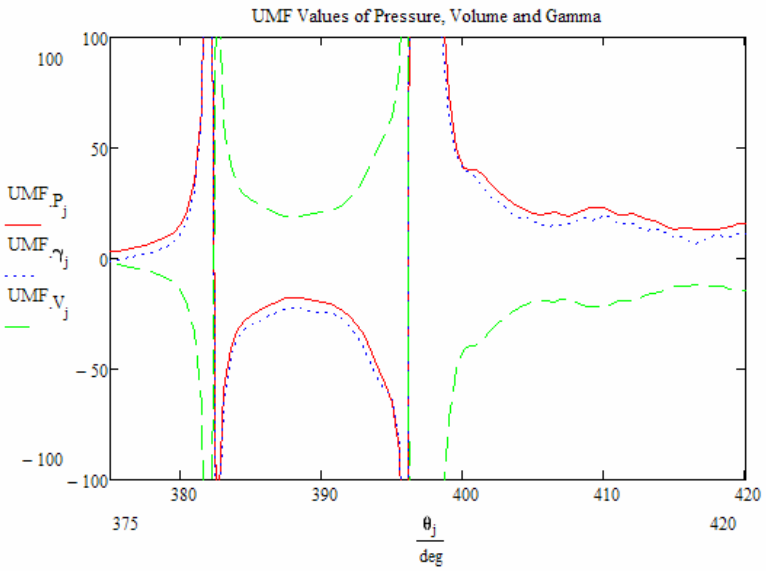

Figure C.26: 55 Degree BTDC Injection Turns (2000) UMF Values

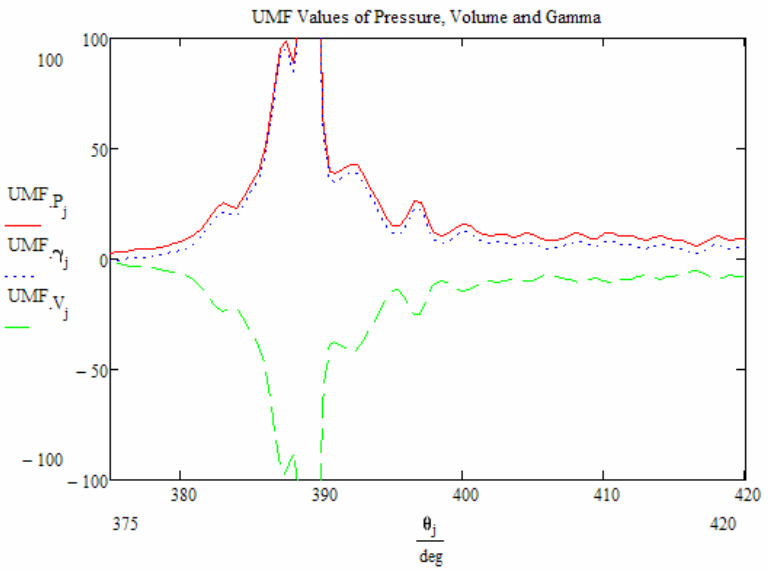

Figure C.27: 55 Degree BTDC Injection
Constant Gamma UMF Values

60 Degree BTDC Injection Timing:

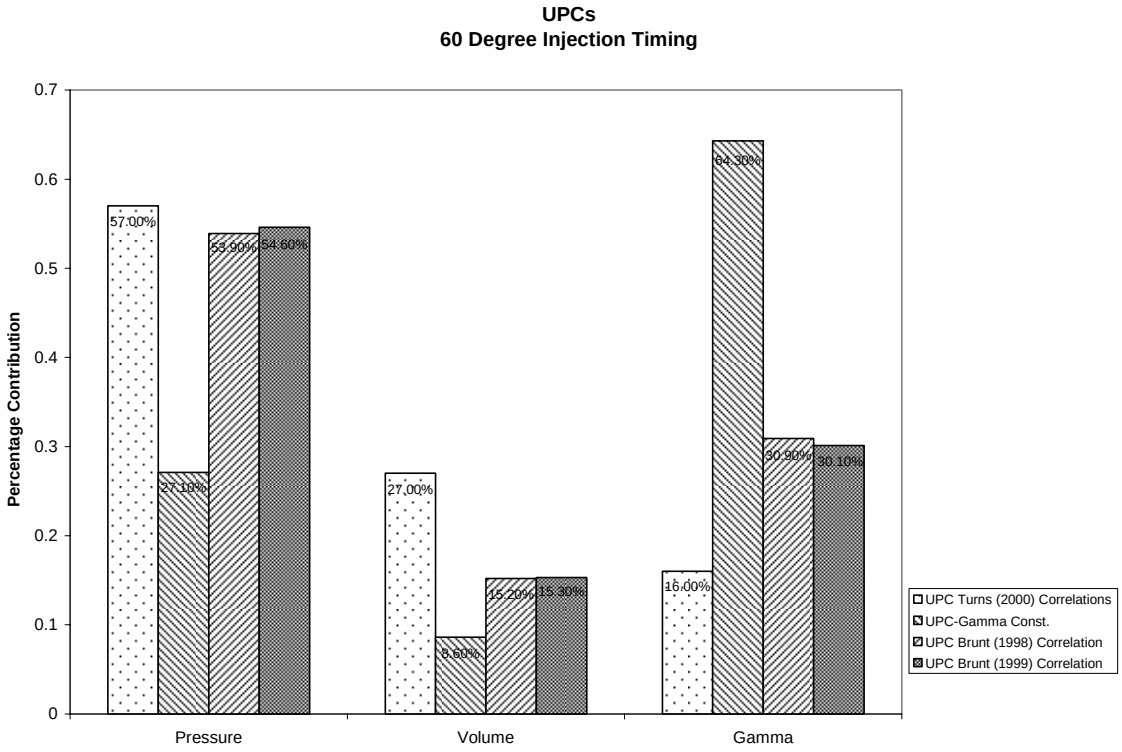

Figure C.28: 60 Degree BTDC Injection UPC Values

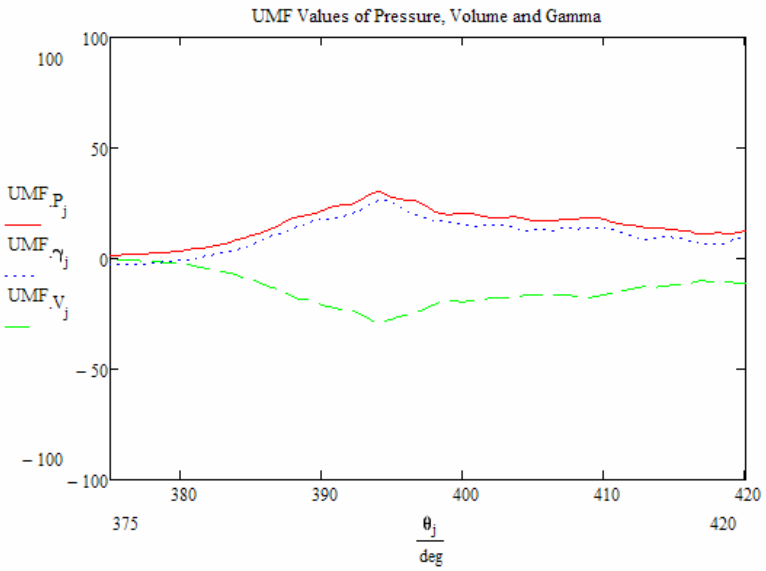

Figure C.29: 60 Degree BTDC Injection Turns (2000) UMF Values

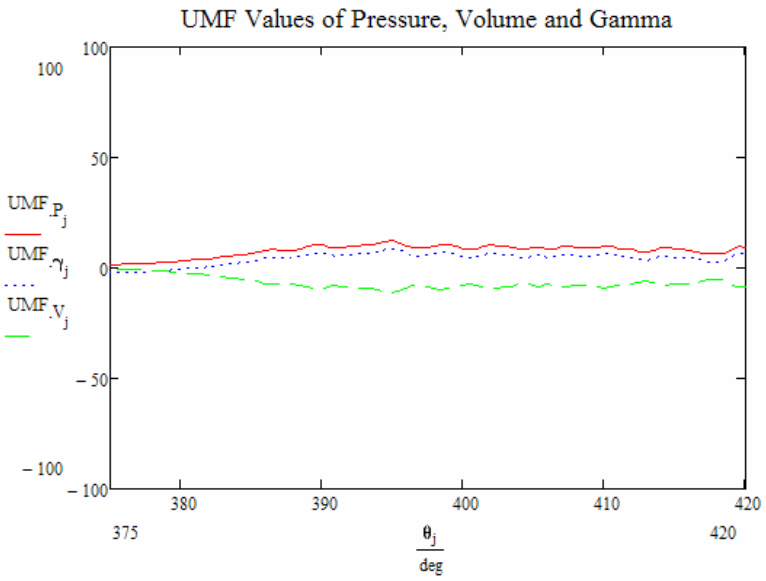

Figure C.30: 60 Degree BTDC Injection
Constant Gamma UMF Values

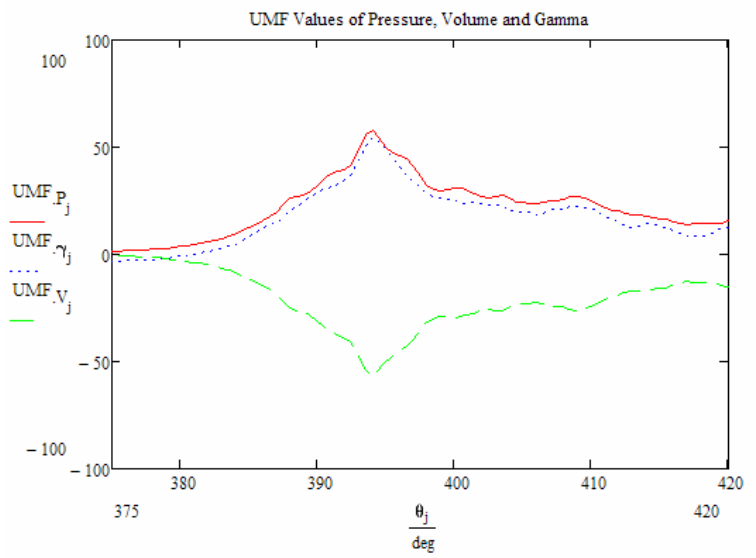

Figure C.31: 60 Degree BTDC Injection
Brunt (1998) UMF Values

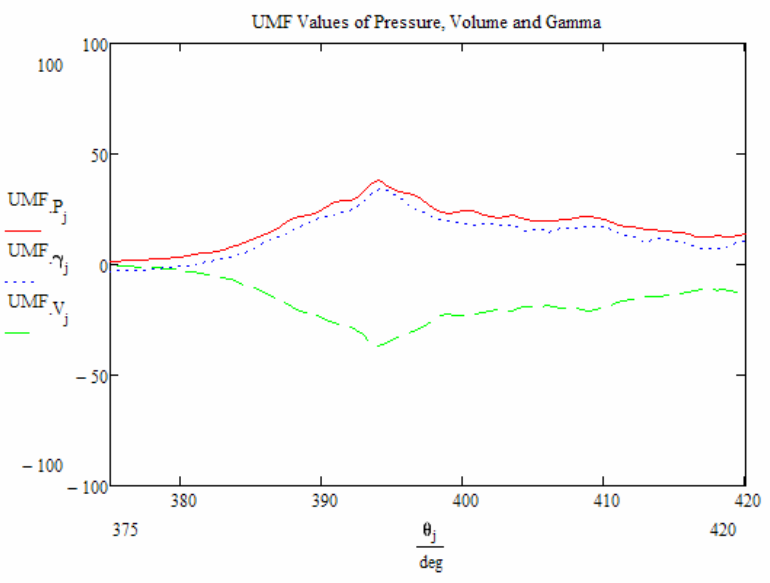

Figure C.32: 60 Degree BTDC Injection
Brunt (1999) UMF Values